

# **CONE PENETRATION TESTING FOR EVALUATING THE LIQUEFACTION POTENTIAL OF SANDS**

**October 1988  
Denver Office**

**Department of the Interior  
of Reclamation**



TECHNICAL REPORT STANDARD TITLE PAGE

1. REPORT NO. <b>REC-ERC-87-9</b>		2. GOVERNMENT ACCESSION NO.		3. RECIPIENT'S CATALOG NO.	
4. TITLE AND SUBTITLE <b>Cone Penetration Testing for Evaluating the Liquefaction Potential of Sands</b>		<div style="border: 1px solid black; padding: 5px; display: inline-block;"> <b>LIBRARY</b>   <b>APR 20 1988</b> </div>		5. REPORT DATE <b>May 1988</b>	
				6. PERFORMING ORGANIZATION CODE <b>D-1542</b>	
7. AUTHOR(S) <b>Robert R. Carter</b>		8. PERFORMING ORGANIZATION REPORT NO. <b>REC-ERC-87-9</b>			
9. PERFORMING ORGANIZATION NAME(S) AND ADDRESS(ES) <b>Bureau of Denver Office Denver, CO 80225</b>		10. WORK UNIT NO.			
		11. CONTRACT OR GRANT NO.			
12. SPONSORING AGENCY NAME AND ADDRESS <b>Same</b>		13. TYPE OF REPORT AND PERIOD COVERED			
		14. SPONSORING AGENCY CODE <b>DIBR</b>			
15. SUPPLEMENTARY NOTES  <b>Microfiche and hard copy available from the Denver office, Denver, Colorado</b>  <p style="text-align: right;">Editor:RC(c)/SA</p>					
16. ABSTRACT <p>The purpose of this report is to present the state of the art for the cone penetration test as an in situ tool for determining the dynamic response of sands during earthquake loading. Although a vast amount of literature has been published over the past 20 years on cone penetration testing, on the dynamic response of sands, and on their correlation, little agreement has been reached in any of these areas. Lack of a common ground has produced both progress and confusion.</p> <p>This report presents not only the current methods of relating cone penetration test data to the dynamic response of sands, but also the current concepts and theories related to each of them. Based on the information presented in this review, the author draws conclusions on the appropriateness and value of established cone penetration resistance – earthquake loading response of sand relationships and on areas in which further research is needed to produce a complete and consistent method for producing such a relationship.</p>					
17. KEY WORDS AND DOCUMENT ANALYSIS <p>a. DESCRIPTORS-- <b>cone penetration test/ soil dynamics/ sands/ soil models/ liquefaction/ compressibility</b></p> <p>b. IDENTIFIERS--</p> <p>c. COSATI Field/Group <b>08M</b>      COWRR: <b>0813</b>      SRIM:</p>					
18. DISTRIBUTION STATEMENT <i>Available from the National Technical Information Service, Operations Division, 5285 Port Royal Road, Springfield, Virginia 22161.</i>  <b>(Microfiche and hard copy available from NTIS)</b>		19. SECURITY CLASS (THIS REPORT) <b>UNCLASSIFIED</b>		21. NO. OF PAGES <b>60</b>	
		20. SECURITY CLASS (THIS PAGE) <b>UNCLASSIFIED</b>		22. PRICE	

**REC-ERC-87-9**

**CONE PENETRATION TESTING  
FOR EVALUATING THE LIQUEFACTION  
POTENTIAL OF SANDS**

by

**Robert R. Carter**

May 1988

Geotechnical Services Branch  
Research and Laboratory Services Division,  
Denver, Colorado



## ACKNOWLEDGMENTS

This report was submitted to the Department of Civil, Environmental, and Architectural Engineering of the Graduate School of the University of Colorado in 1987, in partial fulfillment of the requirements for the degree of Master of Science.

As the Nation's principal conservation agency, the Department of the Interior has responsibility for most of our nationally owned public lands and natural resources. This includes fostering the wisest use of our land and water resources, protecting our fish and wildlife, preserving the environmental and cultural values of our national parks and historical places, and providing for the enjoyment of life through outdoor recreation. The Department assesses our energy and mineral resources and works to assure that their development is in the best interests of all our people. The Department also has a major responsibility for American Indian reservation communities and for people who live in Island Territories under U.S. Administration.

The information contained in this report regarding commercial products or firms may not be used for advertising or promotional purposes and is not to be construed as an endorsement of any product or firm by the Bureau of Reclamation.

## CONTENTS

	Page
Course of study.....	1
Introduction.....	1
Failure mechanisms.....	1
Need for a detailed soil model.....	2
The cone penetration test.....	2
Organization of report.....	3
Notation.....	3
Sources of information.....	4
Soil behavior model.....	4
Introduction.....	4
Stress field around the cone penetrometer.....	5
Strain field around the cone penetrometer.....	7
Effects of earthquake loading on a soil element.....	7
Steady-state soil models for development of a relationship between CPT and earthquake loading.....	10
Evaluation of the steady-state shear strength concept.....	12
Status and use of large-strain behavior models.....	20
Additional problems with association of cone penetration testing to earthquake response of soils.....	25
Cone penetration theory.....	25
Introduction.....	25
General bearing capacity theory.....	25
Janbu and Senneset's method.....	27
Durgunoglu and Mitchell's method.....	27
Comparison of bearing capacity methods.....	28
Cavity expansion theory.....	31
Comparison of cavity expansion theory and bearing capacity theory for predicting soil friction angle.....	35
Effect of compressibility of sands.....	36
Cone penetration practice.....	36
Introduction.....	36
Influencing factors of the CPT.....	36
CPT-SPT correlations.....	38
Liquefaction assessment directly from CPT data.....	40
Cone resistance normalization factor.....	43
Analysis of CPT data to determine input parameters for use in liquefaction analyses.....	48
Piezocone as a possible indicator of sand behavior.....	49
Use of relative density determinations.....	52
Summary, conclusions, and recommendations.....	54
Introduction.....	54
Summary.....	54
Conclusions.....	57
Recommendations.....	57
Bibliography.....	57

## TABLES

Table		Page
1	Lunne and Christoffersen's comparison of $\Phi$ predictions.....	31
2	Summary of CPT calibration chamber tests.....	49
3	Properties of sand tested in calibration chamber studies.....	49

## CONTENTS – Continued

Figure	FIGURES	Page
1	Failure mechanisms in sand caused by earthquake loading .....	1
2	Fugro-type cone penetrometer.....	3
3	Computer plot of the principal stress trajectories, based on 182 measuring points .....	5
4	Direction of principal stresses acting on soil elements in contact with and at a distance from a penetrometer .....	6
5	Yield criteria in unordered principal effective stress space.....	7
6	Soil displacements during penetration of a 60° cone.....	8
7	Contours of maximum shear strain .....	9
8	Cyclic shear stresses on a soil element during ground shaking .....	10
9	Cyclic torsional shear tests on Fuji River sand .....	11
10	Steady-state soil model.....	13
11	Idealized soil model proposed by Robertson .....	14
12	Constant volume plane of idealized soil model showing zones of stable soil behavior and metastable behavior.....	15
13	Typical data from monotonically loaded undrained axisymmetrical triaxial shear tests on sands.....	16
14	Extrapolation of undrained shear stress paths into constant volume plane of idealized soil model.....	17
15	Development of failure plane in highly overconsolidated sands during axisymmetrical triaxial shear test.....	19
16	Development of bulging failure in loose sand during axisymmetrical triaxial shear test .....	20
17	Critical state soil model for sands.....	21
18	Possible critical state model showing projection of CS shear strength from failure void ratio into initial constant volume plane.....	22
19	Critical state model for sands (nonassociated flow rule) .....	23
20	Critical state soil model interpretation of stress paths caused by earthquake and cone penetration loading.....	24
21	Example of electric cone penetrometer record in an alluvial lacustrine deposit .....	26
22	Ridged plastic frictional soil model.....	28
23	Bearing capacity theory failure mechanism .....	29
24	Diagram showing bearing capacity factor (number) as a function of friction angle and $\beta$ .....	30
25	Modified Janbu and Senneset method .....	31
26	Relationship between bearing capacity number and peak friction angle at in situ stress, from large calibration chamber tests.....	32
27	Cavity expansion theory .....	34
28	Variation of predictions of peak triaxial friction angle using bearing capacity and cavity expansion theories.....	35
29	Initial tangent axial compression modulus ( $E_o$ ) of mica-quartz sand mixtures, at different confining pressures ( $\sigma_3$ ), as a function of mica weight percentage.....	37
30	Comparison of different relative density relationships.....	38
31	Variation of $q_c/N$ ratio with mean grain size.....	39
32	Variation of $q_c/N_{60}$ ratio with mean grain size .....	40
33	Example of lack of correlation between $q_c/N_{60}$ and $D_{50}$ .....	41
34	Normalized cone and friction sleeve resistance versus normalized SPT data .....	42
35	Correlation between field liquefaction behavior of silty sands ( $D_{50} < 0.15$ mm) under level ground conditions and standard penetration resistance .....	43
36	Soil classification chart for electric cone showing proposed zone of liquefaction soils .....	44
37	Graphs for determining liquefaction resistance of a sand from normalized cone end bearing ...	45
38	Graph for estimating liquefaction resistance of soils.....	46
39	Summary of normalized tip and sleeve friction CPT data – 1983 U.S.-Japan Joint Study .....	47
40	Relationship between correlation factor $C_o$ and effective overburden pressure .....	48
41	Definition of state parameter $\psi$ .....	50
42	Definition of state parameter $\psi$ in idealized soil model proposed by Robertson.....	51
43	Summary of normalized cone resistance – state relationships for normally consolidated sands.....	52

## CONTENTS – Continued

Figures		Page
44	Location of filter elements for measurement of pore pressure .....	53
45	Conceptual pore pressure distribution in saturated soil during cone penetration .....	53
46	Piezocone data showing lack of response of pore pressure measurements to changing soil types .....	54
47	Conceptual plots of pore pressure decay patterns measured behind the cone.....	55
48	Examples of change in pore pressure measurements due to densification of sands and silts...	56



## COURSE OF STUDY

### Introduction

Before the Niigata and Alaskan earthquakes of 1964, most geotechnical engineers had expressed little concern about the dynamic behavior of saturated sand layers. Regardless of their density, sands were generally considered quite incompressible and stable for foundation and construction uses. The only disadvantages for the universal use of sands considered were the consequences of their high permeabilities: excessive seepage losses, high exit gradients (which could reach critical or flotation gradient levels), and the possibility of adjoining fine-grained soils piping into the voids of the sand. Each of these problems was concerned with the steady-state flow of water through sand. Damage to many structures founded on saturated sand beds and other physical signs of loss of strength in sand layers during the two 1964 earthquakes resulted in the formation of a new area of geotechnical engineering. And new term, "liquefaction," was coined to describe the more visible outcomes of earthquake-related failures.

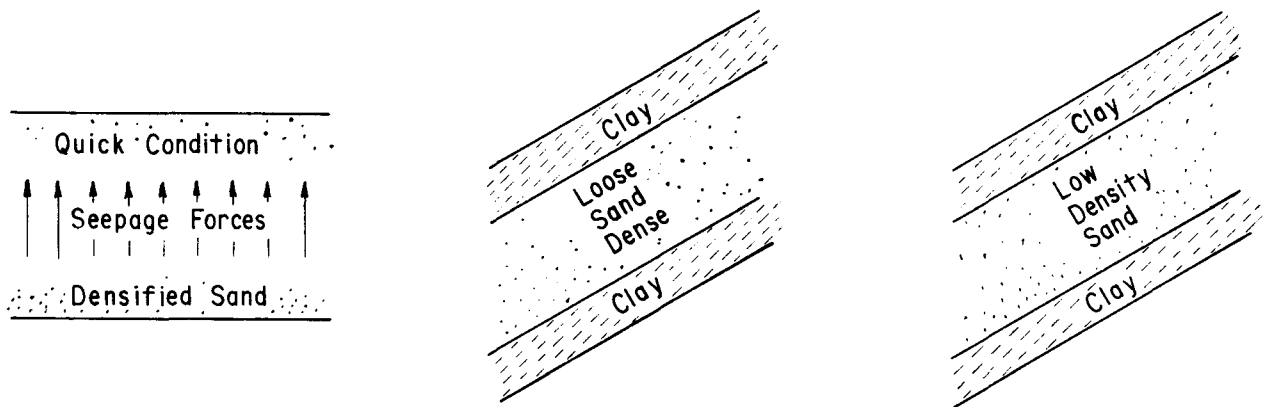
### Failure Mechanisms

The term "liquefaction" has been the focus of almost as much discussion as the problems it was intended to describe [10, 49, 50, 12, 13].\* Initially, the dynamic response of saturated sands was thought to be a single problem – the complete loss of strength during cyclic loading. However, as detailed studies

\* Numbers in brackets refer to entries in the bibliography.

of sand behavior became more numerous, engineers realized that at least three different failure mechanisms were possible (fig. 1). First, loose sands could densify under dynamic loading and internally develop high seepage gradients that could reach critical levels at exposed exit points. Second, if the sand layer was not allowed to drain freely, the sand could virtually settle away from the overlying containment layer, thus spontaneously developing a fluidized zone at the contact of the layers. And third, the sand layer itself could develop high excess pore pressures internally during the shaking; this would reduce the effective stress and cause a corresponding loss of shear strength in the sand. These three failure mechanisms resulting from the different drainage conditions are referred to as globally drained, globally undrained, and locally undrained, respectively [25].

Realizing the possibility of three distinct failure mechanisms developing during dynamic loading and observing the evidence that, in a locally undrained condition, dense sands under low effective confining stresses do not respond to dynamic loading the same way as loose sands under high effective confining stresses led to disagreement over the definition of the term "liquefaction." Researchers, such as Casagrande [10], Castro [12], and Poulos [13], wished to limit the definition to the behavior of loose sands under high effective confining stresses. Consequently, they developed new terms for the other modes of sand behavior and failure mechanisms. At the same time, other researchers, such as Seed [49, 50], and engineering practitioners in general continued to use the term "liquefaction" as originally coined; that is, to describe all the observed detri-



(a) Globally drained. – Rapid densification of the lower portion of the sand layer results in high seepage gradients that approach critical levels in the upper portion.

(b) Globally undrained. – Drainage within the sand layer occurs as in mechanism (a); however, the water is trapped by the upper clay layer, forming a fluidized zone at the contact between layers.

(c) Locally undrained. – High excess pore pressures developed during shaking reduce the effective stress level in the sand, and a corresponding loss in shear strength results.

Figure 1. – Failure mechanisms in sand caused by earthquake loading. After [25].

mental behavior of sand during earthquake loading. Because the current data base used in developing empirical relationships between cone penetration test data and "liquefaction" susceptibility of a sand does not distinguish between the various modes of earthquake-induced failure, the latter (more universal) definition was adopted for this report.

### **Need for a Detailed Soil Model**

In the past, only clean sands were thought to be susceptible to liquefaction. However, many ongoing research programs are investigating the liquefaction susceptibility of silty sands and gravels, and in light of the 1984 Mexico City earthquake, a reevaluation of the dynamic response of clays is underway. Soils in nature rarely separate into thick homogeneous layers of clean sand or lean clay, but often occur as thin interbedded layers of silt, sand, clay, or mixtures of all three. Therefore, a short digression into general soil behavior is included before the specific topic of liquefaction of sands is discussed.

Most soils are granular media that possess distinct properties. These properties may be subdivided into those of the individual grains and those that describe the bulk behavior of the mass. It is the bulk behavioral properties that most interest geotechnical engineers; individual grain properties are of interest only insofar as they influence the observed bulk behavioral properties. The bulk properties include strength properties, which comprise friction and cohesion; hydraulic properties, which comprise conductivity and storage; and deformation properties in shear and confined compression. The major differences between fine-grained soils, such as clays, and coarse-grained soils, such as sands, lie in the relative importance of the two components of strength (fine-grained soils are cohesive, whereas coarse-grained soils are frictional), the magnitude of the hydraulic properties, and the constitutive relationships that relate stresses and strains.

One conceptual model of behavior should exist to describe the behavior of all soil types. The differences in soil types would be reflected within the soil model by the functions that describe the shape and size of the soil model. This model should be able to qualitatively, if not quantitatively, describe the relationships between the bulk behavioral properties of the soil and the stress condition to which a soil element might be subjected. The model should describe the shear strength of the soil, the effects of changes in the effective stress level, rotation of principal stress axes, level of shear strain, volume change, grain crushing, soil fabric, and the relationships between stress and strain and between permeability and rate of loading. Such a model would be very complex and impractical for solving most geotech-

nical problems. However, qualitative understanding of this model would provide an engineer with the basis to logically determine which portions of the model need definition to solve a particular problem and how parameters such as rate of loading, stability, and consolidation interact for a particular problem.

At present, no such general model exists. Yet, without this model of material behavior, approximate solutions limited to particular soil types and loading conditions will continue to be developed and used. Such practice limits the general application of the existing soil models and often stifles the acceptance of other such models. This is evident in the literature for the cone penetration test, wherein many solutions are presented for lean clays and clean sands, but few exist for all other soil types. One of the major stumbling blocks to developing general solutions that tie the particular solutions together is the missing general soil model. As will be demonstrated (in the sections entitled "Soil Behavior Model" and "Cone Penetration Theory"), without this soil model, theoretical interpretation and evaluation of the cone penetration test and the liquefaction susceptibility of a soil are difficult, if not impossible.

### **The Cone Penetration Test**

Progress in soils engineering must continue. Until the definitive soil model is developed, engineers must continue to identify problems and seek new tools for solutions. One such tool for assessing soil properties is the cone penetrometer. It was originally developed in Holland in the 1930's; and since then, penetrometers of various designs and levels of sophistication have been developed throughout the world. In the late 1960's and early 1970's, it became apparent that to develop useful empirical data reduction and design procedures, the dimensions of the penetrometer and the rate at which the penetrometer was advanced should be standardized.

Standards for performing the CPT (cone penetration test) have been developed in Europe [38] and in the United States [2]. Both standards are based on a device that has a 60° truncated cone tip and a projected circular end area of 10 cm<sup>2</sup>. Allowance has been made in both standards for a friction sleeve having a 150-cm<sup>2</sup> surface area located immediately behind the cone. A penetration rate varying between 1.0 and 2.0 cm/s has also been established as a standard.

Recent developments in electronics have resulted in a variety of new measurement capabilities. Originally, hydraulic pressure was used to measure the cone tip resistance and friction sleeve resistance, and the hydraulic pressure was recorded manually. However, advances in computers and

now allow for virtually continuous automatic monitoring and recording of the two resistance components as well as measurement of penetrometer inclination, pore-water pressure developed at the penetrometer-soil interface, and temperature of the penetrometer. New penetrometers, which can measure pore-water conductivity, shear wave velocity of soil layers, hoop stress developed around the penetrometer shaft, and other items of interest, are continuously being developed and studied. Greater accuracy of electric measurements has led to renewed studies of the effects of varying the cone apex angle and the rate of penetration.

For the purpose of liquefaction assessment, the 60° apex angle cone penetrometer, which allows for electronic measurements of tip and sleeve resistance (often referred to as the Fugro-type penetrometer), has found widespread use. Although many of the specialized probes are rapidly advancing the state of the art and deserve further attention, this report concentrates on the more widely accepted and used Fugro-type electric cone penetrometer (fig. 2) and the various configurations of piezocone penetrometers conforming to its geometry.

### Organization of Report

Currently, the use of the cone penetration test as it applies to liquefaction assessment is based on empirical techniques and relationships. To understand how these procedures have evolved and to develop a framework of evaluating the appropriateness of those empirical relationships, this report has been organized into the following parts:

In the section entitled "Soil Behavior Model," a discussion is presented of (1) the behavior of sands during cone penetration testing, earthquake loading, and undrained axisymmetric triaxial shear testing; (2) four idealized soil models based on observations of sand behavior during triaxial shear testing; and (3) the need for a more complete soil model in developing a theoretical link between sand behavior during cone penetration testing and earthquake loading.

In the section entitled "Cone Penetration Theory," a discussion is presented of (1) theoretical models of sand behavior based on cavity expansion and bearing capacity theories; (2) the soil models used when establishing the framework for those theories; (3) comparisons of the various CPT methods of predicting shear strength of sands; (4) the appropriateness of those predictions in relation to liquefaction assessment; and (5) the effect of compressibility of a sand on those predictions.

In the section entitled "Cone Penetration Practice," a discussion is presented of (1) current empirical relationships between cone penetration test data and

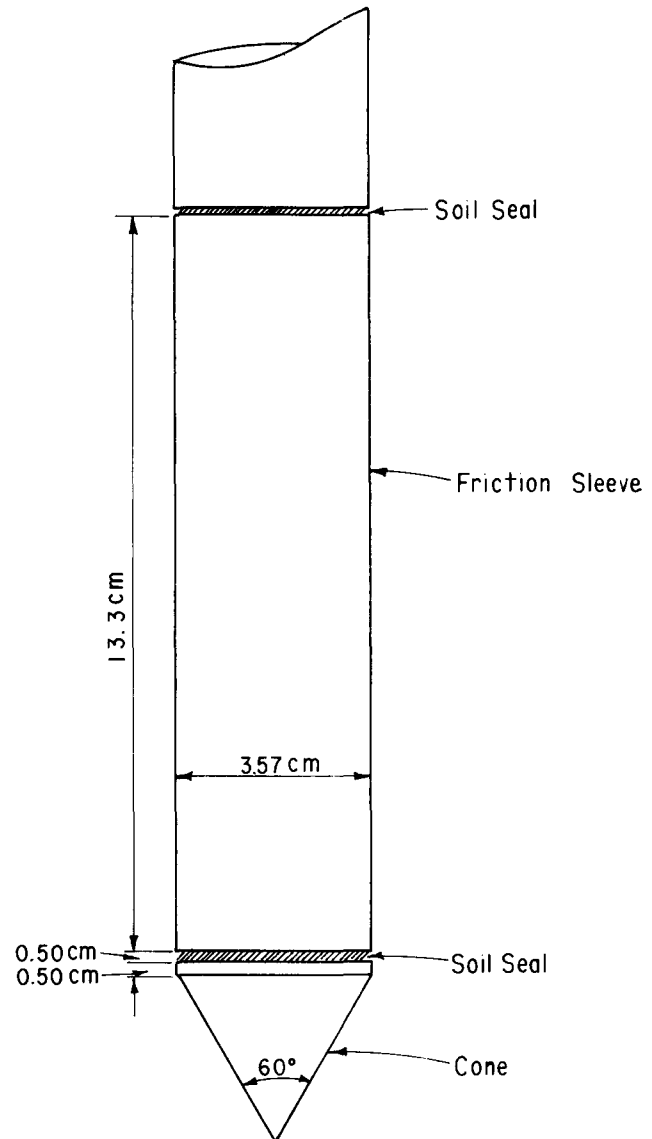


Figure 2. – Fugro-type cone penetrometer.

liquefaction susceptibility; and (2) factors related to sand which influence the data measurements.

In the section entitled "Summary, Conclusions, and Recommendations," a summary of the previous discussions is presented, and conclusions are drawn with respect to (1) the state of the art of cone penetration testing for liquefaction assessment; and (2) areas of further research needed before a sound theoretical or empirical solution can be determined relating cone penetration test results to the liquefaction susceptibility of a sand.

### Notation

The use of the symbols  $P$  and  $Q$  for stress in geotechnical engineering has become confusing and

requires definition. In the United States,  $P'$  and  $Q$  are defined by:

$$P' = 1/2 (\sigma'_1 + \sigma'_3) \quad (1)$$

and

$$Q = 1/2 (\sigma'_1 - \sigma'_3) \quad (2)$$

where:

$\sigma'_1$  = major principal effective stress, and  
 $\sigma'_3$  = minor principal effective stress.

However, in the United Kingdom and many other parts of the world:

$$P' = 1/3 (\sigma'_1 + \sigma'_2 + \sigma'_3) \quad (3)$$

and

$$Q = (\sigma'_1 - \sigma'_3) \quad (4)$$

where:

$\sigma'_2$  = intermediate principal effective stress.

To avoid confusion over the terms  $P'$  and  $Q$ , this report adopts the following notation:

$$I_1' = 1/3 (\sigma'_1 + \sigma'_2 + \sigma'_3) \quad (5)$$

and

$$\tau_m = 1/2 (\sigma'_1 - \sigma'_3) \quad (6)$$

### Sources of Information

Most of the information used in this report originates from the work of Sangrelet [45], Schmertmann [47], Robertson and Campanella [41], the *Proceedings of the European Symposiums on Penetration Testing I and II* [36, 37], ASCE (American Society of Civil Engineers) Conferences on In Situ Testing (1975, 1976) [21], the conference on "Cone Penetration Testing and Experience" [14], the conference on *Liquefaction of Soils During Earthquakes* [25], *Use of In Situ Tests in Geotechnical Engineering* [59], and other publications in the journal *Geotechnique* and in the *Journal of Geotechnical Engineering* of the Geotechnical Engineering Division of ASCE.

## SOIL BEHAVIOR MODEL

### Introduction

This section contains a cursory review of the literature related to (1) the stress and strain fields surrounding the cone penetrometer, (2) the dynamic response of a sand, (3) steady-state shear strength interpretation of large strain behavior of sands, and (4) interpretation of large strain axisymmetrical shear tests. These topics are covered to demonstrate the complexity of the problems associated with linking the behavior of sand in terms of a theoretical model representing its behavior during earthquake loading to the loading conditions of and measurements ob-

tained from a cone penetrometer. The purpose of this exercise is not to provide a conclusive relationship between the loading conditions, but to present the state of the art in understanding the similarities and differences between the loading conditions. This section should provide the reader with an appreciation of the complexities involved with deriving a theoretical relationship between earthquake loading and CPT loading and the associated problems of implementing that theory into an analysis of the behavior of a soil.

### Stress Field Around the Cone Penetrometer

Allersma [1] reported the results of a "photoelastic" study of penetration into a medium of crushed pyrex glass particles. The purpose of the study was to investigate the orientation of principal stress directions in two dimensions during advancement of penetrometers into a homogeneous particulate medium. The penetrometers used in the study had blunt ends or ends formed by a 60° wedge-shaped point. A computer-generated plot of the principal stress trajectories for the 60° wedge penetrometer used in the study is shown on figure 3. The general pattern of major principal stress in the vicinity of the wedge and immediately above the wedge emanates from the penetrometer and rotates toward the undisturbed in situ stress field as the trajectory progresses away from the penetrometer.

Although boundary effects may have influenced the exact shape of the principal stress trajectories in Allersma's study, the general pattern agrees with that expected for a cone penetrometer. To illustrate this point, consider the case of a cone during penetration of a sand as shown on figure 4. Sand elements A and D are located far from the penetrometer in the vertical and horizontal directions, respectively, and do not sense the presence of the penetrometer. For a one-dimensional, "normally" consolidated sand, the major principal stress axis is vertical and the minor principal stress axis is horizontal for these two sand elements. Sand element B is in contact with the face of the cone, and the major principal stress axis is orientated at an angle  $\psi$  downward from the normal to the cone face (where  $\psi$  is the interfacial friction angle between the cone and the sand). Element B is in a state of axisymmetry, and the minor and intermediate stresses acting on element B are not equal. Since elements A and B are located along the same vertical plane, it is apparent that the principal stress axis of a sand element in front of the cone must be rotating as the cone approaches that element. A comparison of the principal stress axis for elements C and D, which are located along the same horizontal plane, shows that the principal stress axis again rotates an angle of  $\psi + 90^\circ$  with respect to the penetrometer. Whether or not elements A and B and elements C and D are located along the same

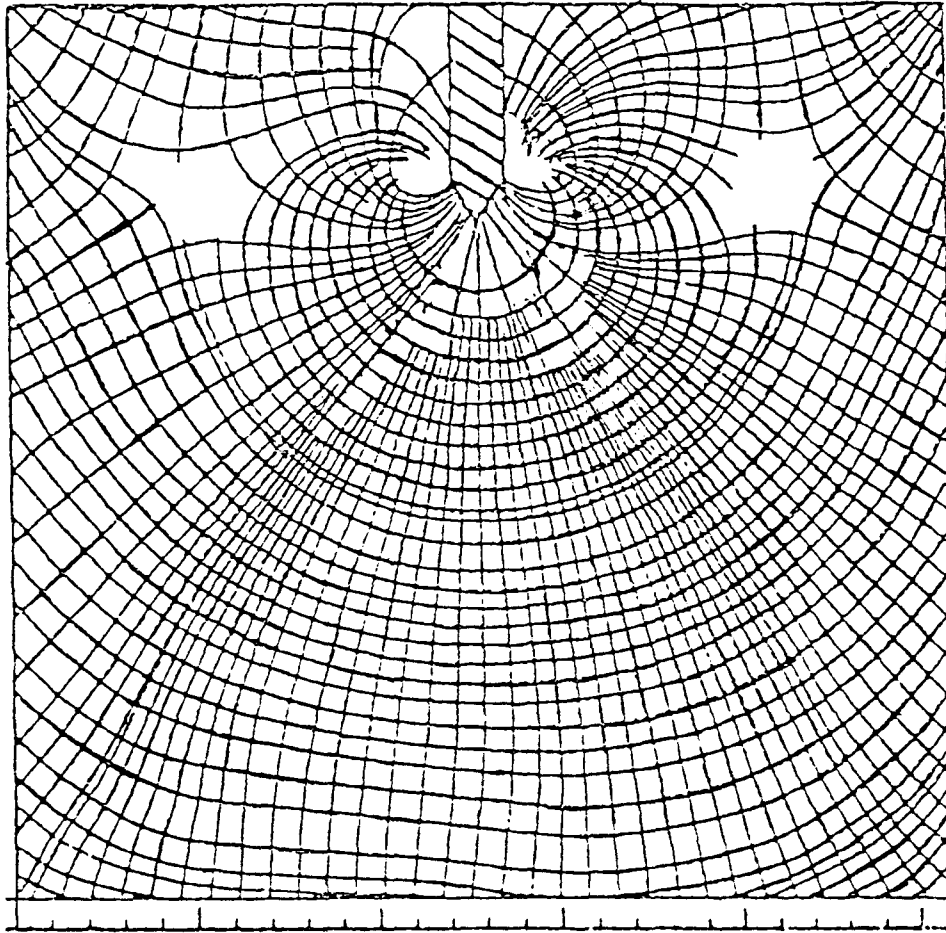


Figure 3. – Computer plot of the principal stress trajectories, based on 182 measuring points. From [1].

principal stress trajectories depends on the stress level induced by the cone and the manner in which the sand surrounding the probe dissipates the stress field (i.e., it is entirely possible for a single stress trajectory beginning at the tip to terminate at the body of the penetrometer as shown on fig. 3).

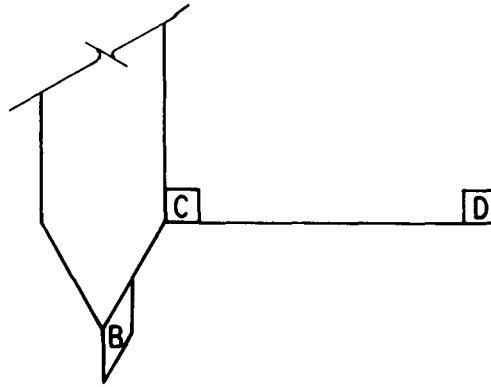
Wroth [65] recognized the effect of the rotation of the principal stress axis on the behavior of soils and suggested using the direct simple shear test instead of the axisymmetrical triaxial compression shear test. He thought it more accurately modeled the stress path to failure for the sand surrounding the cone penetrometer. This recommendation is based on the understanding that the simple shear test causes the stress path for a soil element to rotate from triaxial compression at the beginning of a test to triaxial extension at failure.

The importance of Wroth's recommendation can be illustrated with the aid of figure 5. If soils were to behave according to the Von Mises yield criterion, the shear strength of the soil would be the same in

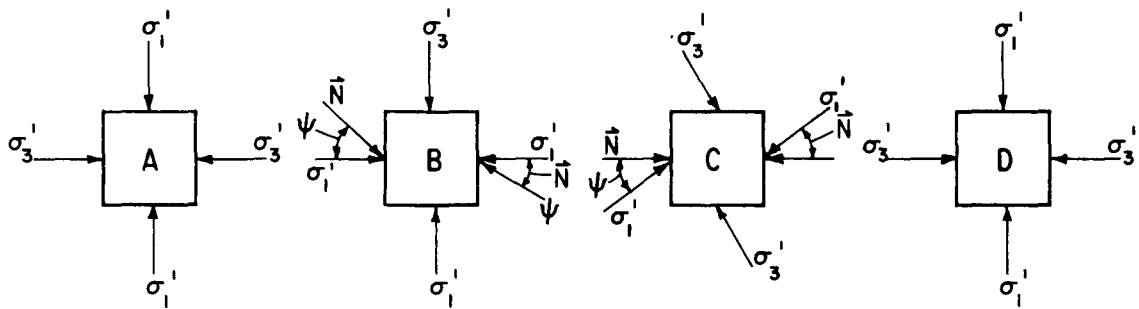
triaxial compression and triaxial extension. However, soils are usually assumed to behave according to the Mohr-Coulomb criteria or more elaborate criteria such as the one devised by Matsuoka [28]. For both of these yield criteria, the shear strength of the sand is less for any stress path to failure than it is for triaxial compression, and the shear strength measured in triaxial extension forms the lower bound. Thus, selection of the shear strength from a test that causes the soil to fail in triaxial extension would be a conservative approach that would more accurately represent the stress path to failure of a soil element near the penetrometer.

### Strain Field Around the Cone Penetrometer

Little has been published about the displacement and strain fields in sands surrounding the cone penetrometer. To develop an understanding of the possible disturbance effects of a penetrometer passing through a sand, a review of some of the work published on strain fields in clays surrounding the penetrometer must be performed. Levadoux and Baligh



(a) Location of soil elements with respect to penetrometer.



(b) Stresses on element A. (c) Stresses on element B. (d) Stresses on element C. (e) Stresses on element D.

Figure 4. – Direction of principal stresses acting on soil elements in contact with and at a distance from a penetrometer.

[24] conducted an extensive study on the displacement and strain fields surrounding cone penetrometers having 18° and 60° apex angles. Figure 6 presents the predicted displacement patterns using cavity expansion theory for five elements of clay located at distances ranging from 1.0 to 5.0 times the cone radius away from the centerline of the cone. It is interesting to note that all particles first move down and then horizontally away from the cone as it approaches. As one would expect, particles nearest the cone move the most. Translating the displacements to shear strain, Levadoux and Baligh developed the set of shear strain contours shown on figure 7.

Levadoux and Baligh were concerned with the penetration of clay, which is assumed to fail in undrained shear. Their analysis closely follows that devised for ideal plastic flow of metals, which are essentially incompressible. For sands, the penetration rate of 2.0 cm/s is considered slow enough to permit drainage within the failure zone of the sand. Drainage of pore water allows the volume to change, and a pattern of volumetric strains similar to that shown on figure 7 could be expected. Furthermore, sand particles are much larger than clay particles. This, in conjunction with the possibility for high dilatancy in sand, would cause the strain contours to expand outward, thereby enlarging the disturbance zone. The exact

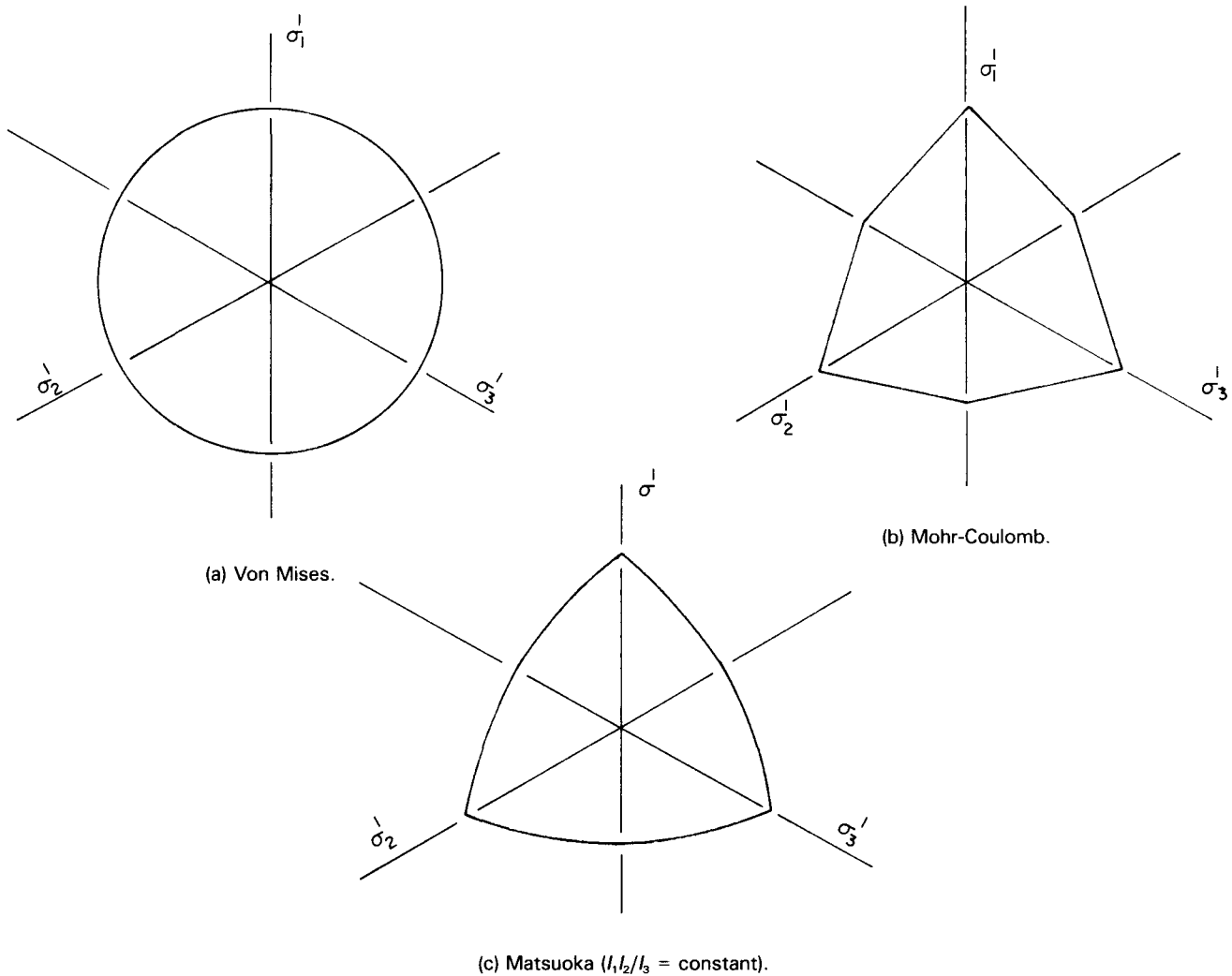


Figure 5. – Yield criteria in unordered principal effective stress space.

extent of the outward expansion would be a function of the size of sand particles, the amount of grain crushing, the initial density, the amount of dilatancy, and the compressibility of the sand.

Assuming that most sands fail at shear strains of less than 5 percent and that beyond failure they may show effects of strain hardening or softening with continued straining makes it difficult to estimate the size and shape of the shear and volumetric strain contours for sands. In essence, one can assume that the cone penetrometer induces large strains in the sand near the penetrometer and that the level of these strains decreases with distance from the penetrometer. Thus, a single measurement of cone tip resistance is a function of the shear strength and compressibility of soil elements encompassing the range from in situ conditions to large volumetric and shear strain conditions. The combination of shear strain, volumetric strain, and the rotation of principal stress axis pro-

duces a complex relationship between the measured cone resistance and the "shear strength" of sands.

#### Effects of Earthquake Loading on a Soil Element

The stress path of a soil element during earthquake loading is complicated. Shear and compressive waves traveling in a three-dimensional medium do not necessarily align themselves with the orientation of static principal stresses. In practice, earthquake loading is usually considered rapid enough for sands to be loaded in an undrained condition by the shear and compressive waves transmitted through the pore water and the soil skeleton. Because the compressive wave speed in the water phase is faster than in the soil skeleton and because shear waves may not be transmitted through the pore water, shear waves are assumed to be the most hazardous for soil stability. This assumption is reflected in current dynamic analysis procedures by the overwhelming degree of attention paid to the shear behavior of sands.

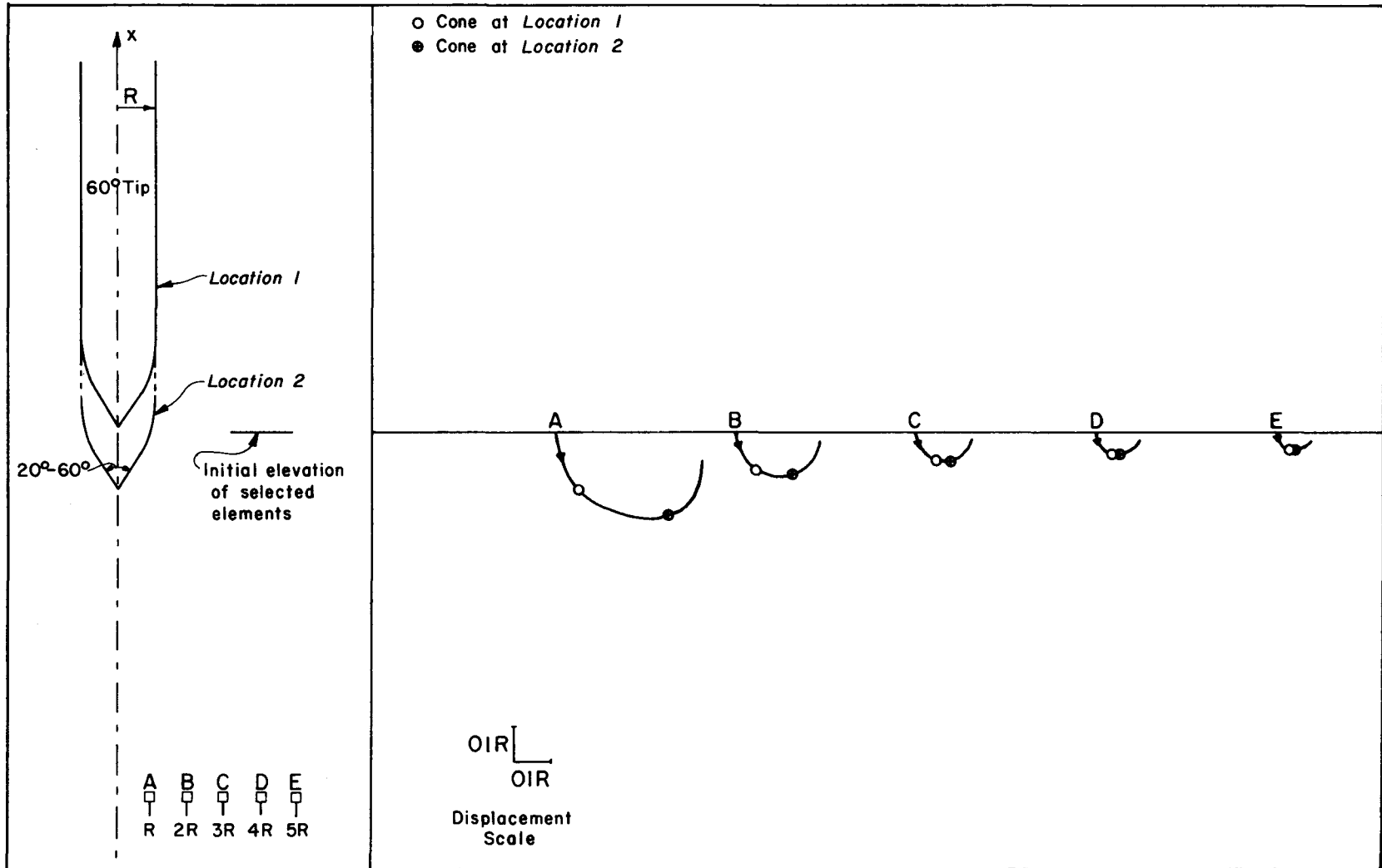


Figure 6. - Soil displacements during penetration of a 60° cone. From [24].

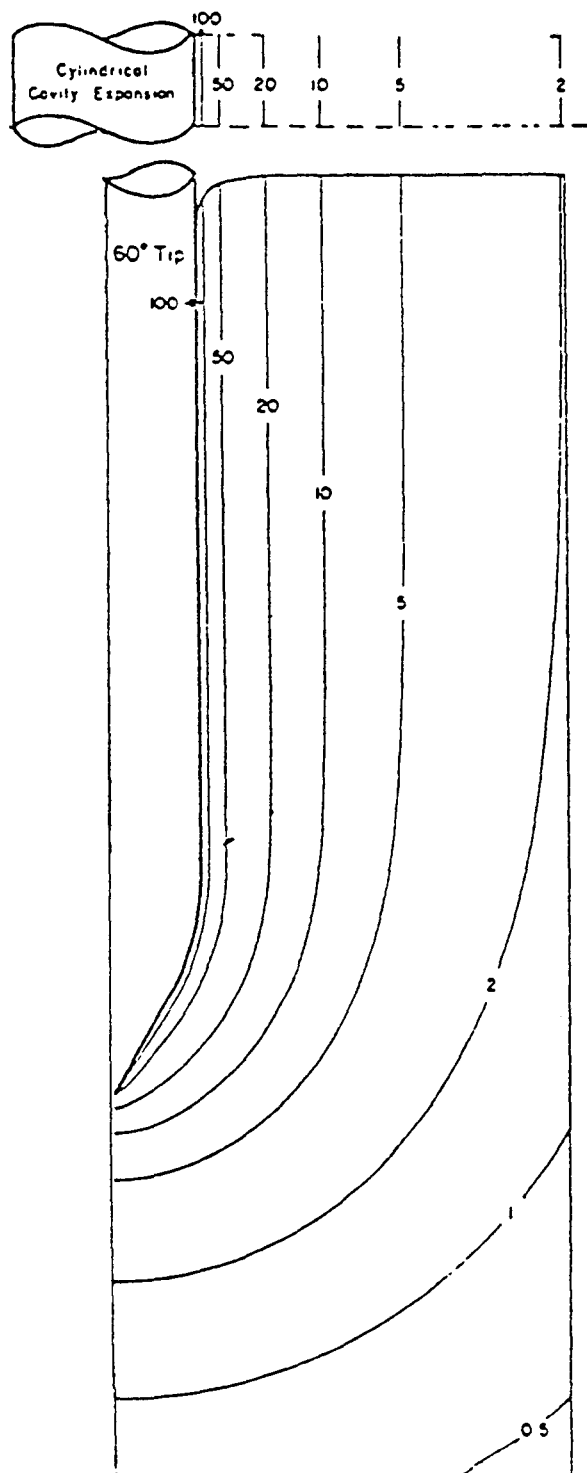


Figure 7. - Contours of maximum shear strain,  $\max. = \frac{1}{2}(\epsilon_1 - \epsilon_3)$ . From [24].

A second assumption limiting the direction of shear wave propagation vertically upward from bedrock is also common practice. This assumption means that the planes of maximum shear stress and principal

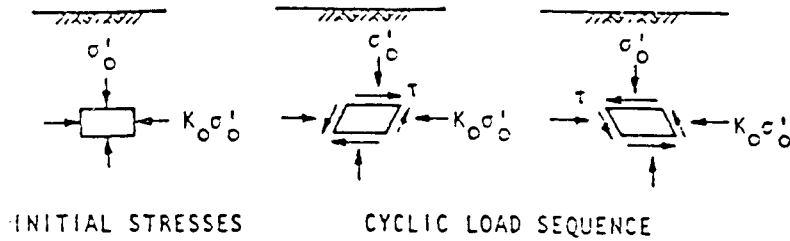
normal stress in a normally consolidated soil layer would rotate as indicated by Seed and Idriss [51] on figure 8.

The undrained loading condition combined with a high-frequency earthquake motion will result in a volumetric strain increment of zero during one or more cycles of loading. However, dissipation of excess pore-water pressures developed by plastic shear strains during sustained static or several cycles of earthquake loading will cause time-delayed volumetric strain.

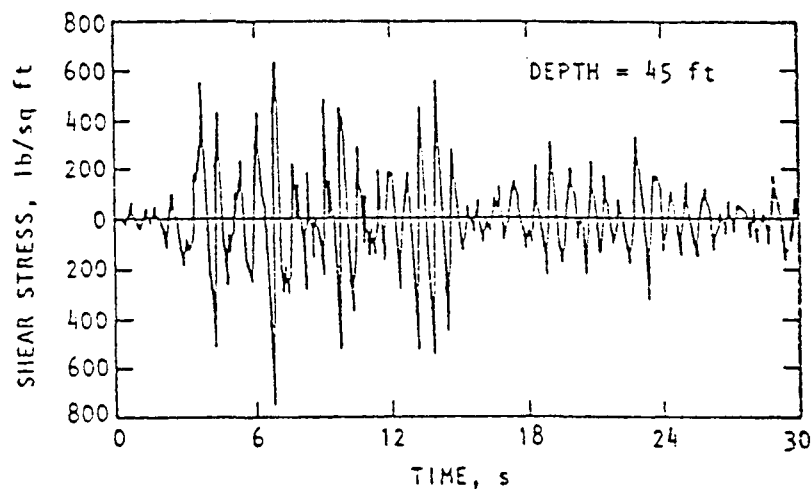
To understand how shear strains can cause excess pore pressures to develop, it may be useful to review the results of cyclic torsional shear tests as performed by Nagase [31] (fig. 9). Initially, the soil is in an isotropic stress state and in equilibrium. As the shear stress is increased, the soil particles gradually unlock, translate, and rotate relative to one another, and the soil mass develops plastic shear strains. Upon reduction of the shear stress a certain amount of nonrecoverable shear strain and excess pore pressure will have developed due to the disruption of the soil structure. Repeated rapid application of the shear stress causes additional disruption to the soil structure, and additional excess pore pressure develops. Because the cyclic loads are of constant magnitude in this example (fig. 9), the amount of disruption caused by each additional cycle becomes progressively less until individual soil particles must bypass one another to cause further deformation in the soil. At this point, Tatsuoka and Ishihara [56] stated that a "phase transformation" occurs as the soil dilates positively and temporarily reduces the excess pore pressure previously developed.

The effects of increasing and decreasing the excess pore-water pressure in a sand are to decrease and increase the effective stress levels, respectively. It is conceivable then that at the phase transformation plane, the disrupted sand structure, if not permitted to drain, must dilate to adjust to the imposed stress level. It is also interesting that at each crossing of the isotropic compression line (even after the onset of positive dilation), a small amount of additional excess pore pressure has accumulated. This accumulation continues until either the soil structure is completely disrupted and a pore-pressure ratio ( $u/\sigma'_{o}$ ) of 100 percent is reached or, for the case of a dense sand under application of moderate cyclic shear stress levels, the stress level can cause no further disruption to the soil structure.

If the pore pressure developed during cyclic loading is allowed to drain under an effective stress state that is less than those represented by the phase transformation plane, the sand will consolidate (negative dilation occurs) and a positive volumetric strain



(a) Idealized field loading conditions.



(b) Shear stress variation determined by response analysis.

Figure 8. - Cyclic shear stresses on a soil element during ground shaking. From [51]. (1 lb/ft<sup>2</sup> = 0.047880 kPa; 1 ft = 0.3048 m).

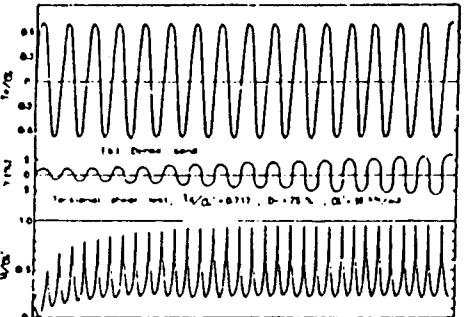
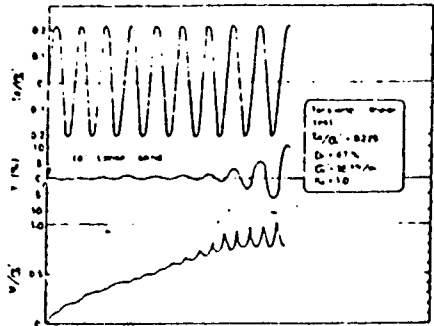
will result. If, on the other hand, a substantial static shear stress level is maintained during drainage (effective stress state greater than the phase transformation plane), the soil may dilate and a negative volumetric strain may occur.

Although the test data used for this example were interpreted to represent the behavior of a soil element during earthquake loading, there are many problems associated with dynamic testing of sands. First, to cyclically load a sand uniformly, the rate of application must be rapid enough to preclude redistribution of void ratio within the specimen. Second, such rapid loading conditions usually lead to problems in interpreting the effects of end plate momentum and membrane penetration and to other test procedural problems. Finally, the stress paths followed during laboratory testing may not resemble those of a soil element in the field, and geotechnical engineers have yet to resolve the significance of this aspect.

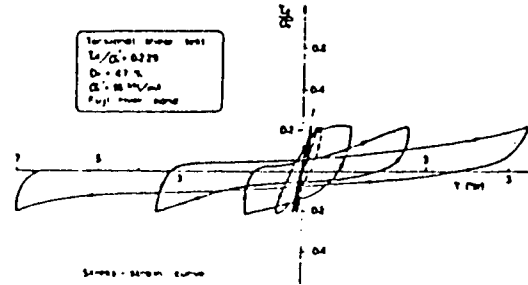
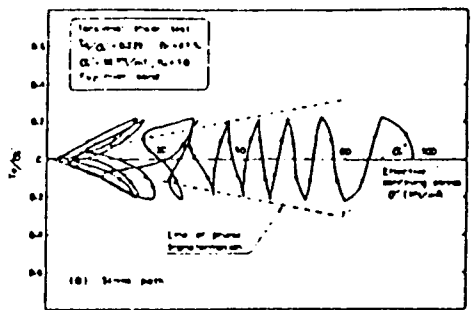
### Steady-State Soil Models for Development of a Relationship Between CPT and Earthquake Loading

A theoretical model for evaluating the earthquake response of sands has been proposed by Castro [11], Casagrande [10], Castro and Poulos [13], and Poulos [35]. This model is based on a concept of residual shear strength of a soil during steady-state deformation at a critical volume.

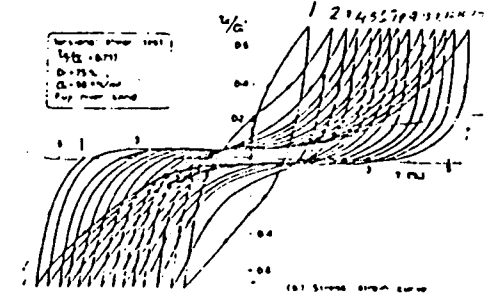
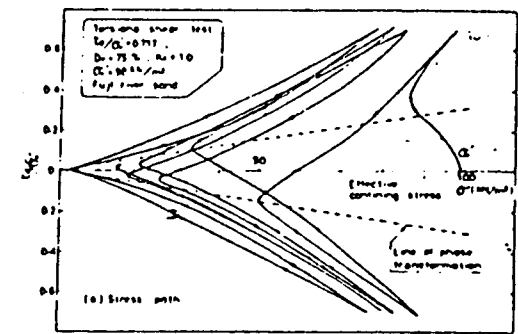
This method, known as the steady-state concept, proposes a beginning for understanding and analyzing soil behavior at large shear strains. As discussed in the subsection entitled "Strain Field Around the Cone Penetrometer," the cone penetrometer causes large shear strains near the probe. Earthquakes of magnitudes greater than 6 on the Richter scale may cause a collapse of loose sand and large shear strains in a soil mass. However, the loading of sand during an earthquake occurs essentially in an undrained



(a) Records of cyclic torsional shear tests.



(b) Stress path and stress-strain curve for loose sand obtained from the cyclic torsion shear test.



(c) Stress path and stress-strain curve for dense sand obtained from the cyclic torsional shear test.

Figure 9. – Cyclic torsional shear tests on Fuji River sand. From [31].

(constant volume) mode, whereas the cone penetrometer loading in sands occurs in a drained mode. To conceptually relate the two loading paths, a large strain soil model is required.

The steady-state concept is illustrated on figure 10, which consists of two graphs that should be considered simultaneously. The first graph shows the steady-state (i.e., residual) shear strength of a sand as a function of the void ratio. The second graph depicts the steady-state line in a plot of the void ratio versus the log of the effective minor principal stress. When considered together, these two graphs define a residual shear strength value of a sand in a three-dimensional shear stress versus log effective minor principal stress versus void ratio space. What is missing in this conceptual model is the stress-strain relationship required to cause a soil to reach the steady-state shear strength from an initial stress state. This missing information is usually deduced from the deviator stress-axial strain curves of axisymmetric triaxial shear tests performed on sands under undrained loading conditions.

In an attempt to form a more complete large-strain soil model and to link peak shear strength with steady-state strength, Robertson [39] proposed the idealized soil model shown on figure 11. The model consists of an elastic-compressive zone, a plastic-compressive zone, and a plastic-dilative zone. The behavioral zones are contained within a strength envelope of possible soil states in the three-dimensional shear stress-mean normal effective stress-void ratio space. Soils subjected to changes in effective stress states contained within the elastic-compressive zone develop fully recoverable elastic shear and volumetric strains; thus, no significant disruptions to the soil structure or lasting excess pore pressures are developed. Soils subjected to effective stress states contained within the plastic-compressive zone will attempt to decrease in void ratio and develop plastic shear and volumetric strains or, during conditions of undrained loading, develop plastic shear strains and positive excess pore pressures. Soils subjected to effective stress states, which enter into the plastic-dilative zone, will attempt to increase in void ratio and develop plastic shear and volumetric strains or, for conditions of undrained loading, develop plastic shear strains and negative excess pore pressures.

The boundary between the elastic-compressive and plastic compressive zones is formed by the mineral-to-mineral friction angle,  $\Phi\mu$ . This angle has been shown by Rowe [44] and others to be constant for a given mineral type and is represented in the idealized soil model by a plane of constant slope. Robertson named this plane the FD (flow deformation) plane. The boundary between the plastic-compressive and plastic-dilative zones is formed by the PT

(phase transformation) plane identified by Tatsuoka and Ishihara [56]. Robertson concluded that the PT plane was not a constant angle plane as indicated by Tatsuoka and Ishihara and that it would intercept the FD plane before reaching the void ratio axis. The intersection of the PT and FD planes would form a line that would represent the steady-state shear strength of a soil. The "peak" shear strength of a soil would be represented by the intersection of a "Roscoe" surface and the strength envelope.

Although the idealized soil model is still incomplete (strains are not quantified) and has not been acknowledged by the authors of the steady-state model, it is easy to visualize and effectively relates the initial stress-void ratio state of a soil to its steady-state shear strength.

Common practice for determining the steady-state shear strength of a sand is to obtain high quality "undisturbed" samples of sands and test them in an axisymmetrical triaxial shear apparatus under undrained conditions. Before and after sampling, transporting, and handling of the samples, careful measurements are taken to back-calculate the in situ void ratio from the void ratio of the specimens determined in the triaxial apparatus. The specimens are then consolidated to the calculated in situ or proposed future effective stress level and subsequently sheared monotonically to approximately 30 percent axial strain.

If the specimens in the triaxial apparatus are dilative (develop negative excess pore pressures at failure) and the analyses of the in situ void ratio determine that the soil will be dilative in the field, then the assumption is made that a locally undrained flow failure cannot occur. If the in situ stress path is determined to be contractive and the static shear stress is greater than the steady-state shear strength of the soil, then a flow failure may occur. Within the context of the idealized soil model for any given void ratio, soils that plot in zone A of figure 12 are dilative and not susceptible to flow failures. Soil elements that are loaded in zone B are contractive and may develop positive excess pore pressures during dynamic loading, but they are not susceptible to flow failure. Only the elements in zone C are both contractive and susceptible to flow failure.

### **Evaluation of the Steady-State Shear Strength Concept**

A set of soil data for the axisymmetrical triaxial shear tests for a hypothetical sand is shown on figure 13. The stress paths shown represent five of the most commonly observed during undrained loading of silts and sands. They are typical of stress paths in an undrained triaxial shear test carried out to 30 percent axial strain.

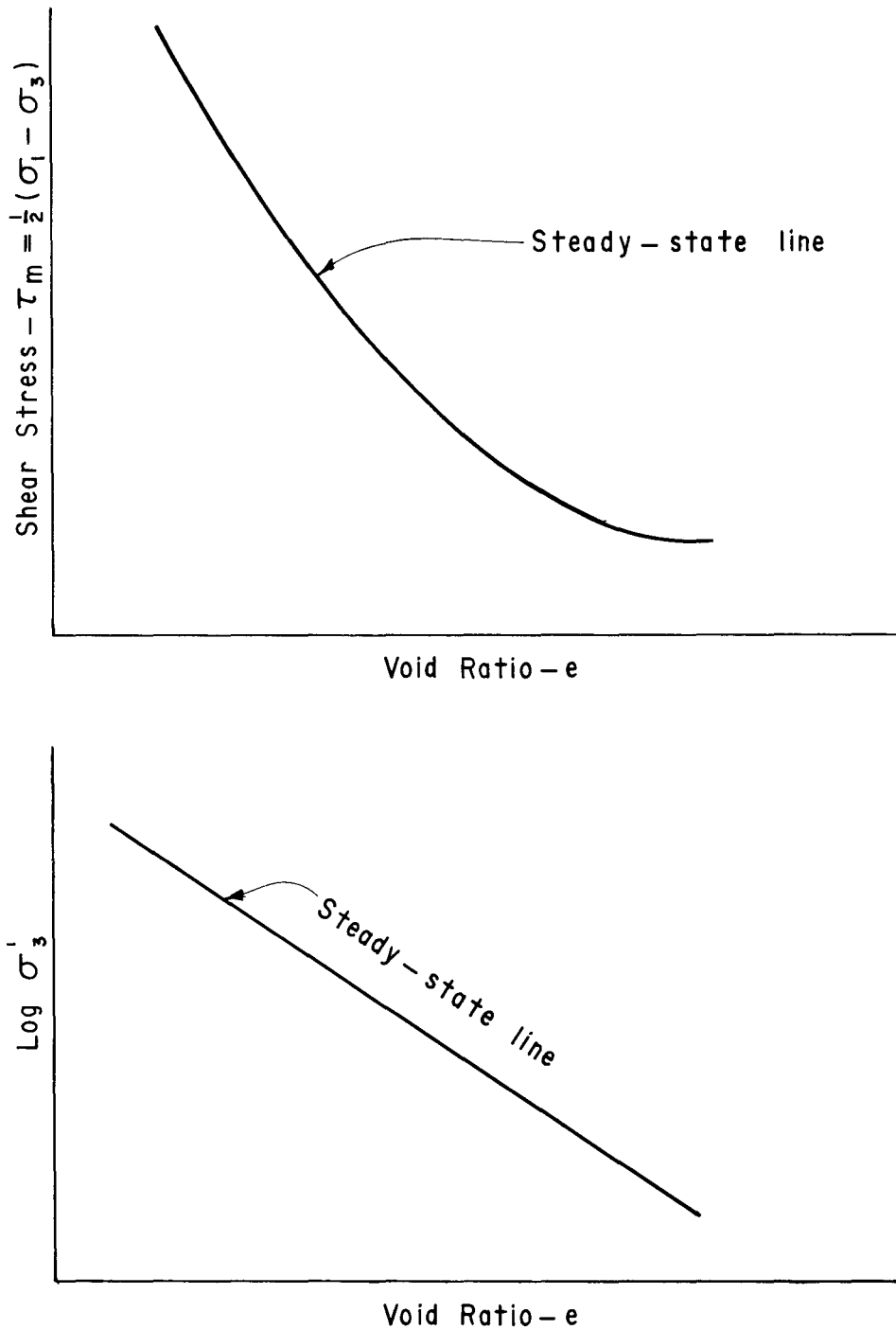


Figure 10. - Steady-state soil model.

Figure 13 shows that the stress paths for this hypothetical soil indicate a distinct pattern for each of the five placement void ratios when the soil is isotropically consolidated to the same mean normal stress. Path 1, which is at the highest void ratio, begins to generate positive pore pressures (fig. 13(c)) at the slightest increment of shear stress and continues to generate additional positive pore pressures

throughout the test. On the stress space plot, path 1 moves immediately through lower levels of mean normal stress with increases in the shear stress until a peak shear stress is reached. From the peak shear stress, path 1 will either begin to drop in both shear stress and mean normal stress until the test is terminated, or, as shown, path 1 will reach a peak shear stress and remain there to the end of the test.

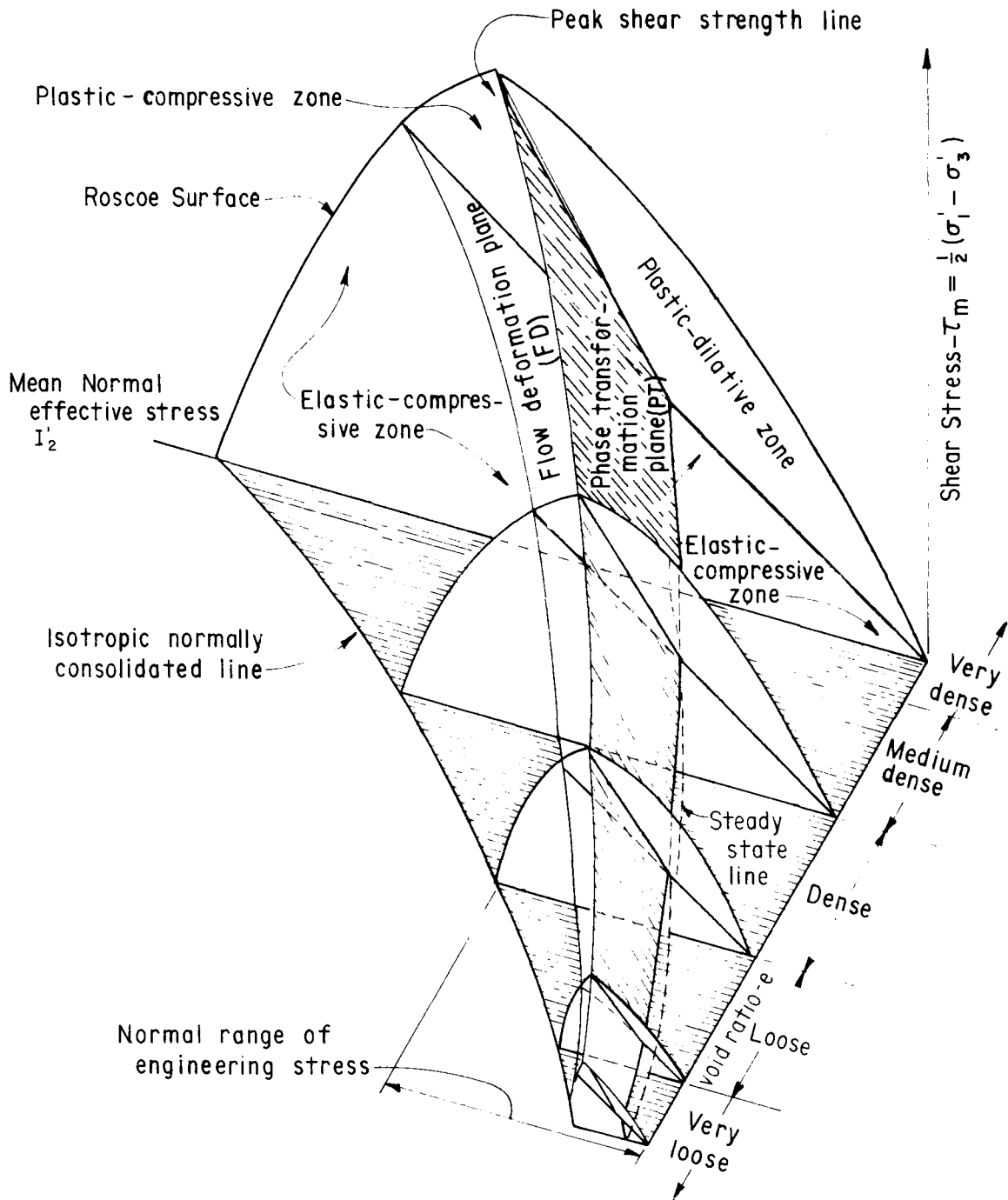


Figure 11. – Idealized soil model proposed by Robertson [39].

Stress path 2 follows the identical pattern as stress path 1 except for a slightly more vertical intercept with the mean normal stress axis. On the shear stress-axial strain plot (fig. 13(b)), path 1 may begin to drop towards the end of the test but will never level off at a constant value as does path 2. In the excess pore pressure-axial strain plot (fig. 13(c)), path 2 develops a certain level of excess pore pres-

sure and ceases to generate additional positive excess pore pressures.

Stress path 3 (fig. 13(a)) rises almost vertically from the mean normal stress axis to a point of maximum stress ratio ( $\tau/l'_1$ ), then the path bends to the right and increases in shear stress with increases in the mean normal stress. Finally, stress path 3 reaches a

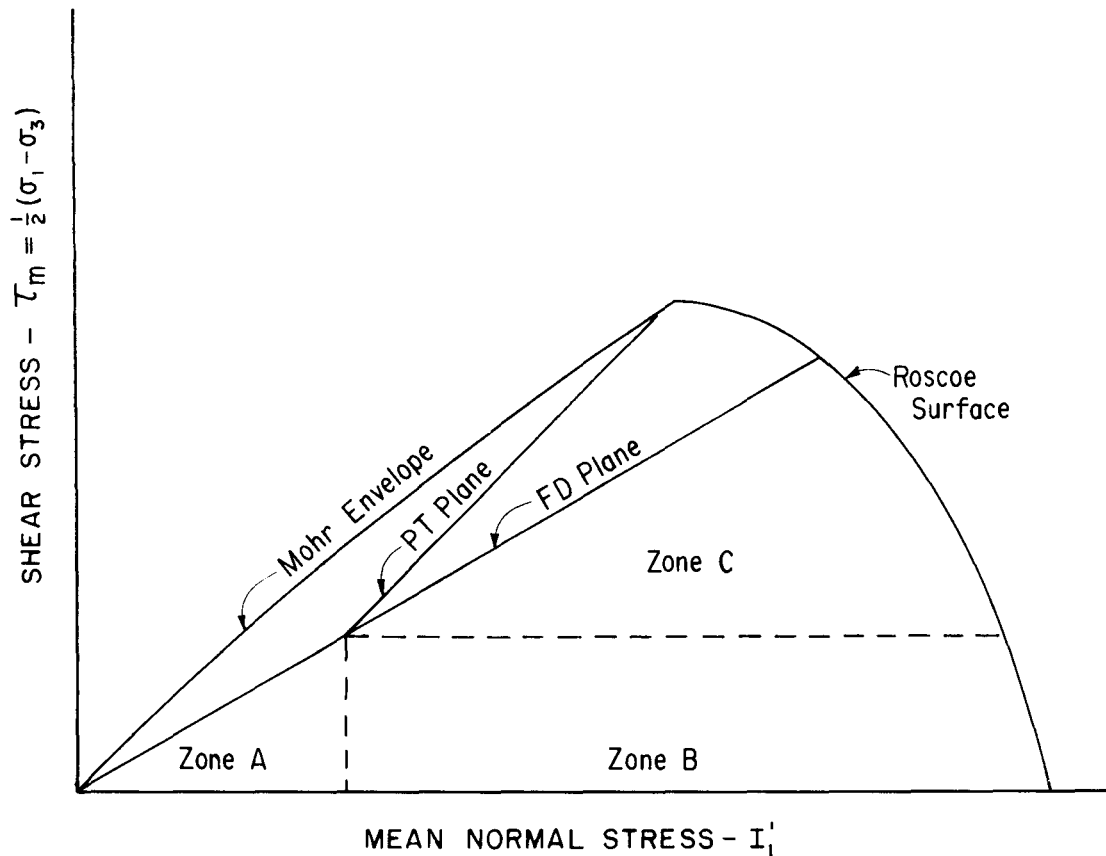


Figure 12. – Constant volume plane of idealized soil model showing zones of stable soil behavior (zones A and B) and metastable behavior (zone C).

maximum shear stress and begins to bend back to the left and drop under its previous path. On the shear stress-axial strain and the excess pore pressure-axial strain plots, paths 2 and 3 follow almost identical trends, the only differences are the magnitudes of shear stress and excess pore pressure developed.

Stress path 4 has a less vertical rise from the mean normal stress axis than does path 3, and shortly before reaching the maximum stress ratio, stress path 4 has a slight hump. This slight hump, which may result in the first maximum stress ratio ( $\tau_m/I_1'$ ), is sometimes referred by that name. Path 4 finally reaches a value of maximum stress ratio and, like path 3, bends to the right. However, unlike path 3, path 4 does not make a final bend back to the left. In the shear stress-axial strain plot, path 4 is similar to path 3; however, instead of dropping off to a lower level of shear stress after reaching a peak, path 4 begins to climb again to higher values of shear stress. On the excess pore pressure-axial strain plot, path 4 actually tends toward dilation before reaching the axial strain of the first maximum stress ratio, and it continues to develop additional negative excess pore pressure through the remainder of the test.

Stress path 5 is identical to stress path 4 except that the hump at first maximum stress ratio is missing. On the shear stress-axial strain plot, path 5 has no tendency to reach a maximum value and drop off, but continues to rise throughout the test. And on the excess pore pressure-axial strain plot, path 5 has only a minor compressive tendency at the beginning of the test before turning dilative. In some tests, paths similar to path 5 have achieved maximum values of shear stress and negative excess pore pressure and have leveled off on all three plots.

Extrapolating the five stress paths shown on figure 13 into a constant void ratio plane that is part of the idealized soil model yields the strength envelope shown on figure 14. The first maximum stress ratio of stress path 4 occurs as the stress path passes through the plastic-compressive zone between the FD and PT planes. The PT plane forms the focal line for all stress paths, and the steady-state shear strength at the intersection of the PT and FD planes becomes the ultimate ending point of all stress paths.

The stress paths shown on figures 13 and 14 were scaled to illustrate the idealized soil model proposed

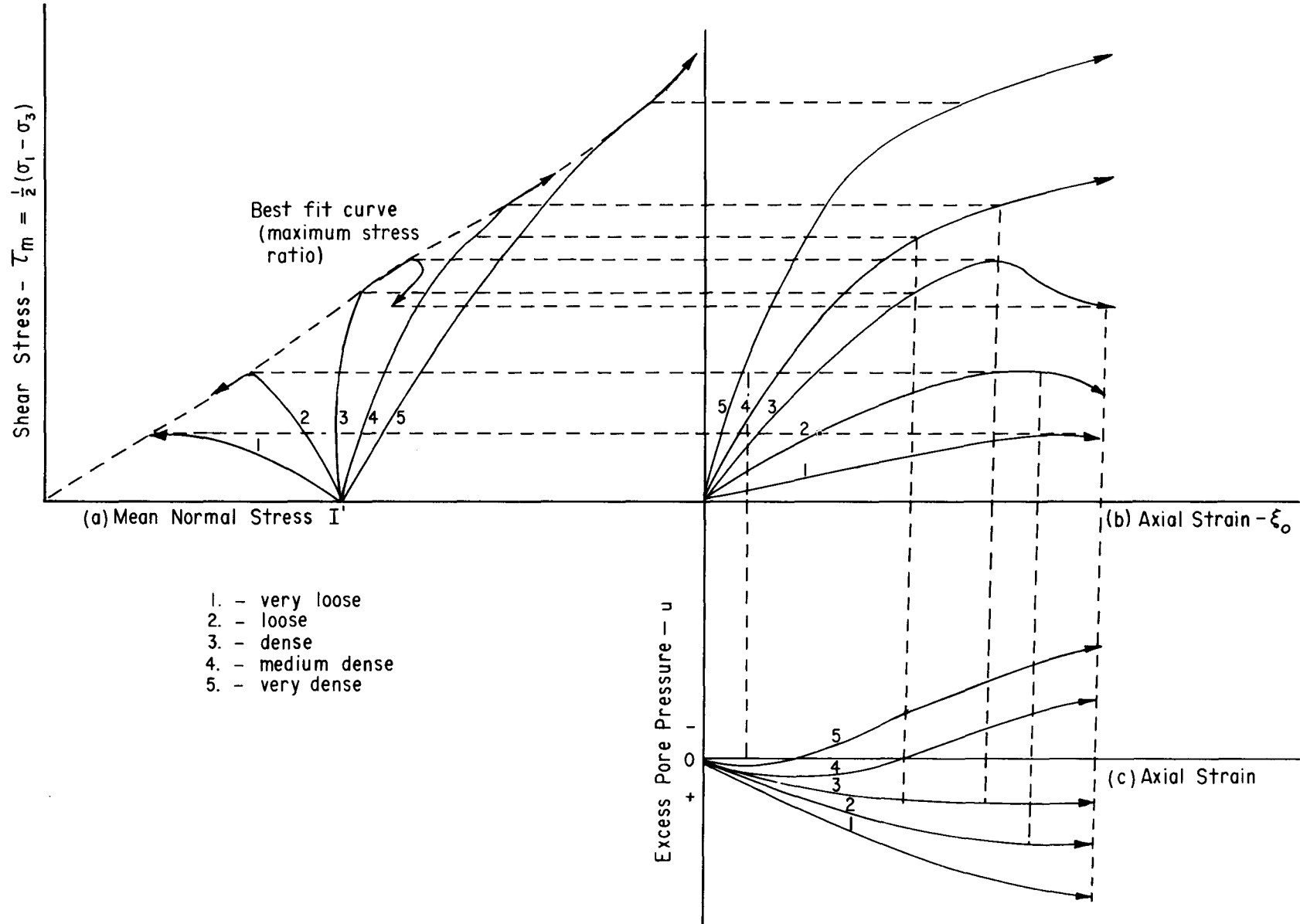


Figure 13. - Typical data from monotonically loaded undrained axisymmetrical triaxial shear tests on sands.

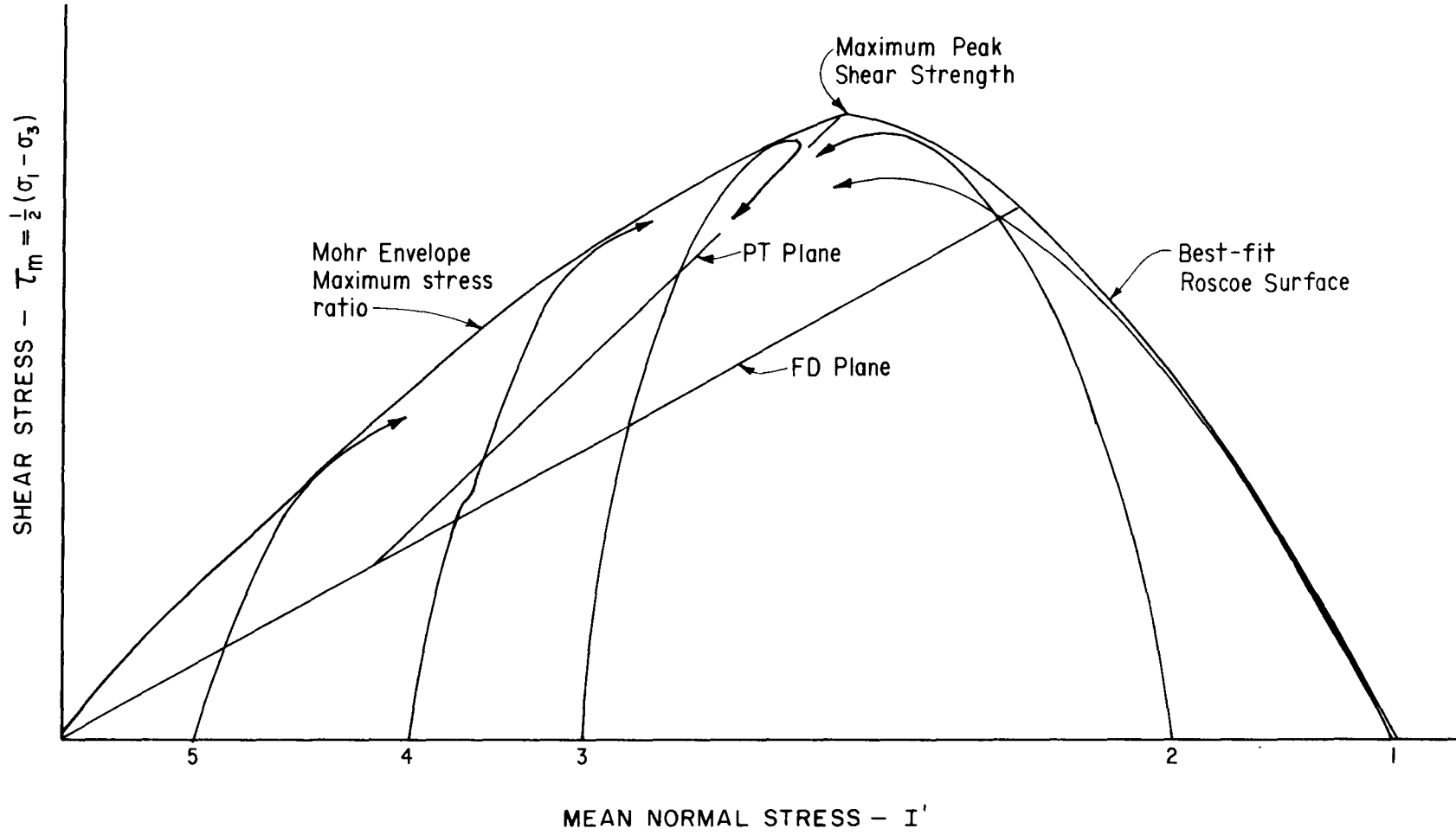


Figure 14. - Extrapolation of undrained shear stress paths into constant volume plane of idealized soil model.

by Robertson. However, one should not forget that the general shape of the stress paths was taken from data collected during axisymmetric undrained triaxial compression shear tests performed on real soils. Note that the soil specimens were loaded with normal stresses and failed in shear, and that reviewing actual data without considering the failure mechanisms of the soil specimens can lead to premature judgments about the shear behavior of soils.

Heavily overconsolidated soils as represented by stress paths 3, 4, and 5 usually fail along a narrow shear band, as shown on figure 15(a). Shear and possible volumetric strains are concentrated along this band in the latter (high strain) stages of the test. The concentrated shear band (zone A) could actually be increasing in void ratio at a rate necessary to allow failure. To maintain an overall net volume change equal to zero, the ends of the specimen (zone B) would have to compress. In other words, the specimen boundaries remain undrained; but the actual failure zone occurs in a drained state. Void ratio calculations for an undrained shear test are made from the boundary measurements, and an average void ratio is assumed to apply uniformly throughout the specimen. This calculated void ratio may greatly underestimate the actual void ratio within the shear band.

An unknown void ratio can account for part of the deviation of stress paths 3, 4, and 5 from the failure envelope. Additional deviation such as the final bend of stress path 3 (fig. 14) as it follows the PT plane may be explained by errors in the calculation of the cross-sectional area in the axial direction. The usual method for computing the cross-sectional area in an undrained triaxial shear test is to divide the volume of the specimen by its length at the stage of the test when a measurement is made. For the banded failure mechanism at high strains (as shown on fig. 15(c)), the axial projection of the cross-sectional area decreases as the test progresses; yet, the computations would indicate that the area increases. The miscalculation of cross-sectional area would cause the calculated axial stress ( $\sigma'_a$ ) to be far less than the actual axial stress within the failure zone. The combination of unknown void ratio and cross-sectional area miscalculations have long been realized as problems with axisymmetric triaxial tests on overconsolidated soils at high strains. As a result, they are not generally recommended for use in defining the steady-state line during a steady-state investigation.

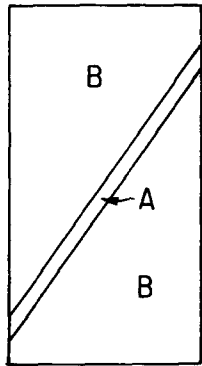
Lightly overconsolidated and normally consolidated soils as represented by stress paths 1 and 2 (figs. 13 and 14) tend to develop the bulging failures shown on figure 16. The reason for this type of failure is that the soil skeleton tends to collapse rather than shear and dilate. In the early stages of the test, the

collapse is fairly uniform throughout the specimen, as shown on figure 16(b). However, later in the test, the bulge is much larger in the middle of the sample than on either end (fig. 16(c)). This concentration of the bulge is generally attributed to end-plate friction between the loading platens and the soil specimen. The result in these tests is that using the average cross-sectional area, as opposed to the actual cross-sectional area, causes the stress calculation to be overestimated for the central portion of the failure zone toward the end of the test. Again, homogeneity of void ratio is assumed throughout the specimen even though there is little proof such a condition actually exists. It is feasible that stress concentrations at both ends of the specimen will cause the soil to compress at the ends forcing water into the center of the specimen. This would make the center of the specimen increase in void ratio.

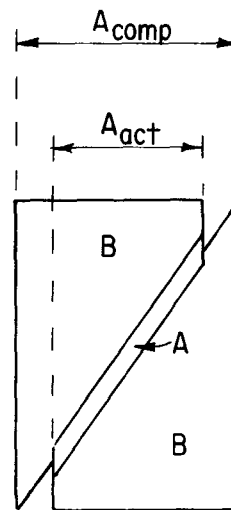
The result of the error in calculations and lack of understanding of the large-strain behavior of sands during the axisymmetric triaxial shear test is that calculations based on boundary measurements at large strains (i.e., 30 percent axial strain) are unreliable. The PT and FD planes might well exist for small strains, but the intersection might just as likely be located along the void ratio axis, as shown on figure 17. The uncertainty of calculations for large strain behavior of the actual failure surfaces allows one to speculate that the actual sand behavior may be explained by a CS (critical state) model, as shown on figure 18. For this model, the steady-state shear strength of a soil, as determined by axisymmetrical triaxial shear testing, would be a poor estimate of the critical state shear strength at an unknown void ratio projected into the calculated average void ratio plane for the specimen.

In the discussion of soil models thus far, little has been mentioned of flow rules or direction of strain increment vectors. The most common assumptions with critical state models are the application of (1) an associated flow rule (the plastic potentials and yield curves coincide), and (2) the normality condition (strain increment vector is orthogonal to the plastic potential). These assumptions imply that the critical state shear strength for any void ratio is also the peak shear strength for that void ratio. The first two (explicit) assumptions are generally made for convenience and have generally proved valid or conservative for clays (see [3]).

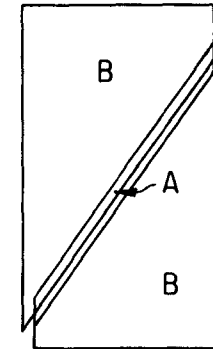
Tatsuoka [55] has shown that either the normality rule or the associated flow rule may not be a valid assumption for the description of sand behavior. Maintaining the assumption of the normality condition and using a nonassociated flow rule allows for the construction of a critical state soil model, as shown on figure 19. For this critical state model, the



(a) Failure zone A begins to develop at low strains.

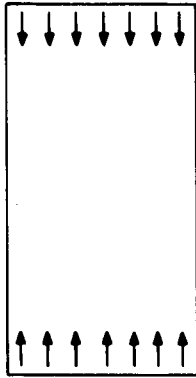


(c) At large strains, wedge failure affects stress calculations.

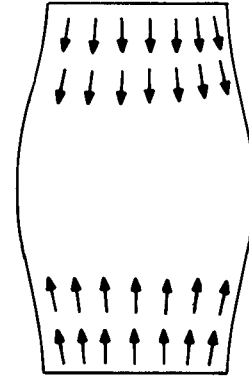


(b) At moderate strains, failure zone A dilates and wedge failure is pronounced.

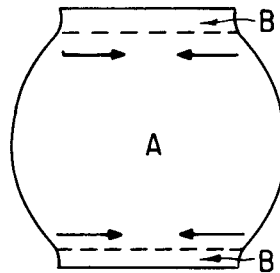
Figure 15. – Development of failure plane in highly overconsolidated sands during axisymmetrical triaxial shear test.



(a) At low strains, stress and strain are uniform.



(b) At moderate strains, center begins to bulge. Stress concentrations develop near specimen ends.



(c) At high strains, stress concentrations in ends of specimen are more pronounced.

Figure 16. – Development of bulging failure in loose sand during axisymmetrical triaxial shear test.

critical state shear strength at any void ratio is less than the peak shear strength. The significance of this model is that undrained triaxial shear path 2 (fig. 13) can be explained without reference to any effects of redistribution of void ratio within the test specimen.

#### Status and Use of Large-Strain Behavior Models

The amount of literature on soil models is constantly increasing. Models such as the Prevost model [19], the snail track model [48], and the Poorooshasb model [33 and 34] continue to be advanced. However, as was demonstrated in the examination of the steady-state, critical state, and idealized soil models, the problem with soil models in general remains the interpretation of tests used to determine the soil properties.

The previous discussion on soil modeling and axisymmetrical triaxial shear testing was performed to indicate the complexities involved with attempting to develop a soil model to relate small-strain behavior of sands to their large-strain and remolded behaviors. Each of the soil models chosen for discussion was selected as much for ease in graphical representation as for technical accuracy and completeness in de-

scribing sand behavior. For this reason, it should be expected that each soil model contains a piece of the picture of sand behavior, but that none of the models provides a complete, definitive explanation of sand behavior or of the relationship between the sands behavior during the drained CPT loading and that during undrained earthquake loading.

To illustrate the need for such a model, consider an isotropically consolidated critical state model with associated flow rule and normality condition, as shown on figure 17. Ignoring the effects of stress direction rotation, the stress path of an "isotropically consolidated" sand element during earthquake loading could be traced (fig. 20(a)). The stress path of this same sand element during the CPT could also be traced (figs. 20(b) and (c)). Relationships between the constant-volume cyclic loading stress path induced by the earthquake and the changing-volume monotonic loading stress path of the CPT could be drawn through the functions that describe the various components of the soil model. In this manner, the CPT stress path could be theoretically linked to the earthquake loading stress path and the liquefaction susceptibility of a sand element.

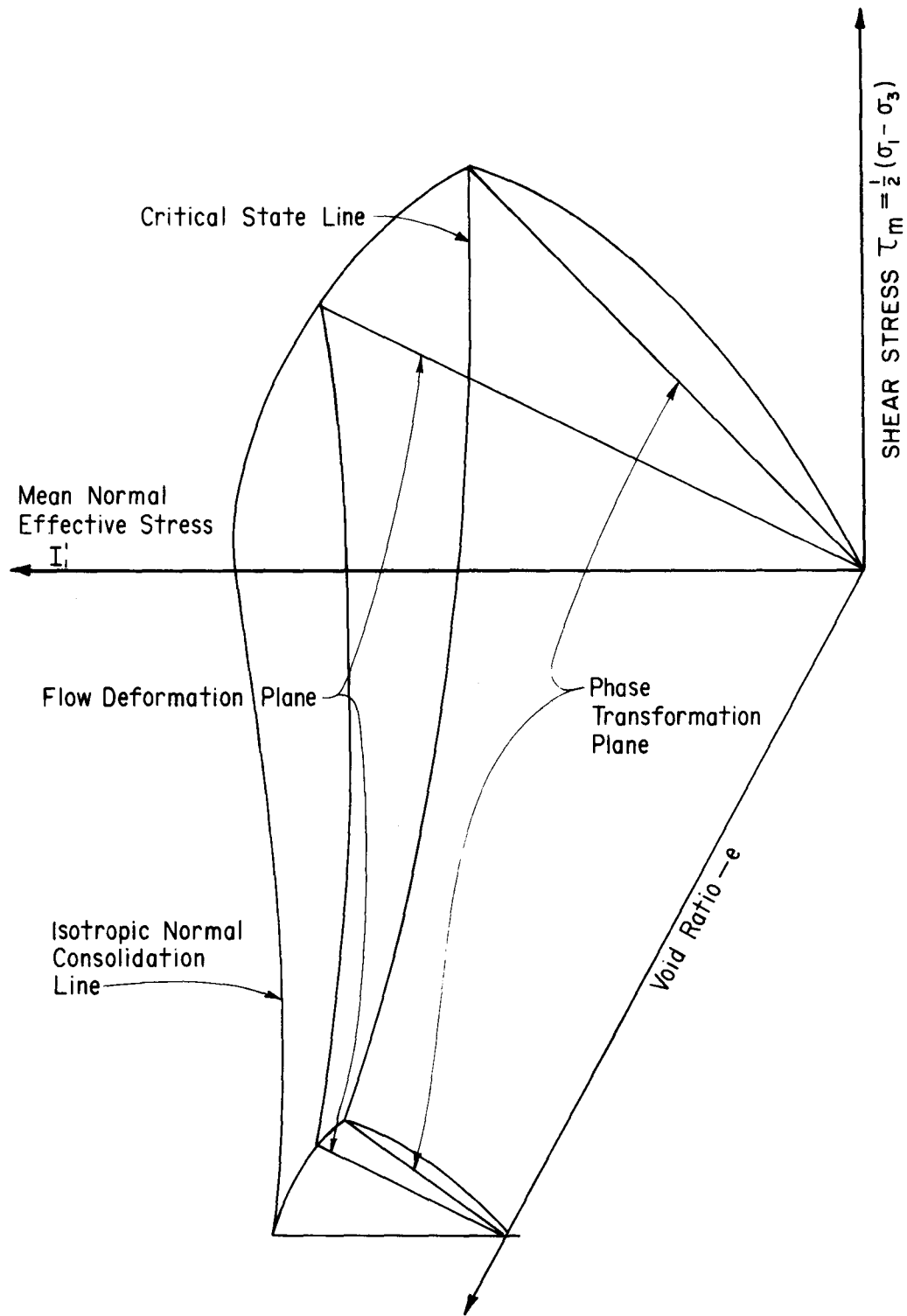


Figure 17. – Critical state soil model for sands.

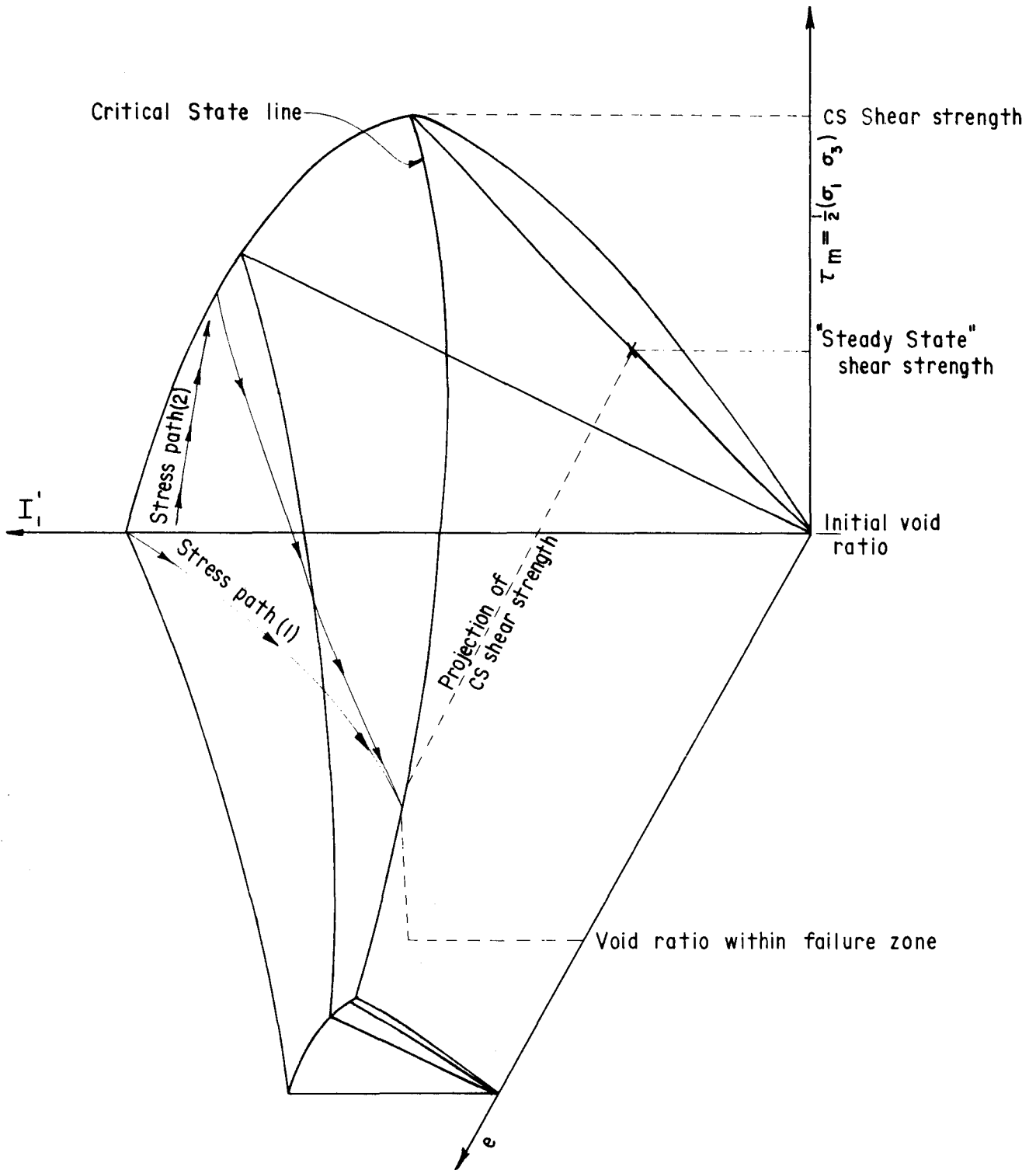


Figure 18. – Possible critical state model showing projection of CS shear strength from failure void ratio into initial constant volume plane.

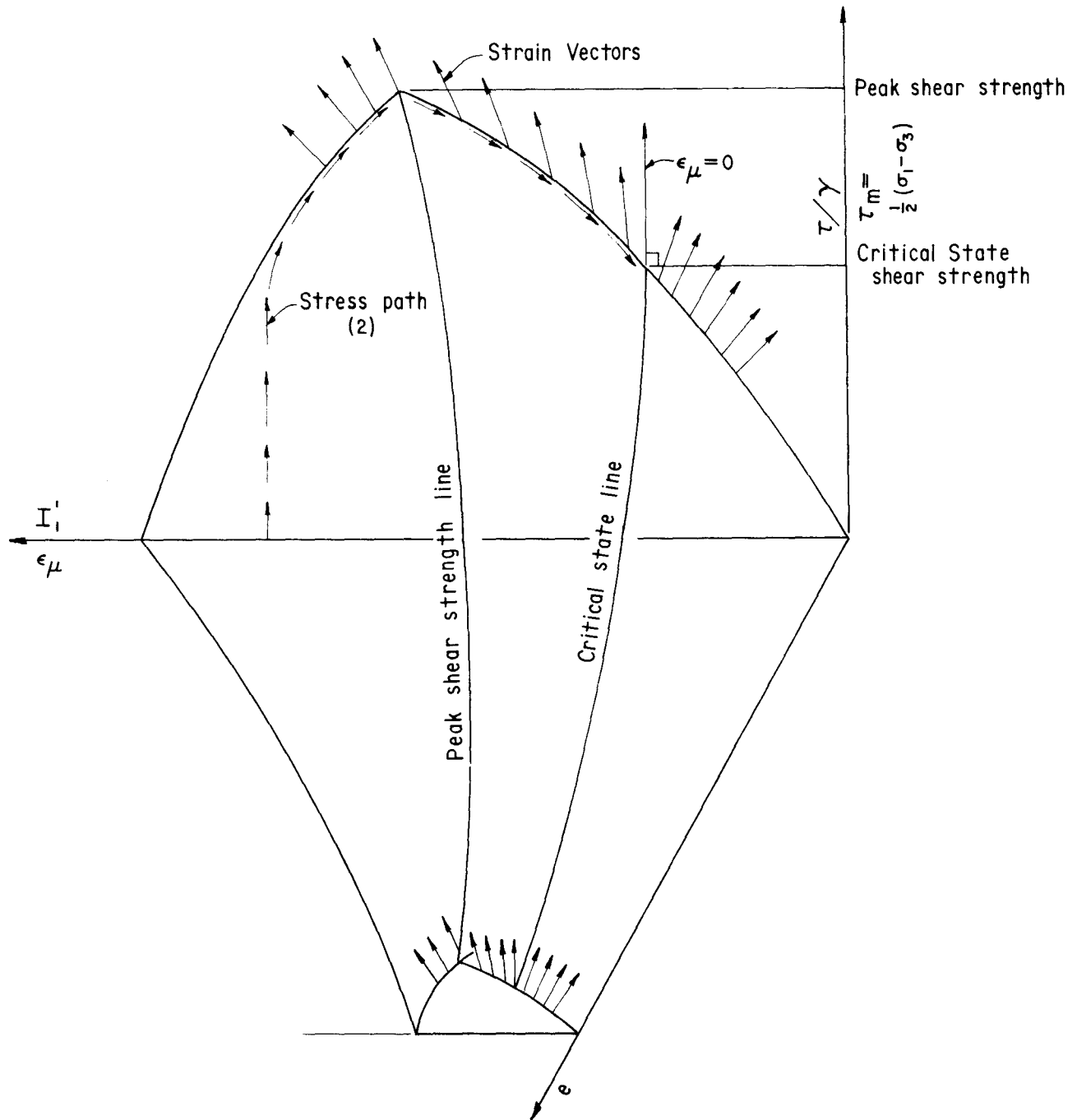
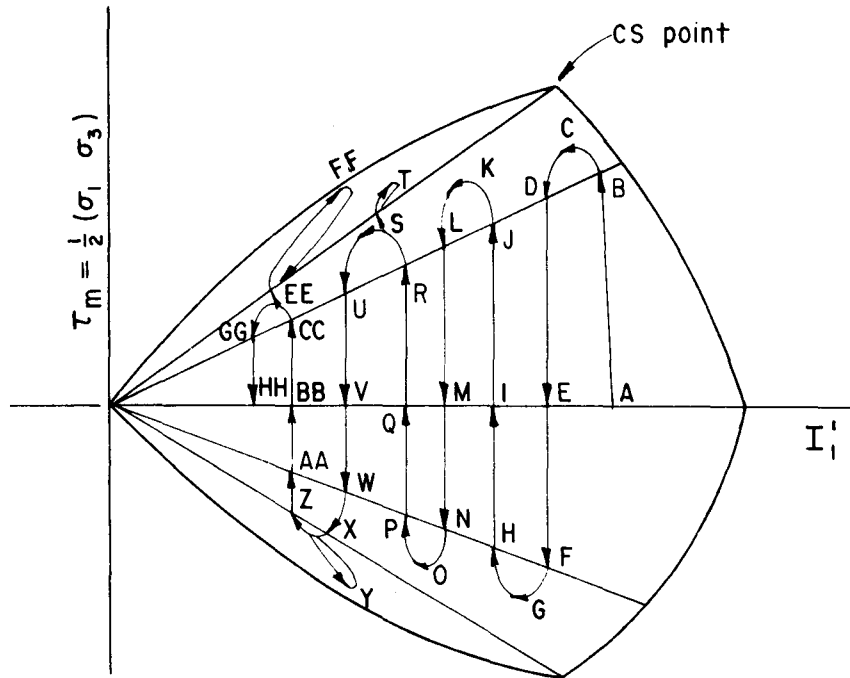


Figure 19. – Critical state model for sands (nonassociated flow rule).

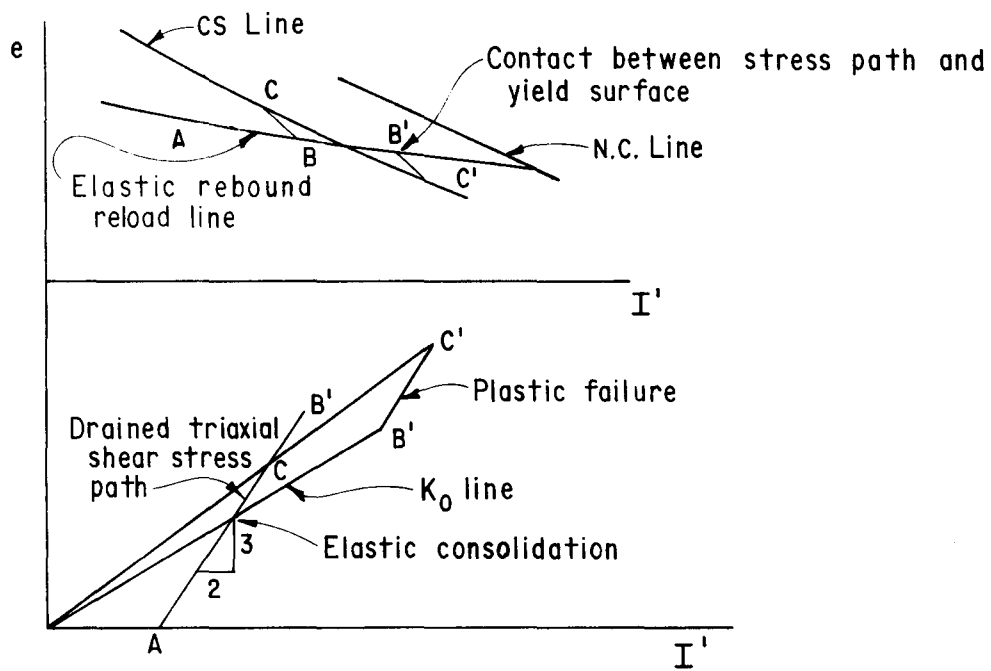
Once the problem of selecting a soil model and test data interpretation is resolved, a new problem arises: How to use the soil model to develop an analytical procedure to evaluate a real structure? Currently, finite element methods form the basis of many of the more popular analytical procedures for evaluating soil behavior and soil structures. Complicated soil models of the aforementioned types are not easily incorporated into the finite element method. Vast computer storage and high-speed calculations would be re-

quired for such a combination of analytical procedures and soil models. While it is true that a finite element analytical procedure is of little value without a proper material model, it is also true that an accurate soil model is of little value if it cannot be used to evaluate a real problem.

The conclusion of this discussion on soil models is that to theoretically link the behavior of sands during earthquake loading to the measurements obtained



(a) Stress path for soil element during earthquake loading - constant volume plane



(b) Possible stress paths for soil element during cone penetration test

Figure 20. - Critical state soil model interpretation of stress paths caused by earthquake and cone penetration loading.

during the cone penetration test requires a realistic soil model, a procedure for obtaining the soil parameters to describe the soil model, and a computer analysis capable of implementing the soil model. Currently, an abundance of soil models exists, but their accuracy in relating the large-strain drained behavior to the undrained behavior of a sand is questionable. Finite element computer analysis procedures are limited in their ability to handle many of the proposed soil models by the necessity for large-memory, high-speed computers. Finally, soil tests to determine the properties that describe a soil model are either nonexistent or are in research and development stages and not available to the entire engineering community. Thus, the primary needs for a complete large-strain soil model are (1) qualitative evaluation of the limitations of current analytical techniques; and (2) proper selection of soil parameters for developing empirical relationships. The latter need is demonstrated in the section entitled "Cone Penetration Practice."

#### Additional Problems with Association of Cone Penetration Testing to Earthquake Response of Soils

Additional problems associated with application of a theoretical relationship between CPT loading and earthquake loading of real soil deposits arise from the nature of these deposits. Seldom is a real homogeneous clean sand deposit of several feet in thickness encountered. Cone penetration tests performed in areas of alluvial-lacustrine deposits are generally spiked with peaks and valleys, as shown on figure 21. In deposits of gravel, sand, silt, and clay, continuous profiles from one sounding hole to the next are difficult to correlate, and layers are so thin that assuming the full failure strength of a layer is developed during the CPT is highly misleading. Even for soils deposited in a deltaic environment, thin seasonal layering is evident. Guidelines related to the thickness of a layer required before full end bearing resistance is developed within that layer have been proposed by Schmertmann [47], Robertson and Campanella [41], and others. A general rule of thumb of approximately 15 cone diameters (0.5 m) is often used. Thus, the use of theoretical models and analytical procedures for interpretation of CPT data for real soil deposits always requires some degree of experience and judgment on the part of the engineer.

In addition to the problems related to the layering of real soil deposits, the drainage condition of real soils is seldom known during performance of the CPT. The assumptions of drained failure for clean sands and undrained failure for clays during the CPT may be justified, but questions remain on (1) the drainage condition during CPT sounding in silty or clayey sands and gravels, and (2) whether earthquake-related

structural problems are only limited to sands and gravels.

## CONE PENETRATION THEORY

### Introduction

Theoretical modeling and interpretation of CPT data have developed primarily in terms of limit equilibrium and limit plasticity, and pragmatically in terms of general bearing capacity theory [17, 23] or cavity expansion theory [5, 60]. While some theoretical advancements have recently been proposed along the lines of strain path methods, which are based on ideal plastic flow concepts [24], a significant amount of current research in this area has focused on clays not generally susceptible to liquefaction during earthquake loading. Therefore, this section concentrates on the limit equilibrium theories.

### General Bearing Capacity Theory

The CPT was originally developed as a tool for pile design. The cone penetrometer itself was assumed to be a model pile; therefore, early analytical techniques for interpreting CPT data developed from concepts used to analyze the bearing capacity of piles. Using equations of the same form to interpret model and prototype piles provided the added convenience of lumping the effects of differences in end bearing, skin friction, and insertion rate into a single empirically derived scale effect parameter.

Pile load design is based on two components of resistance, skin friction ( $f$ ) and end bearing ( $q$ ). By assuming uncoupled contributions from the two components, the total pile load capacity ( $Q$ ) may be calculated by superposition as:

$$Q = qA_e + fA_s \quad (7)$$

where:

$$\begin{aligned} A_e &= \text{end area of pile, and} \\ A_s &= \text{side area of pile.} \end{aligned}$$

Buisman [8] and Terzaghi [57] proposed a general equation for bearing capacity in the following form:

$$\frac{Q}{B} = q = cN_c + \gamma \left( \frac{B}{2} \right) N_\gamma + \gamma DN_q \quad (8)$$

where:

$$\begin{aligned} B &= \text{base width or diameter,} \\ \gamma &= \text{total unit weight of soil,} \\ D &= \text{embedment depth,} \\ c &= \text{cohesion, or cohesive strength} \\ &\quad \text{of soil, and} \end{aligned}$$

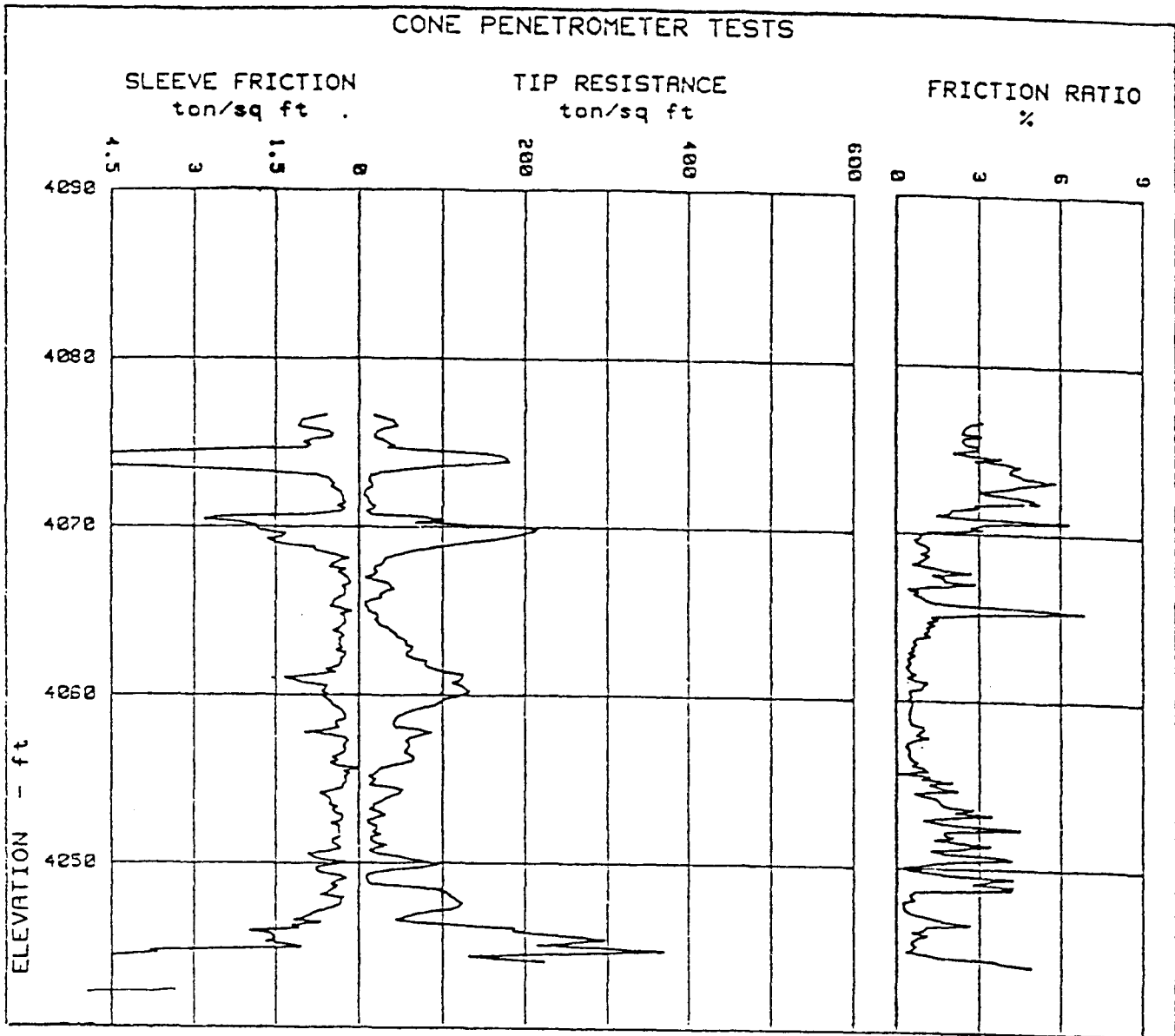


Figure 21. - Example of electric cone penetrometer record in an alluvial lacustrine deposit. (1 ton/ft<sup>2</sup> = 9 765.34 kg/m<sup>2</sup>).

$N_c, N_\gamma, N_q$  = dimensionless bearing capacity factors for deep or shallow foundations.

and

$$q_c = \gamma DN_q \quad (10)$$

For a cone penetrometer at great depth ( $D \gg B$ ), the term  $\gamma(B/2)N_\gamma$  becomes negligible. For penetration in clays, the process is assumed to take place under undrained conditions where the friction angle ( $\Phi'$ ) is zero and  $N_q = 1.0$ . For penetration into sands, the cohesion ( $c$ ) is usually assumed to be zero. Thus, the end bearing capacity equations for penetration in clays and sands, respectively, become:

$$q_c = S_u N_k + P_o \quad (9)$$

where:

- $q_c$  = end bearing pressure of a cone penetrometer ( $Q/B$ ),
- $S_u$  = undrained shear strength of clay,
- $P_o$  = total vertical overburden pressure ( $\sigma_{vo}$ ), and
- $N_k$  = empirical, dimensionless cone bearing capacity factor, which includes scale effects.

The skin friction component of pile capacity is often assumed to be proportional to the undrained shear strength of a clay or the drained friction angle ( $\Phi'$ ) of sands. The general forms of the equations that describe skin adhesion and friction components of cone resistance for clay and sand, respectively, are:

$$S_u = \alpha f_s \quad (11)$$

and

$$\Phi' = \frac{(\tan^{-1}\beta) f_s}{\gamma B} \quad (12)$$

where:

$\alpha, \beta$  = dimensionless cone correlation factors, and  
 $f_s$  = cone friction sleeve measurement.

The soil model most often used to describe shear behavior for bearing capacity theory is a rigid plastic model (fig. 22). One example of the use of these general bearing capacity equations was presented by Meyerhof [29]. The failure mechanism assumed by Meyerhof is illustrated on figure 23(a).

### Janbu and Senneset's Method

Janbu and Senneset [23] recognized the need for maintaining the simplicity of the general bearing capacity equations while accounting for the varying volume changes exhibited by sands during shear. The basis of this method lies in the separation of shear strength and volume change. The shear strength of sands is given by the equation:

$$\tau_f = (a + \sigma') \tan \Phi' \quad (13)$$

where:

$\tau_f$  = shear strength at failure,  
 $a$  = attraction =  $c' \cot \Phi'$ ,  
 $\sigma'$  = effective normal stress, and  
 $c'$  = effective cohesion.

The compressibility of a sand is introduced into this method in the description of the failure mechanism analyzed. To describe the failure mechanism related to the end bearing of the cone penetrometer and to calculate the nondimensionalized bearing capacity factor,  $N_q$ , as a function of compressibility, the angle  $\beta$  between the horizontal plane and the limits of the bearing capacity failure mechanism (fig. 23(b)) was introduced. Angle  $\beta$  is a function of the volume change characteristics of the soil during shear and must be estimated either by trial and error based on laboratory shear test data or by experience in a particular area. Positive angles of  $\beta$  correspond to decreases in volume during shear, and negative angles

of  $\beta$  correspond to increases in volume. Once a  $\beta$  angle has been selected, a bearing capacity factor  $N_q$  may be calculated as a function of  $\Phi'$  by the equation:

$$N_q = N_q e^{(\pi - 2\beta \tan \Phi')} \quad (14)$$

where:

$$N_q = \tan^2 \left( 45 + \frac{\Phi'}{2} \right)$$

The relationship between cone end bearing and drained friction angle may be calculated from the expression:

$$q_c = N_p (\sigma'_{vo} + a) \quad (15)$$

where:

$N_p = N_q - 1$ , and  
 $\sigma'_{vo}$  = vertical effective stress.

For a cohesionless soil in which adhesion ( $a$ ) is assumed to equal zero, equation (15) may be rearranged to the form:

$$\frac{q_c}{\sigma'_{vo}} = N_p = N_q - 1 \quad (16)$$

For  $\beta = -15^\circ, 0^\circ$ , and  $+15^\circ$ , Robertson and Campanella [40] presented the plot shown on figure 24 for the relationship between drained friction angle ( $\Phi'$ ) and bearing capacity factor ( $N_q$ ) as a function of  $\beta$ . Figure 24 shows that assuming  $\Phi' = 42^\circ$ ,  $N_q$  may vary from approximately 40 to 150 as  $\beta$  varies from  $+15^\circ$  in a compressible sand to  $-15^\circ$  in a dilatant sand.

The problem with this method is that the engineer must assume a value of  $\beta$  to determine a bearing capacity factor and friction angle. Implicit in the assumption of  $\beta$  is the friction angle itself. Thus, determinations of  $\beta$  must be made by other means, such as sampling and laboratory testing, to prevent errors when entering new site locations.

### Durgunoglu and Mitchell's Method

Durgunoglu and Mitchell's method for determining the drained friction angle of a sand is based on the failure mechanism shown on figure 23(c). The bearing capacity failure mechanism is divided into two zones: zone AOC of plane shear and zone COE of radial shear. The governing equation for this mechanism of shear behavior is:

$$q = \gamma' BN_{\gamma q} \xi_{\gamma q} \quad (17)$$

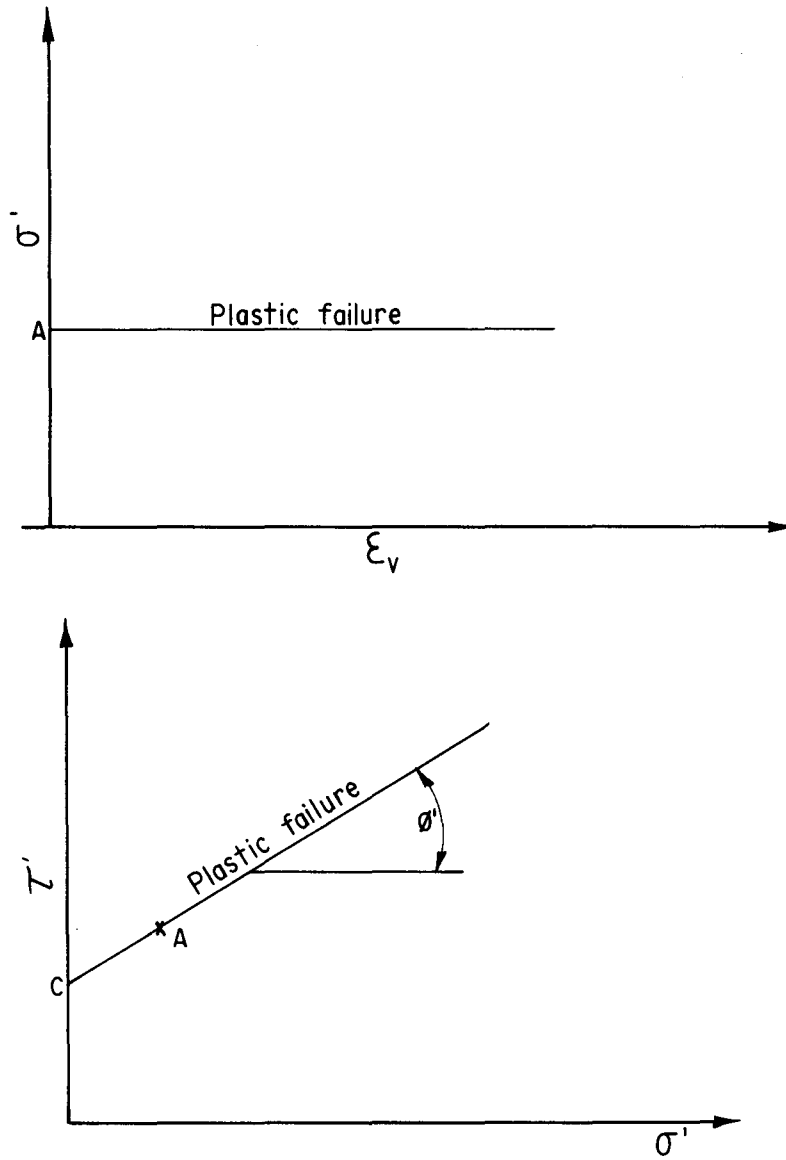


Figure 22. – Ridged plastic frictional soil model.

where:

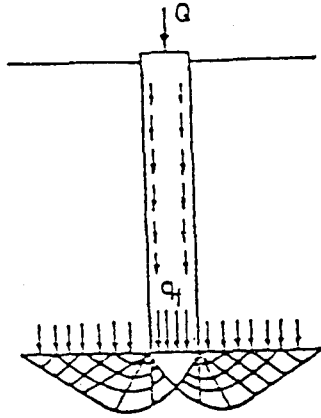
- $\gamma'$  = effective soil unit weight,
- $B$  = cone diameter,
- $N_{\gamma q}$  = bearing capacity factor for wedge penetration, and
- $\xi_{\gamma q}$  = shape factor to convert wedge factor to cone factor.

The simplicity of this basic equation is overshadowed by the rather complex set of equations for  $N_{\gamma q}$  and the semiempirical equation describing  $\xi_{\gamma q}$ . Although  $N_{\gamma q}$  was derived by means of theoretical approaches that did not include volume change characteristics of sands during drained shear, the use of a semiempirical equation for  $\xi_{\gamma q}$  implicitly assumed volume change characteristics similar to those of the sands

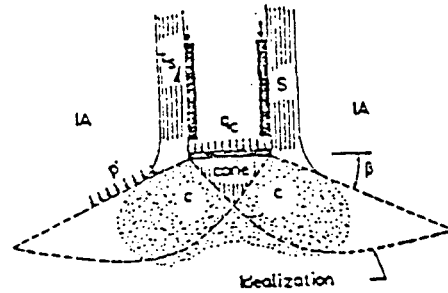
tested to develop the equation. As with any equation that incorporates empirically derived terms, the equation for  $\xi_{\gamma q}$  would be valid for only the materials and test conditions represented in the empirical data base. Thus, use of Durgunoglu and Mitchell's method in soils not represented in the empirical data base would result in errors of unknown magnitude. A comparison of Durgunoglu and Mitchell's failure mechanism with Janbu and Senneset's suggests that  $\xi_{\gamma q}$  was originally developed for dense sands that expand in volume during shear.

#### Comparison of Bearing Capacity Methods

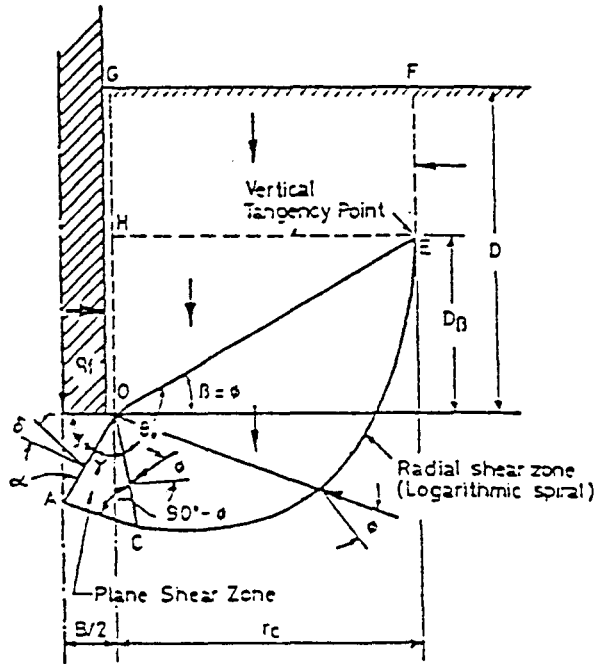
Lunne and Christoffersen [26] compared four methods for predicting drained shear strength from CPT



(a) Typical slip line solution to bearing capacity failure of cone penetrometer. From [29].



(b) Failure mechanism for bearing capacity failure of cone penetrometer. Proposed in [23].



(c) Failure mechanism for bearing capacity failure. Proposed in [17].

Figure 23. – Bearing capacity theory failure mechanism.

data. Three of the methods (Meyerhof [29], Durgunoglu and Mitchell [17]; and Janbu and Senneset [23]) were based on conventional bearing capacity theory. The fourth method (Schmertmann [47]) was an empirical method based primarily on results obtained in large calibration test chambers.

Lunne and Christoffersen's study compared the drained friction angle of the soil as determined by

drained triaxial compression testing with the friction angles predicted by the four methods. Table 1 shows the results of this comparison. For the purpose of conducting this comparison, values of  $a = 0$  and  $\beta = 0$  were assumed for Janbu and Senneset's method. This assumption lead to a consistent over-prediction of  $\Phi'$  of between  $3^\circ$  and  $5^\circ$  for the three sets of chamber test results presented. For example, if  $\beta = -15^\circ$  for the Chapman's (1979) test results

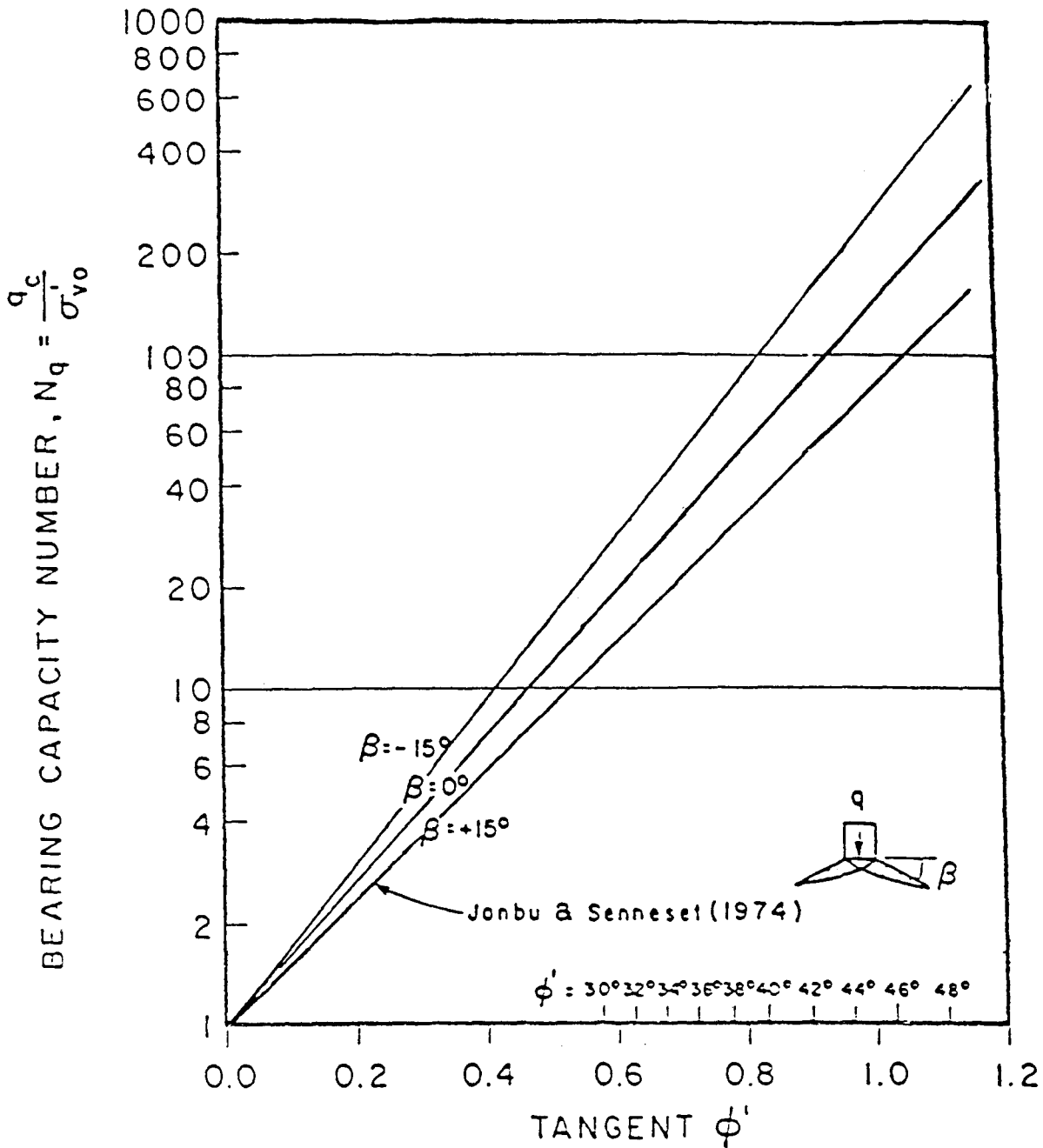


Figure 24. – Diagram showing bearing capacity factor number as a function of friction angle and  $\beta$ . After [40].

had been assumed, it can be seen from figure 24 ( $N_q = \text{constant}$ ) that the estimate of  $\Phi'$  would have been approximately  $39^\circ$  instead of  $42^\circ$ . Durgunoglu and Mitchell's method required no assumption of volume change characteristics and resulted in a very accurate prediction of  $\Phi'$ . This indicates that the conditions represented by the three chamber test studies were very similar to those conditions used by Durgunoglu and Mitchell in developing their semi-empirical equation for  $\xi_{\gamma q}$ .

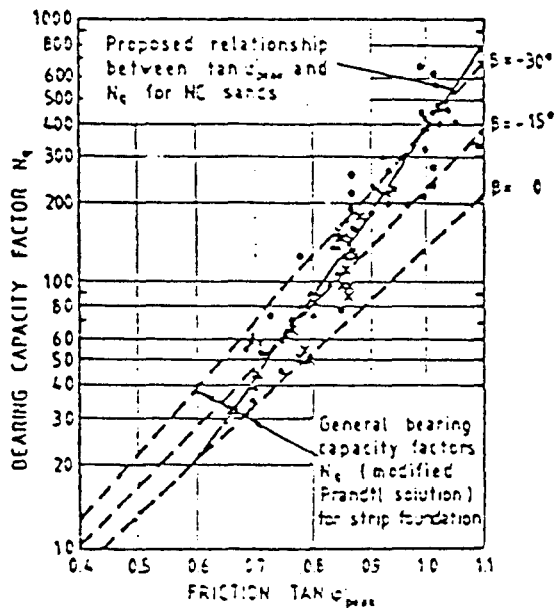
Using the assumption of  $\beta = 0^\circ$ , Lunne and Christoffersen devised a modification to Janbu and Senneset's method whereby  $N_q$  is defined by:

$$N_q = \tan^2\left(45 + \frac{\Phi'}{2}\right) e^{\left[\left(\frac{\pi}{3}\right) + 4\Phi'\right]\tan\Phi'} \quad (18)$$

The relationship for this expression of  $N_q$  as a function of  $\tan\Phi$  is shown on figure 25. The comparison of the modified Janbu and Senneset method with the

Table 1. – Lunne and Christofferson's comparison of  $\Phi$  predictions. From [26].

Reference	Test type	No. of tests	OCR	Method of interpretation, $\phi'$ (degrees)					Drained triaxial compression tests $\phi'_{peak}$ (degrees)
				Meyerhof 1961	Durgunoglu and Mitchell	Janbu and Senneset ( $\alpha=0, \beta=0$ )	Modified Schmertmann	Modified Janbu and Senneset	
Parkin et al. (1980)	Chamber	40	1	40	42	47	41	42	42
Chapman (1979)	Chamber	16	1	36	39	42	41	39	39
Bellotti et al. (1983)	Chamber	30	1	37	39	42	40	39	39
Average deviation from $\phi'_{peak}$ determined in laboratory				-2	0	-4	0	0	
Parkin et al. (1980)	Chamber	20	8	42	43		40		
Chapman (1979)	Chamber	11	2-7.7	39	41		40		
Bellotti et al. (1983)	Chamber	21	1.9-9.9	37	38		39		
Dahlberg (1975)	Field	8	>1	39	40		39		
North Sea (Mitchell and Lunne, 1978)	Field	2	>1	44	44		42		
Average OC sand				39	40		40		



LEGEND:

- NGI CHAMBER TESTS
- CHAPMAN (1979) TESTS
- BALDI ET AL (1983) TESTS

NOTE:

EFFECT OF DIAMETER RATIO ACCOUNTED FOR (Fig 1)

Bearing capacity factor  $N_q$  vs.  $\tan \phi'_{peak}$  from tests on NC sands.

Figure 25. – Modified Janbu and Senneset method. From [26].

chamber results brought this method into agreement with the results of Durgunoglu and Mitchell, Schmertmann, and the triaxial shear test. Figure 25 shows that the apparent effect of the modification is to make  $\beta$  a function of the friction angle ( $\Phi'$ ) of the sand and to ignore the compressibility of sands that were not a part of this study and that differed in their relationship between  $\Phi'$  and  $\beta$ . Based upon their findings, Lunne and Christoffersen recommended:

1. Use of a modified Janbu and Senneset method,
2. Use of Durgunoglu and Mitchell's method with  $K_o = 0.4$ , and
3. Use of the modified Schmertmann method whereby relative density is determined from a revised chart.

Robertson and Campanella [40] compared data from Durgunoglu and Mitchell's [17] and Janbu and Senneset's [23] methods of predicting the friction angle with data from large chamber tests (fig. 26). Robertson and Campanella concluded that the scatter in the data reflected the effect of compressibility on the end bearing value. They also concluded that the reasonably good predictions of undrained shear strength of sands using Durgunoglu and Mitchell's and Janbu and Senneset's methods resulted from the use of highly incompressible, predominately quartz and feldspar sands that contained very low percentages of mica. For more highly compressible carbonate sands, Robertson and Campanella suggested that both methods would produce conservatively low estimates of the friction angle.

Cavity Expansion Theory

Vesic [60] recognized the need to incorporate compressibility of a soil directly into the equations for

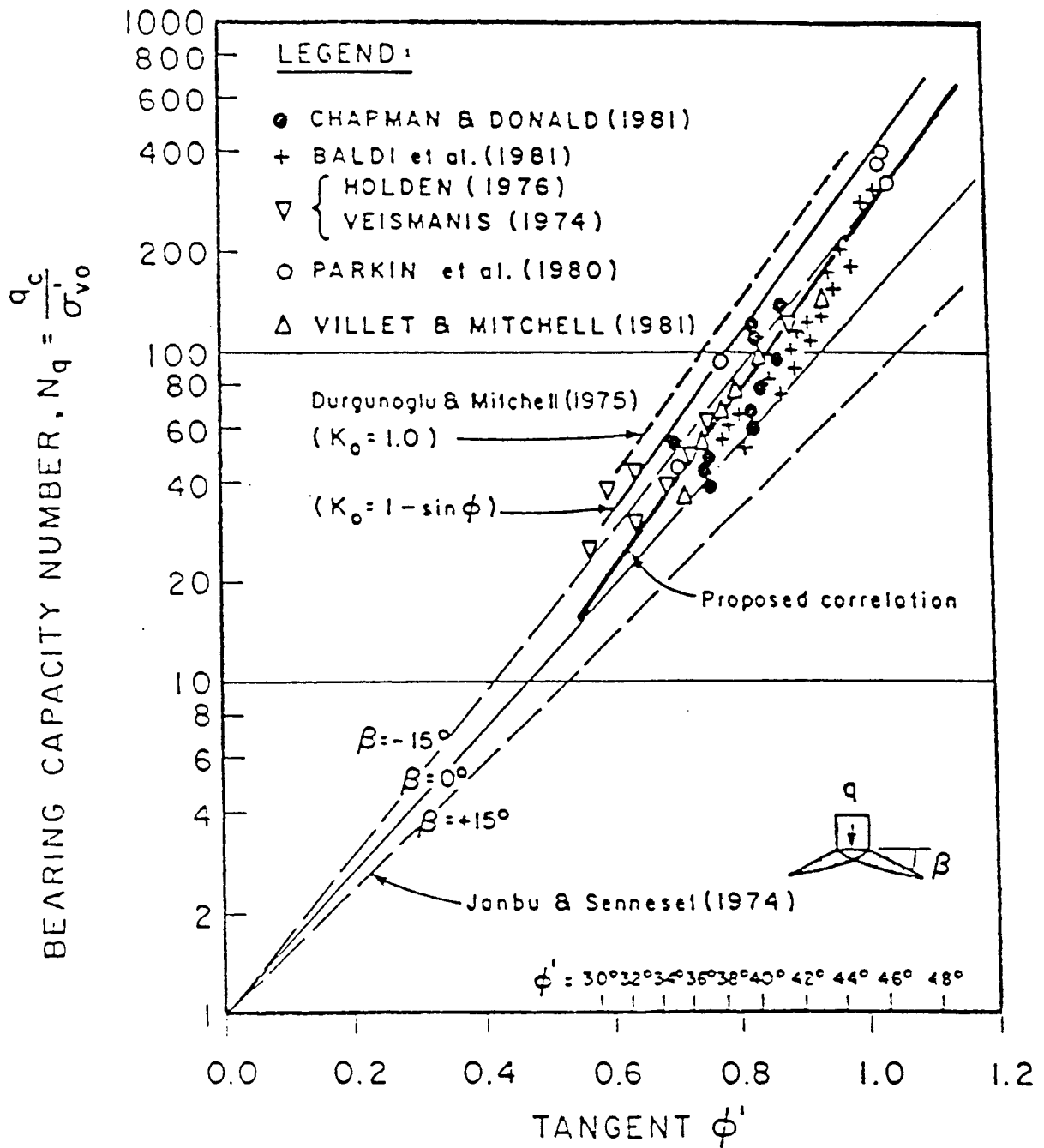


Figure 26. – Relationship between bearing capacity number and peak friction angle at in situ stress, from large calibration chamber tests. From [40].

determining cone resistance. At that time (1972), bearing capacity theories did not recognize compressibility, which Vesic thought to be of great importance. To formulate the basic equations of cavity expansion, Vesic assumed that the cone opened a spherically shaped cavity while the penetrometer shaft maintained an open cylindrical cavity. In his formulation, Vesic assumed that (1) each cavity is not influenced by the presence of the other (i.e., an un-

coupled effect); (2) the soil within the zone of plastic failure behaves as a compressible plastic continuum with a strength envelope defined by Mohr-Coulomb strength parameters ( $c$  and  $\Phi$ ) and an average volumetric strain ( $\Delta$ ); (3) the soil beyond the plastic zone behaves as a linearly deformable (elastic), isotropic solid defined by an elastic modulus ( $E$ ) and a Poisson's ratio ( $\nu$ ); and (4) before application of load, the entire soil mass is subjected to an isotropic effective

stress ( $\sigma'$ ), and the body forces within the plastic zone are negligible. The soil model and failure mechanism for these assumptions are shown on figure 27.

From considerations of static equilibrium of an element within the plastic zone of failure (fig. 27), the governing equations for spherical and cylindrical cavity expansion, respectively, are given by:

$$\frac{\delta\sigma_r}{\delta_r} + \frac{2(\sigma_r - \sigma_\theta)}{r} = 0 \text{ (spherical cavity)} \quad (19)$$

$$\frac{\delta\sigma_r}{\delta_r} + \frac{\sigma_r - \sigma_\theta}{r} = 0 \text{ (cylindrical cavity)} \quad (20)$$

where:

- $\sigma_r$  = normal stress on the element in the radial direction,
- $\sigma_\theta$  = normal stress on the element in the circumferential direction(s), and
- $r$  = distance from the center of the cavity to the element.

With "minor" additional simplifying assumptions, Vesic proposed the solutions of spherical and cylindrical cavity expansion, respectively, in the forms:

$$P_u = cF_c + qF_q \text{ (spherical cavity)} \quad (21)$$

$$P_u = cF'_c + q'F'_q \text{ (cylindrical cavity)} \quad (22)$$

where:

- $P_u$  = cavity pressure,
- $c$  = cohesion,
- $q$  = mean normal effective stress,  $I_1'$ ,
- $q'$  = horizontal effective stress,  $\sigma_h'$ ,
- $F_c, F_q, F'_c,$  and  $F'_q$  = dimensionless cavity expansion terms for a spherical cavity.

$$F_c = (F_q - 1)\cot\Phi' \quad (23)$$

and

$$F_q = \frac{3(1 + \sin\Phi')}{3 - \sin\Phi'} \left( I_{rr} \right) \frac{4 \sin\Phi'}{3(1 + \sin\Phi')} \quad (24)$$

where:

$$I_{rr} = \zeta_v J = \frac{I_r}{(1 + I_r \Delta)} \quad (25)$$

- $I_r$  = rigidity index ( $G/\tau_f$ ),
- $\zeta_v$  = volume change factor,
- $\Delta$  = average volumetric strain,
- $G$  = shear modulus, and
- $\tau_f$  = shear stress at failure.

And for a cylindrical cavity:

$$F'_c = (F'_q - 1)\cot\Phi' \quad (26)$$

and

$$F'_q = \frac{(1 + \sin\Phi')(I'_{rr} \sec\Phi') \sin\Phi'}{1 - \sin\Phi'} \quad (27)$$

where:

$$I'_{rr} = \zeta_v' J' = \frac{I_r}{1 + I_r \Delta \sec\Phi'} \quad (28)$$

To solve equations (21) and (22) for the cavity expansion pressures, the friction angle, the rigidity index, and the average volumetric strain within the plastic zone must be known. For CPT generated results, the only known parameter is the cavity expansion pressure; the soil properties are the unknowns. Any justifiable assumptions related to the soil properties that will decrease the number of unknowns will greatly improve the accuracy of the results.

The CPT is usually performed at a rate of 2.0 cm/s, which has generally been accepted as fast enough to cause clays to fail in undrained shear, sand to fail in drained shear, and most other soil types to fail in partially drained shear. This assumption of drainage conditions during shear allows for the simplifying assumptions of  $\Phi' = 0$  and  $\Delta = 0$  for failure in clays, thus reducing equations (21) and (22) to:

$$P_u = S_u \left[ \frac{4}{3(\ln I_r + 1)} \right] + \frac{\sigma_{vo} + 2\sigma_{ho}}{3} \quad (29)$$

for spherical cavity expansion, and

$$P_u = S_u(\ln I_r + 1) + \sigma_{ho} \quad (30)$$

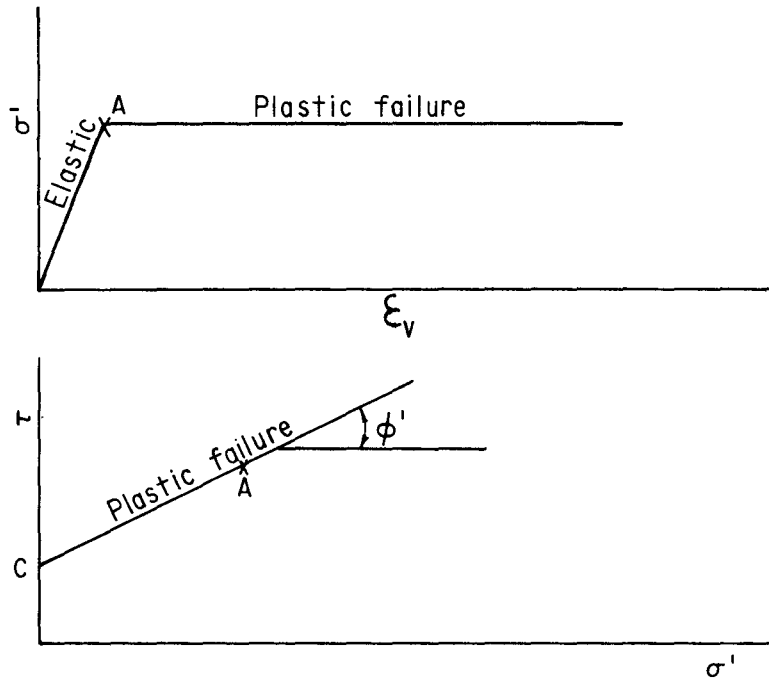
for cylindrical cavity expansion

where:

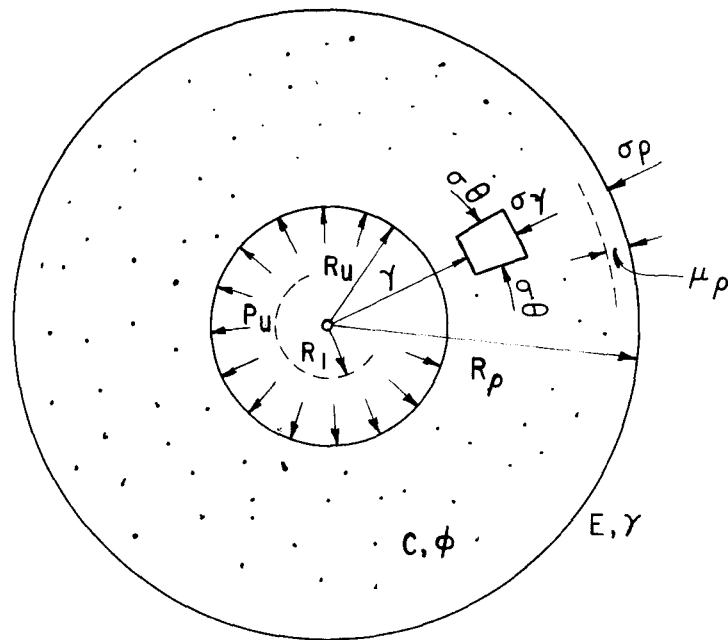
$S_u$  = undrained shear strength.

Equations (29) and (30) are very similar in form to equation (9) from bearing capacity theory. Like equation (9), they require additional assumptions of stress state to create a closed form solution to the problem.

Unfortunately, most liquefaction problems involving loss of shear strength occur in sands and silty sands. For these materials, the CPT failure condition is assumed to be drained or partially drained; and the simplifying assumptions of  $\Phi' = 0$  and  $\Delta = 0$  cannot be justified. Thus, additional soil testing, currently laboratory shear and volumetric testing, is presumed to be required to identify  $\Phi'$ , estimate  $\Delta$ , and solve equations (21) and (22) for either a spherical or cylindrical cavity. Selection of  $\Phi'$  becomes even more



(a) Elastic-plastic soil model.



(b) Expansion of cavity. [60].

Figure 27. - Cavity expansion theory.

complicated for cavity expansion theory than for bearing capacity theory because the cone penetrometer involves a lesser degree of empiricism and higher stresses in the soil than traditional laboratory testing.

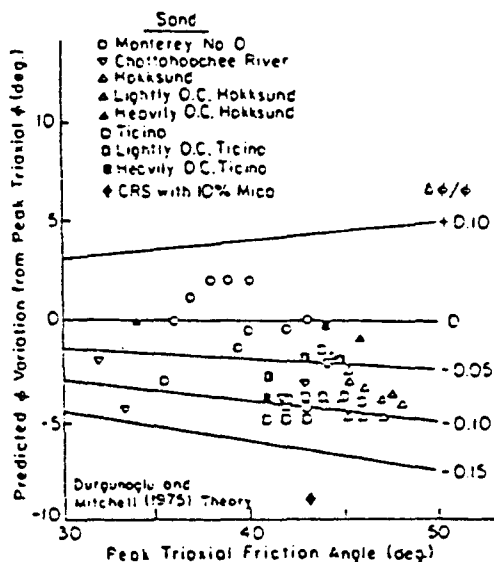
Cavity expansion theory assumes the soil must compress during failure. The stress levels measured during cone penetration testing of sand often exceed grain crushing levels and force general agreement with this volume change assumption; however, laboratory tests to determine  $\Phi'$  are conducted at much lower stresses where sands often display tendencies to expand during shear. Although no exact guidelines have been found in the literature to account for this discrepancy and its effect on the selection of  $\Phi'$  for cavity expansion theory, because of the large strains induced into the soil, it appears as though  $\Phi'_{cv}$  (critical volume friction angle) would be a proper selection.

Baligh [5] further advanced the cavity expansion theory to account for a nonlinear soil strength envelope. This extension further complicates cavity expansion theory and requires even more soils information to achieve a solution. This need for extensive laboratory or in situ soil testing to solve the equations, although theoretically attractive, invariably negates the need for solving the equations in the first place.

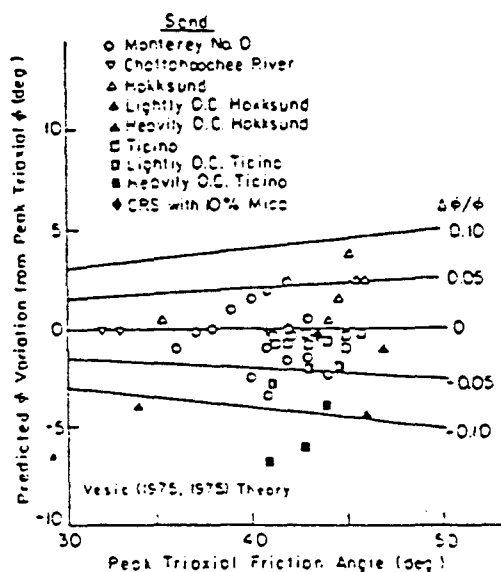
### Comparison of Cavity Expansion Theory and Bearing Capacity Theory for Predicting Soil Friction Angle

A recent comparison between Vesic's cavity expansion theory and Durgunoglu and Mitchell's bearing capacity theory for predicting peak (drained) triaxial friction angle was reported by Mitchell and Keaveny [30]. Plots of the predicted variation from the peak triaxial friction angle versus the measured peak angle for sand tested in large calibration chambers as determined by triaxial shear tests presented in their report are shown on figure 28. Figure 28 shows that the variation in predicted values using cavity expansion theory is less than the variation produced from bearing capacity theory. For cavity expansion predictions in this study, Mitchell and Keaveny chose to use a modulus of deformation ( $E$ ) corresponding to the secant modulus at 50 percent deviator stress at failure rather than the initial tangent modulus suggested by Vesic [61, 62].

The most obvious reason for the closer agreement of cavity expansion predictions with measured triaxial shear results is exemplified by the CRS (Chattahoochee River Sand) containing 10 percent mica. As will be shown in the next subsection ("Effect of Compressibility of Sands"), a mica content of 10 percent has a dramatic impact on the compressibility of sands, and therefore on the measured end bearing



(a) Variation between predicted and peak triaxial friction angle using the Durgunoglu and Mitchell's theory [17].



(b) Variation between predicted and peak triaxial friction angle using Vesic's theory [61, 62].

Figure 28. - Variation of predictions of peak triaxial friction angle using bearing capacity and cavity expansion theories. From [30].

value of the cone penetrometer. Yet, the peak friction angle of a sand is not nearly so affected by the mica content. The direct incorporation of compressibility within cavity expansion theory prediction of peak friction angle accounts for the greater degree of accuracy in predicting the peak friction angle for this sand.

## CONE PENETRATION PRACTICE

As suggested by Mitchell and Keaveny, accurately predicting peak friction angle is important when predicting end bearing pile load capacity. For such predictions, conservative estimates of friction angle for compressible sands, as generally obtained from theories based on bearing capacity, will grossly underestimate the end bearing capacity of the pile. This comparison suggests that, when an accurate prediction of peak friction angle is required for computational purposes, the cavity expansion theory, along with the necessity of sampling and additional laboratory testing, is justified.

The relationship between the drained friction angle, as determined by the CPT methods, and the undrained steady-state friction angle (as previously described in the section "Soil Behavior Model") has not yet been explored. One of the primary aspects of a complete soil model would be to develop this relationship and thereby deduce the undrained peak and residual shear strengths of a soil directly from CPT data.

### Effect of Compressibility of Sands

Compressibility of a sand has been mentioned in connection with both bearing capacity and cavity expansion theories. It is generally recognized that increases in compressibility of a sand lower the end bearing tip resistance. For a clean quartz sand, the primary causes for a change in compressibility relate to changes in relative density (i.e., void ratio) and grain crushing. For sands in situ, compressibility is also a function of cementation, stress condition, mineralogy, and many other factors. For example, Harris et al. [20] have shown that small changes in percentages of mica, between 0 and 10 percent, can have significant effects on the initial tangent modulus  $E_o$  (fig. 29) as well as a secant modulus to 50 percent deviator stress at failure.

Robertson and Campanella [40] prepared the graph on figure 30 to illustrate the effect of compressibility on predictions of relative density. Summarized in this diagram are methods of predicting relative density ( $D_r$ ) proposed by Schmertmann [46]; Baldi et al. [4]; and Villet and Mitchell [63]. Note the relationships between curve 3 at  $D_r = 40$  percent and curve 1 at  $D_r = 40$  percent and  $D_r = 80$  percent. The dynamic behavior of a sand at  $D_r = 80$  percent is very different from that at  $D_r = 40$  percent; yet without knowing the compressibility of the granular structures being tested, estimates of relative density can easily vary by as much as  $\pm 20$  percent from the mean. From the standpoint of mica content, this could mean that a change of only a few percentage points between 0 and 10 percent could change the predicted behavior significantly.

### Introduction

The lack of a good theoretical soil model and an accurate analytical technique to link CPT data to undrained shear strength of potentially liquefiable soils has led engineers to seek empirical relationships for design and analysis in earthquake prone areas. By developing empirical CPT models, engineers hope to separate soils exhibiting stable or safe behavior from those that are unstable or potentially unsafe. The CPT data are often used for locating and focusing attention on the specific zones of soil whose behavior is questionable. Once such a zone has been located and fully delineated by the CPT, other in situ tests, such as the standard penetration test or sampling and laboratory testing, verify the CPT results and provide more detailed design information.

Although theory may not fully substantiate the CPT-soil empirical relationships, these relationships should be based on a logical set of first-order, soil-test condition, influencing factors. If these factors are not fully understood, the limitations on the validity of the empirical correlations are unknown. Thus, the validity of empirical correlations developed in one location for one soil under one set of boundary conditions is unknown for use in another location where soil or boundary conditions are different. Therefore, a complete empirical relationship should present methods for evaluating the changes in the influencing factors as well as provide guidelines for design. For this reason, this section not only presents the CPT empirical relationships currently used for estimating the liquefaction susceptibility of soils, but also attempts to define the factors that may have influenced the development of those relationships.

### Influencing Factors of the CPT

The factors that influence measured CPT values may be placed in three categories: first, factors resulting from penetrometer design and geometry; second, factors related to soil properties; and third, factors related to the stress field in the soil caused by the penetration of the tool. The latter is the soil-structure interaction factor.

Robertson and Campanella [41] pointed out the effects of machine tolerances on individual penetrometer elements, the effects of temperature on electronic components, and the effects of unequal surface areas of cone tip and sleeve components. Levadoux and Baligh [24] investigated the effects of changing the cone apex angle for penetration in clays. Lunne et al. [27] presented further methods for evaluating the effects of thermal shift, load cell range, and other factors related to penetrometer design.

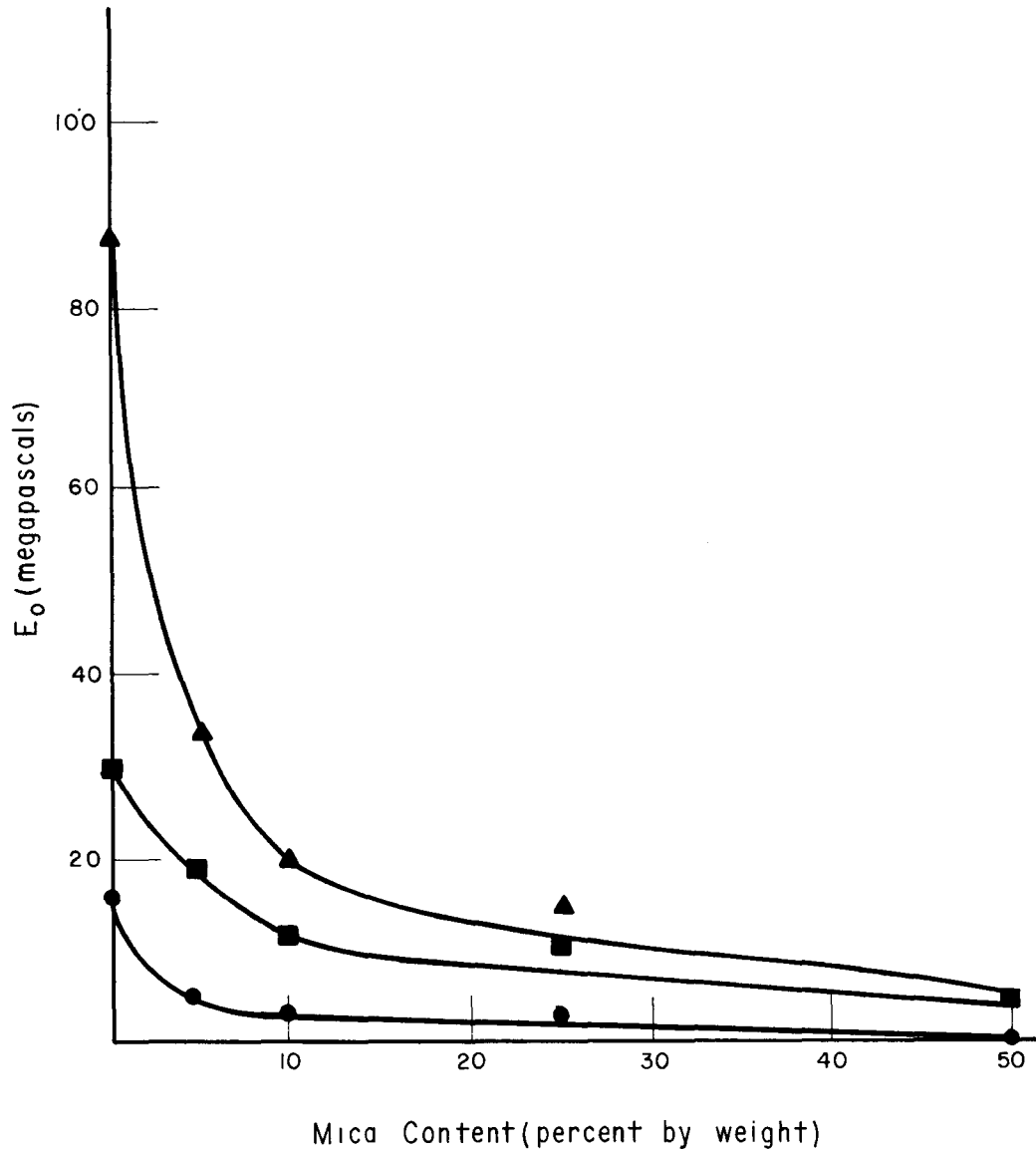


Figure 29. — Initial tangent axial compression modulus ( $E_o$ ) of mica-quartz sand mixtures at different confining pressures ( $\sigma_3$ ) as a function of mica weight percentage. After [20].

With the exception of unequal cone area, the effects of these penetrometer factors may be minimized through careful design and machining of the penetrometer itself. For the purpose of liquefaction assessment, the unequal cone area factor is negligible because of the low pore pressures surrounding the penetrometer and the high tip resistance encountered in penetration of even loose sand. Penetration rate, which has received attention in the literature, is mostly viewed as a deviation from the standardized CPT procedure and remains in the research stage. With the exception of the use of a 15-cm<sup>2</sup> cone, changes in the standard CPT procedure and external design have not been introduced into engineering practice for liquefaction assessment purposes.

Soil properties that influence penetration measurements are compressibility, shear strength, permeability, and layer thickness. The influences of layer thickness, compressibility, and shear strength were discussed in previous sections. Permeability becomes very important as liquefaction assessment moves toward fine sands and silty sands, for which the CPT may result in partially drained or undrained failure of the soil. The piezocone penetrometer may be more useful in identifying this condition.

Schmertmann [47] discussed the influence that a variable stress field might have on penetrometer measurements in terms of change in vertical stress, rate of change in horizontal stress, and the in situ ratio

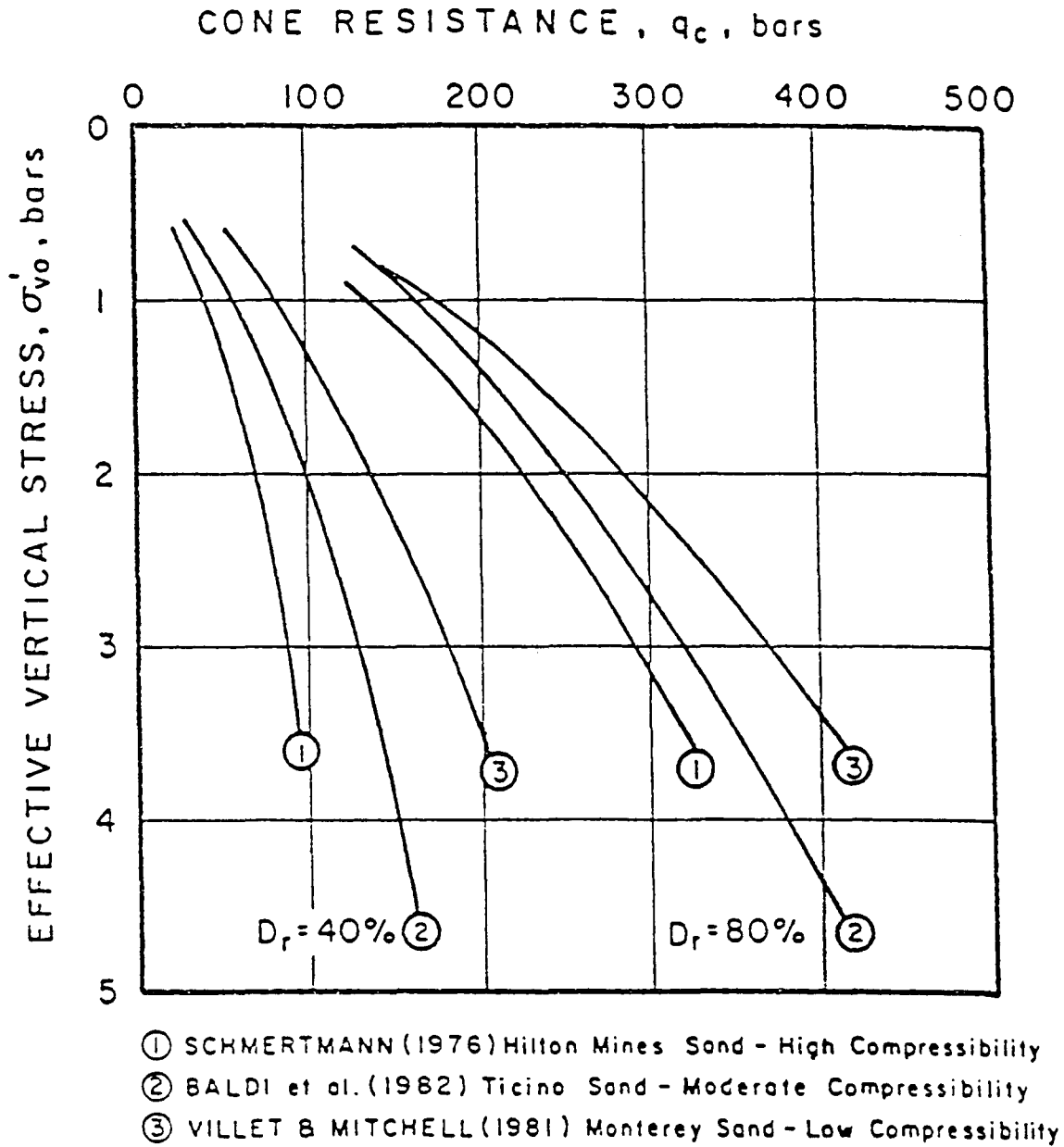


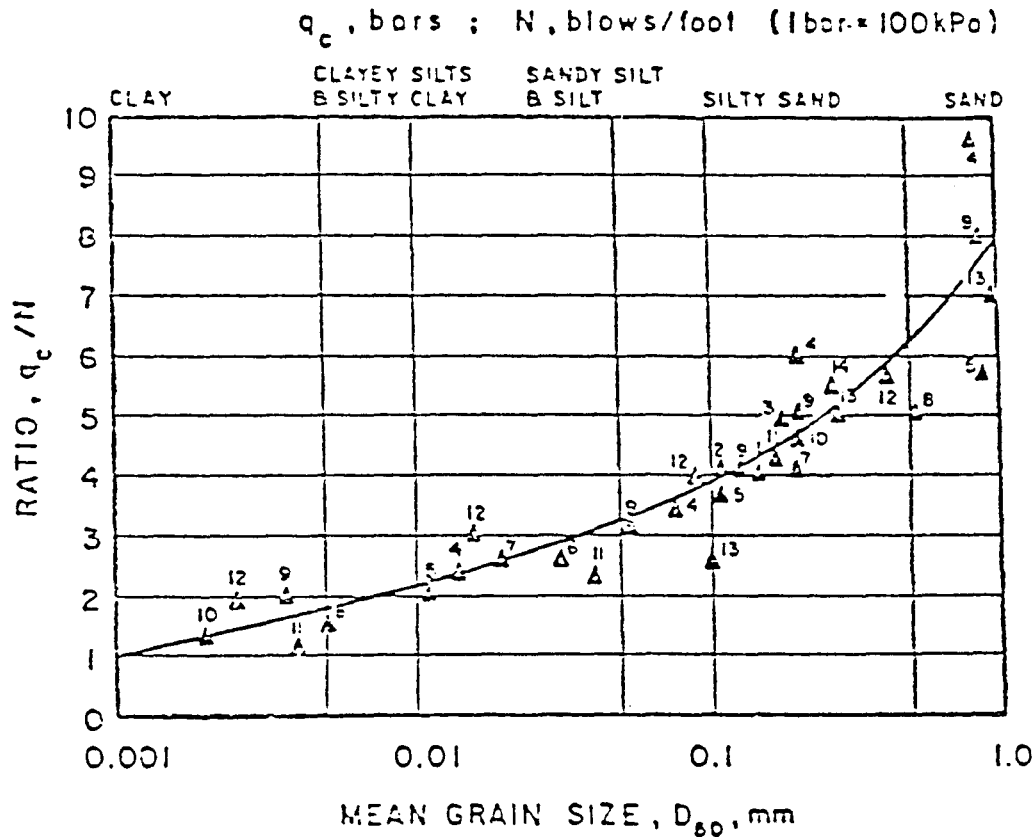
Figure 30. - Comparison of different relative density relationships. From [40].

of horizontal to effective vertical stresses ( $K_0$ ). The general trend is for cone resistance to increase with an increase in mean normal effective stress. The rate of increase in tip resistance is not expected to be linear with changes in effective stress condition, just as soil properties such as compressibility and shear strength are neither linearly related to nor constant with changes in void ratio associated with changes in stress condition.

#### CPT-SPT Correlations

The SPT (standard penetration test) has been used extensively for liquefaction assessment in the United

States, Japan, China, and other countries. To make use of this extensive SPT data base, many investigators have tried to develop relationships between CPT and SPT results. The early conversion attempts were made to determine a constant for the ratio of cone tip resistance to SPT blow count ( $q_c/N$ ). Robertson et al. [43] noted that many of the different  $q_c/N$  ratios reported in the literature had some degree of correlation with mean grain size ( $D_{50}$ ) of a sand and developed the chart shown on figure 31. Seed and De Alba [53] updated this curve with new data and presented the graph shown on figure 32. However, Farrar [18] found a great deal of scatter in the correlation with  $D_{50}$  when applied to a variety of sites in Japan, as shown on figure 33.



- |                             |                                  |
|-----------------------------|----------------------------------|
| 1. Meyerhof (1956)          | 8. Camponella et al. (1979)      |
| 2. Meigh and Nixon (1961)   | 9. Nixon (1982)                  |
| 3. Rodin (1961)             | 10. Kruizinga (1982)             |
| 4. De Alencar Veloso (1959) | 11. Douglas (1982)               |
| 5. Schmerlmann (1970)       | 12. Muromachi & Kobayashi (1982) |
| 6. Sutherland (1974)        | 13. Goel (1982)                  |
| 7. Thornburn (1970)         | 14. Ishihara and Koga (1981)     |

Figure 31. - Variation of  $q_c/N$  ratio with mean grain size. From [43].

Olsen [32] suggested that a way to develop a consistent CPT to SPT correlation was through the use of static stress level normalized tip and friction sleeve resistances compared with a normalized SPT blow count, as shown on figure 34. This normalization uses different variables for cone, friction sleeve, and SPT to account for the different stress fields and drainage conditions associated with the procedure of obtaining each measurement. The inclusion of both normalized cone and sleeve data for comparison with normalized SPT blow counts was partly in recognition that the SPT blow count is influenced by both an end bearing component of the sample tube and a frictional component between the sample tube

and soil as the sampler is advanced. The equations recommended by Olsen for normalization of the CPT and SPT data are:

$$q_{cn} = \frac{q_c}{(\sigma_v')^n}; n \approx 0.7 \quad (31)$$

$$f_{sn} = \frac{f_s}{(\sigma_v')^n}; n = 1.0 \quad (32)$$

$$N_1 = \frac{N}{(\sigma_v')^n}; n \approx 0.5 \quad (33)$$

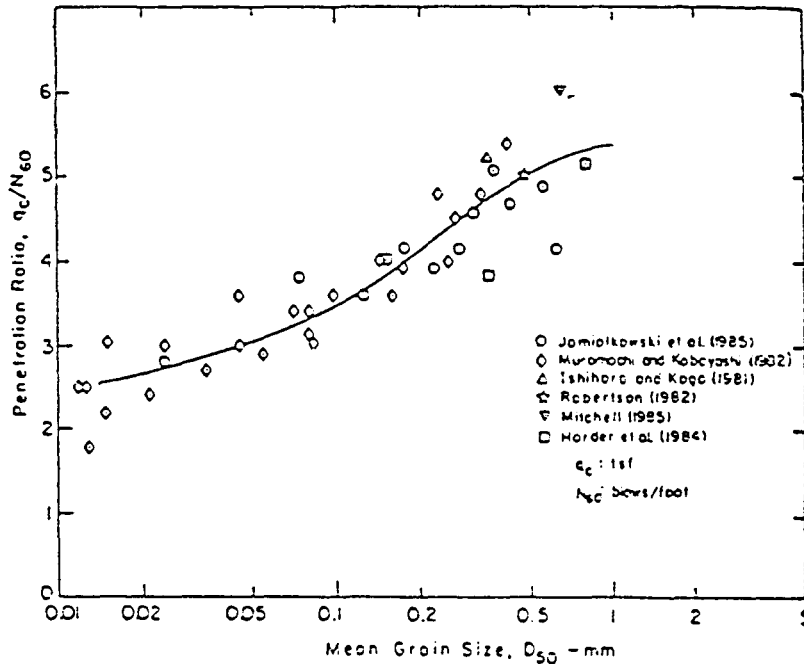


Figure 32. – Variation of  $q_c/N_{60}$  ratio with mean grain size (1 TSF = 96 kPa). From [53].

where:

- $q_{cn}$  = normalized cone bearing,
- $f_{sn}$  = friction sleeve resistance,
- $N_1$  = SPT blow count normalized to 1.0 ton/ft<sup>2</sup>, and
- $1/(\sigma_v')^n$  = normalization factor for stress level.

The factor related to mean particle size is not used in this method, because it is assumed that both the CPT and SPT data are similarly influenced by  $D_{50}$  (i.e., as  $D_{50}$  increases, both  $q$  and  $N_1$  increase proportionately).

From the viewpoint of test conditions, the PST is a quasi-dynamic or impact test, whereas the CPT is a quasi-static test involving a constant penetration rate. That is, the SPT is performed in a discontinuous dynamic manner such that the probe advances at an acceleration rate approaching infinity, resulting in an undrained state of shear in the soil. Conversely, the CPT is performed with a continuous, constant rate of displacement such that the probe advances with an acceleration near zero, resulting in a drained or partially drained shearing state. The approach devised by Olsen [32] tends to account for these differences to a greater degree than the approaches of Robertson et al. [43] or Seed and De Alba [53]. However, based on the author's experience, friction sleeve measurements for subtraction-type cone penetrometers are often unreliable or erratic in sands that contain appreciable amount of coarse sand to travel-sized particles.

Therefore, they should be used with caution when plotted on the log-log scale of Olsen's method. With either method, once the CPT data have been converted to SPT blow counts, Seed and Idriss's [51]  $N_1$  chart (fig. 35) is used to evaluate the soil for liquefaction potential.

#### Liquefaction Assessment Directly From CPT Data

Because of the vast differences of the test conditions imposed during the CPT and the SPT, it is doubtful that either of the CPT to SPT correlations discussed above can now provide a universally applicable method for evaluating the liquefaction susceptibility of a sand. Even though CPT results cannot now be theoretically linked directly to liquefaction susceptibility, it remains more desirable to empirically relate the two directly rather than introduce the uncertainty of CPT to SPT data conversions.

Currently, there are three charts proposed for possible use of CPT data to directly estimate liquefaction potential of soils. The simplest method involves using the chart proposed by Robertson [39] shown on figure 36. This chart is an adaptation of the one developed by Douglas and Olsen [16] for the purpose of soil classification. Robertson noted that soils having sensitive structure tended to plot in zone A of figure 36. These same sensitive soils were those that exhibited the greatest potential for liquefaction during dynamic loading. The advantage of this method is that no computer analysis is needed, and the method may be applied in the field.

RATIO OF CONE RESISTANCE AND SPT  $N_{60}$  VALVE  
VS  
MEAN PARTICLE DIAMETER

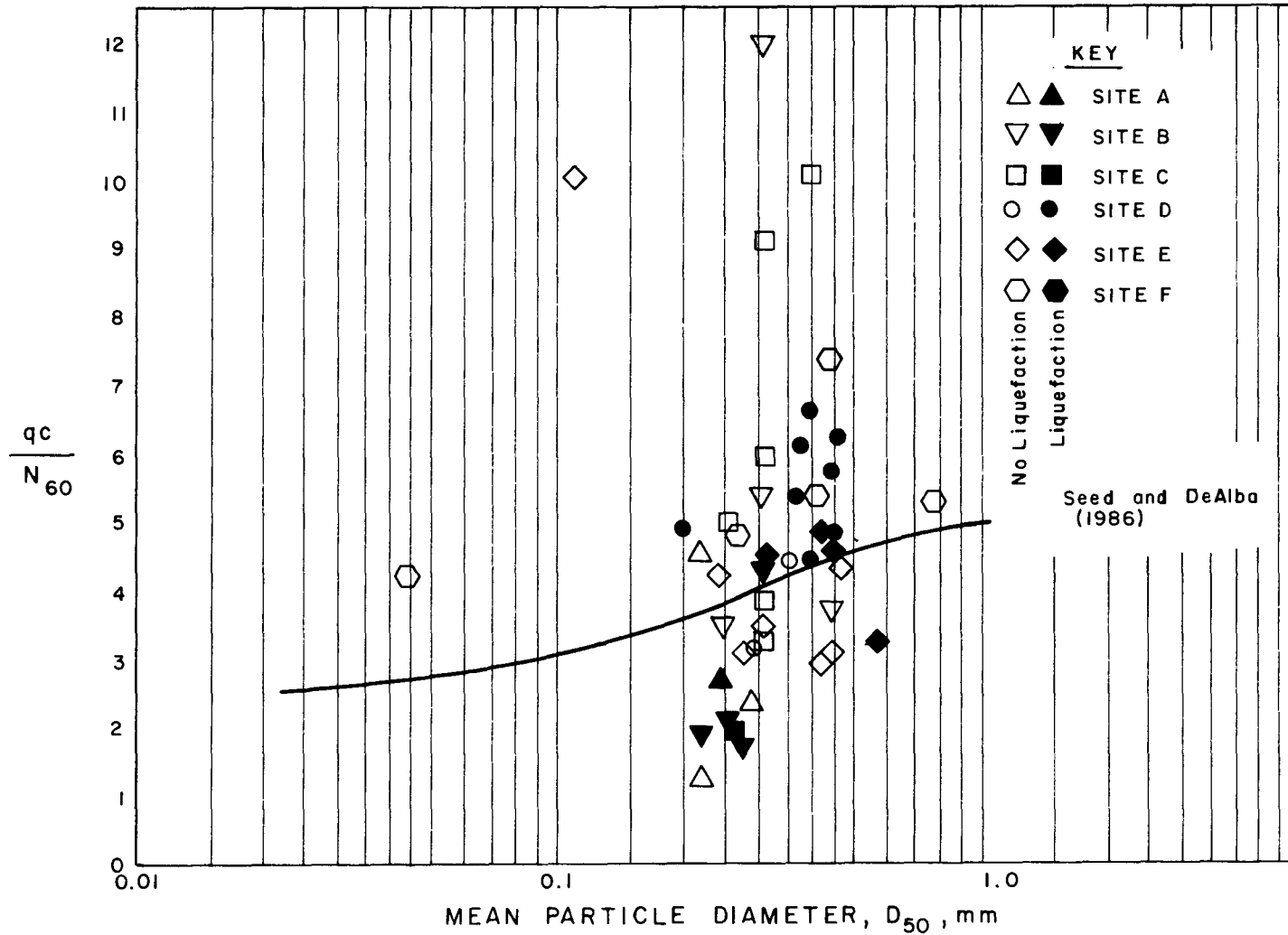


Figure 33. - Example of lack of correlation between  $q_c/N_{60}$  and  $D_{50}$ . From [18].

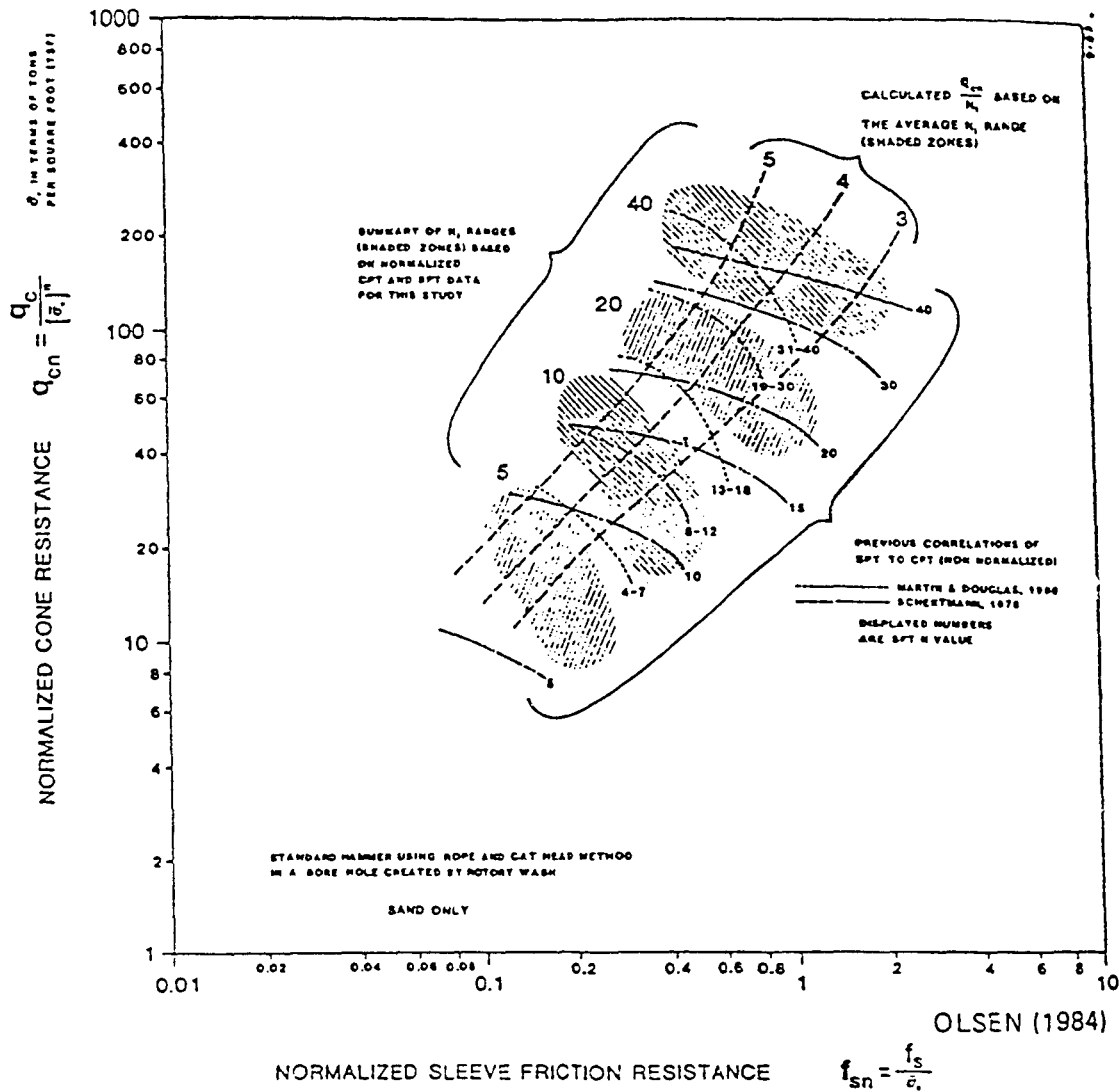


Figure 34. – Normalized cone and friction sleeve resistance versus normalized SPT data. From [32].

Figure 37 shows a second direct method (Seed et al. [52] and Seed and De Alba [53]), that is similar in appearance to the popular SPT- $N_1$  method. In this CPT method, the end bearing tip resistance ( $q_c$ ) is normalized to a 1.0 TSF (tons per square foot) of stress ( $Q_c$ ) (or to 1 MPa, which is used as the reference stress in many countries other than the United States) and compared with an existing data base related to known soil behavior under earthquake loading. However, the CPT- $Q_c$  data base is much smaller than the SPT- $N_1$  data base. Other major disadvantages of this method are (1) the data base is limited to level ground; (2) unlike its SPT counterpart, soil drainage during the CPT allows the compressibility of the soil due to factors other than  $D_{50}$  to play a more important role; and (3) much of the information expressed in this method appears to have been extrapolated from the SPT data base through the use of the highly questionable SPT-CPT relationships.

These disadvantages make the validity of extrapolating the data base into new locations and soil types questionable.

Olsen [32] proposed a third direct chart interpolation method (fig. 38). This method uses normalized tip and sleeve resistances, which are plotted on the chart. Data located within the "tube-shaped" region of the chart represent normally consolidated soils; data on the right side of the tube-shaped region result from overconsolidated soils; and data on the left of the tube-shaped region result from soils that have a sensitive structure. These sensitive soils are considered unstable and likely to liquefy during an earthquake.

Cone end bearing resistance is a function of soil properties while it is changed from an undisturbed infinitesimal strain state into a remolded, large strain

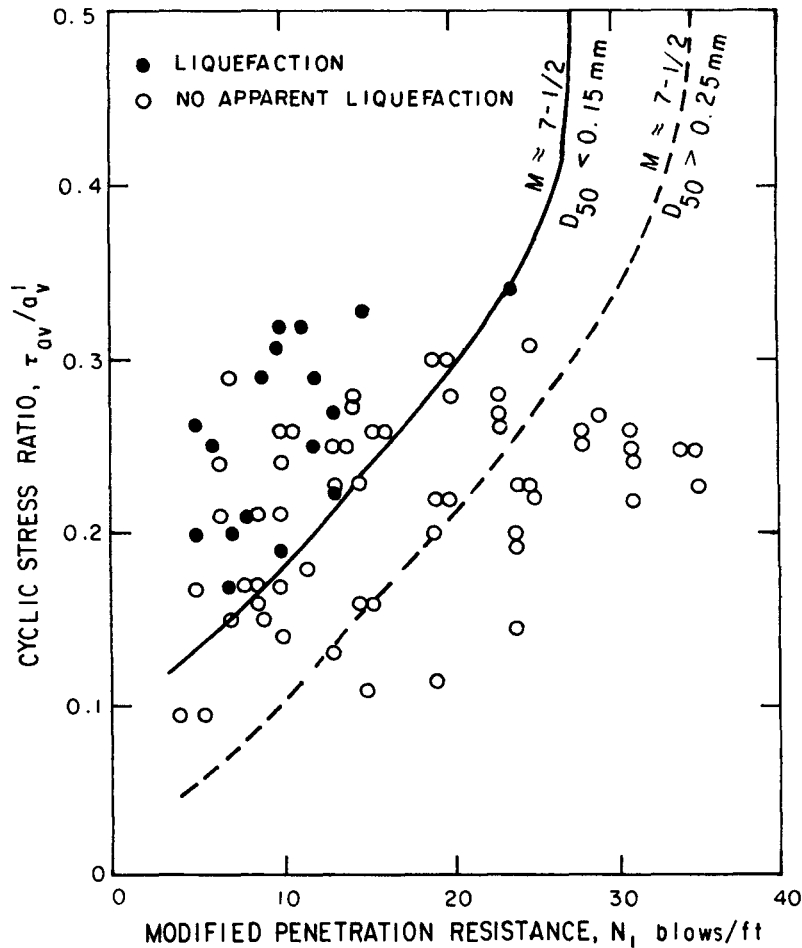


Figure 35. – Correlation between field liquefaction behavior of silty sands ( $D_{50} < 0.15$  mm) under level ground conditions and standard penetration resistance. Data after Tokimatsu and Yoshimi (1981). From [51]. (1 ft = 0.3048 m).

state; while friction sleeve resistance is a function of the soil in the remolded state only. Thus, the trend of higher end bearing and friction sleeve resistances corresponding to lower levels of soil sensitivity is intuitively correct. The problems associated with application of this procedure are that it relies on accurate friction sleeve measurements, and the data base used to develop the chart is unknown. In an effort to check the general validity of the Olsen chart, Farrar [18] applied this procedure to Beggman Friction Mantle mechanical cone data from the 1983 Joint United States-Japan Study. Although the chart was developed for electric cone penetrometers, the mechanical cone data did show an acceptable degree of correlation (see fig. 39).

### Cone Resistance Normalization Factor

With the exception of Robertson's [39] direct approach, all of the remaining empirical liquefaction assessment methods use a type of stress level

normalization equation. Practice within the United States has been to normalize the measurements to a 1.0-TSF (96-kPa) stress level with an equation in the form:

$$Q_{c_1} = c_n q_c \quad (34)$$

where:

- $Q_{c_1}$  = normalized cone end bearing stress,
- $q_c$  = measured cone end bearing stress,
- $c_n = 1/(\sigma'_{vo})^n$ ,
- $\sigma'_{vo}$  = initial vertical effective stress, and
- $n$  = experimentally determined normalization factor.

Although the normalization equation is a curious mix of units and effective stress ( $\sigma'_{vo}$ ) and total stress ( $q_c$ ) parameters, much can be deduced by a review of the literature surrounding the normalization factor ( $n$ ).

Robertson and Campanella [40] presented a graph similar to figure 40 for obtaining  $C_n$ . The results rep-

$$1 \text{ bar} = 100 \text{ kPa} = 1.02 \text{ kg/cm}^2$$

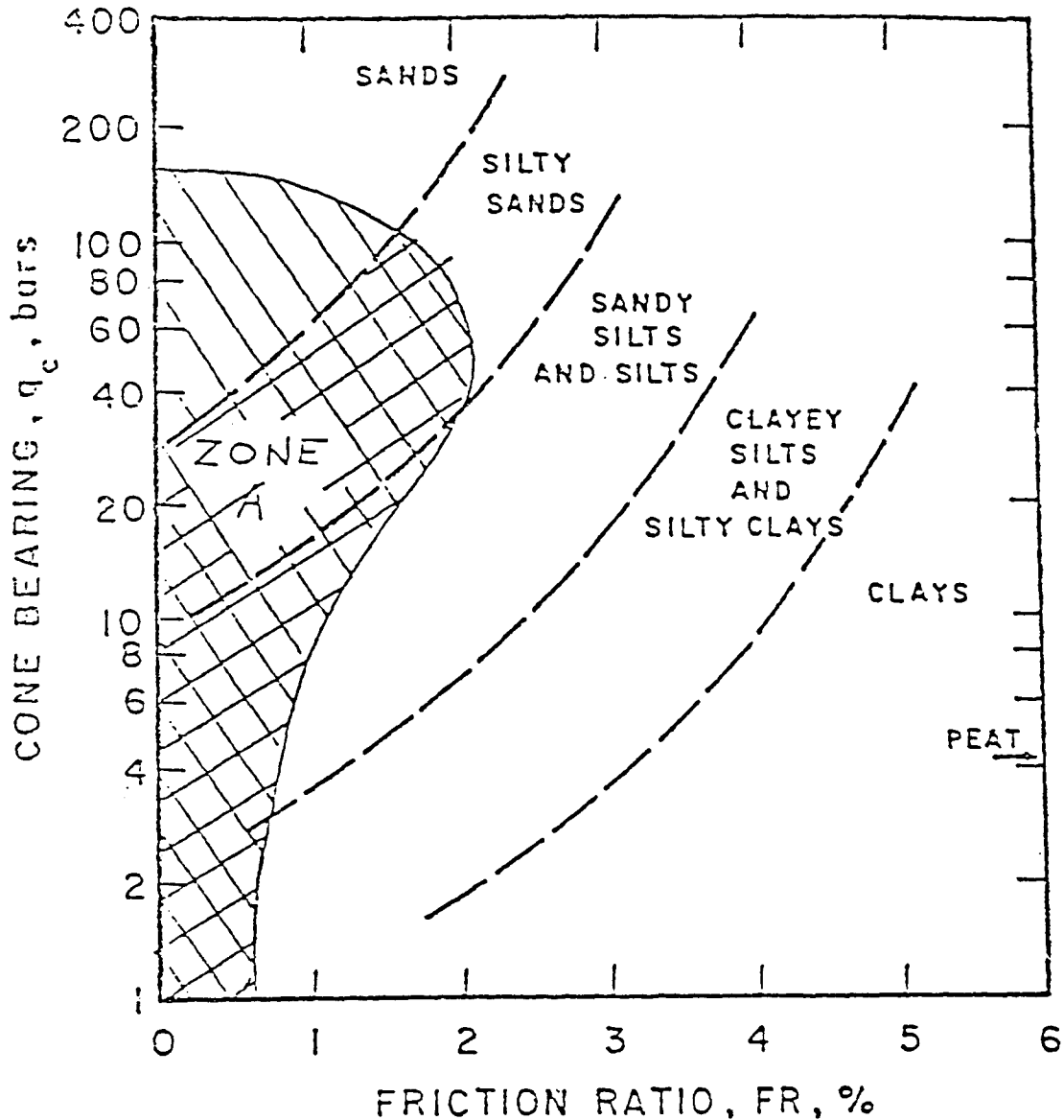


Figure 36. – Soil classification chart for electric cone showing proposed zone of liquefaction soils. From [39].

resented on this figure were based on large calibration chamber tests performed on Ticino sand reported by Baldi et al. [4]. Although no value for  $n$  was given, the response curve may be closely approximated by letting  $n = 0.60$ .

For sands, Olsen [32] recommended a value of  $n = 0.70$ , based upon a review of several large calibration chamber tests. He further recommended that the value of  $n$  should approach 1.0 for clays.

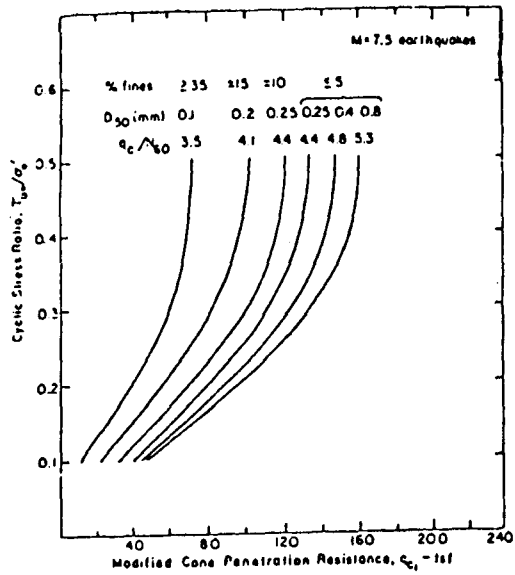
Jamiolkowski et al. [22] summarized several large calibration chamber tests. The expression accompanying this table was:

$$q_c = C_0^{(DRC)} (\sigma'_{vd})^{C_2} \quad (35)$$

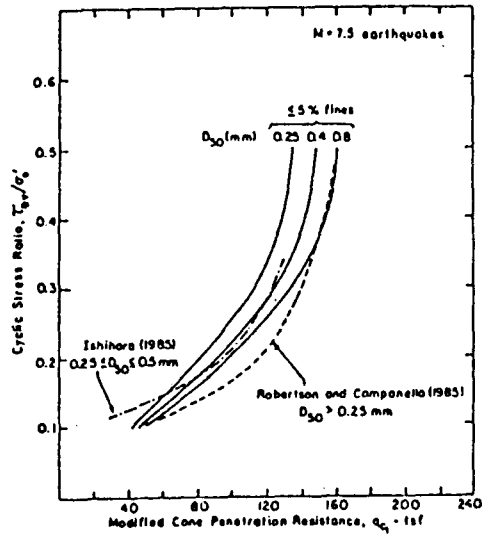
where:

$D_R$  = relative density, and  
 $C_0, C_1, C_2$  = experimentally derived constants.

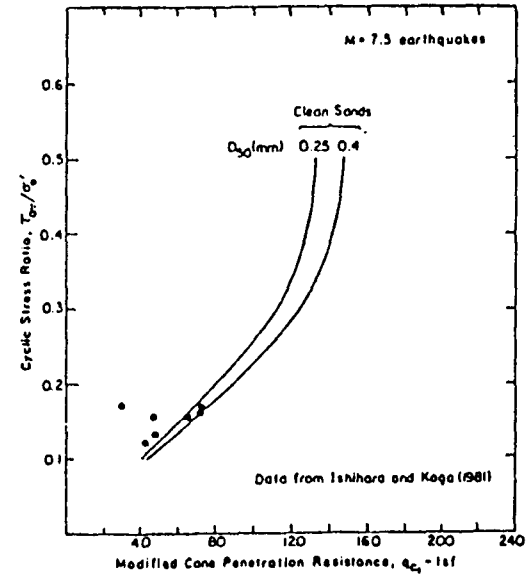
From equation (35), the constant  $C_2$  is equivalent to the value of  $n$  shown in equation (34). The average value for all specimens considered is  $C_2 = 0.72$ . In column  $C_2$  of table 2, the individual values range from 0.584 for the Ticino sand to 0.855 for Melbourne sand. A closer review of the soil properties that lead



(a) Relationship between stress ratio causing liquefaction and cone tip resistance for sands and silty sands.



(b) Comparison of proposed boundary curves for liquefaction resistance evaluations in terms of CPT data.



(c) Comparison of proposed boundary curves and field performance data.

Figure 37. – Graphs for determining liquefaction resistance of a sand from normalized cone end bearing. From [53]. (1 TSF = 96 kPa).

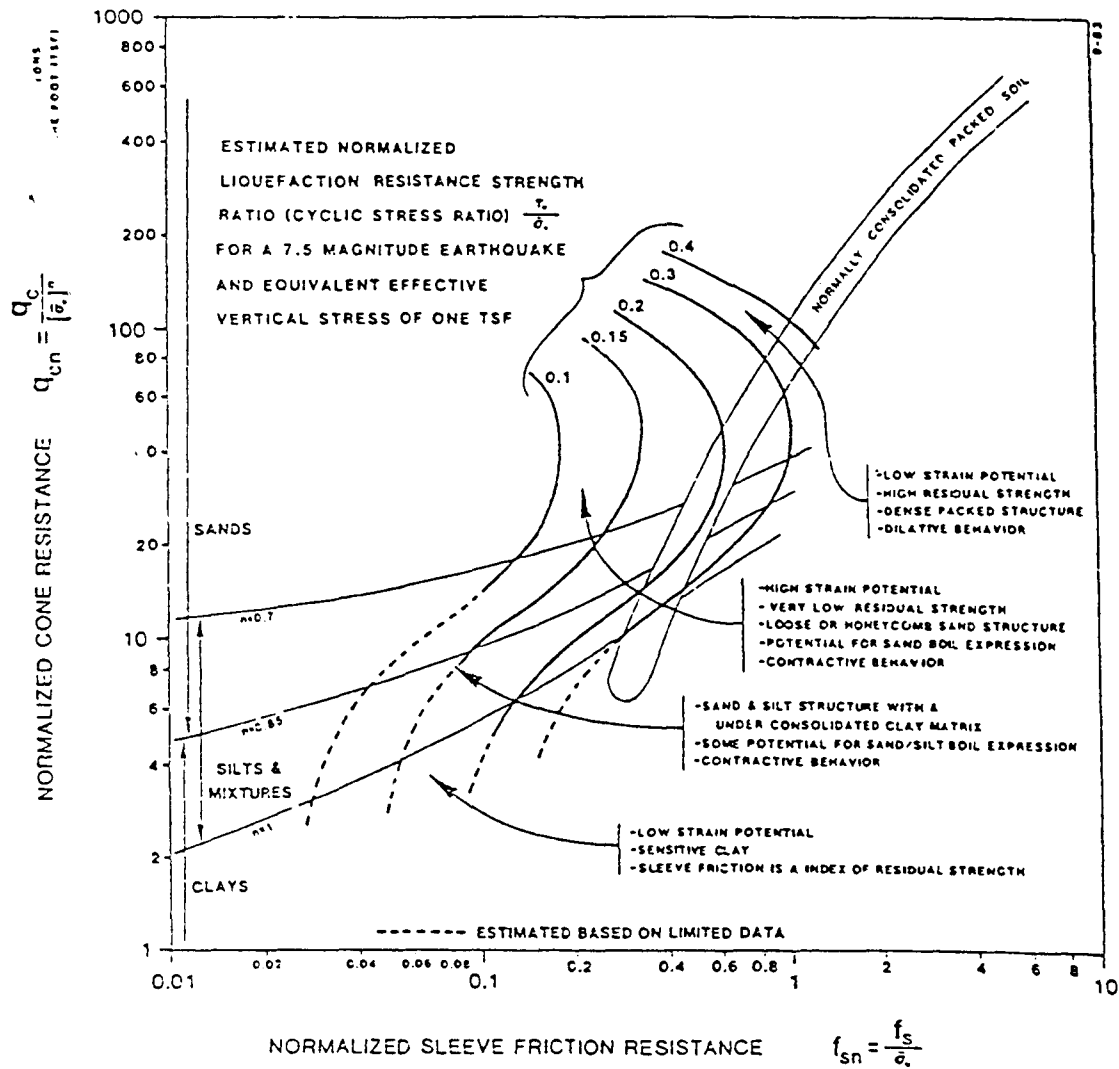


Figure 38. – Graphs for estimating liquefaction resistance of soils. From [32].

to the spread in normalization factors from approximately 0.60 to 0.85 is enhanced by table 3 [41], which presents additional soil properties for many of the sands listed in table 2.

Ticino sand contains approximately 5 percent mica, with a mean grain size of 0.60 mm. The relative density for the Ticino sand ranged from 11 to 95 percent in the experiments. The mineralogic properties of Melbourne sand are not listed in table 3; however, the mean grain size was 0.32 mm and the relative density ranged from 52 to 100 percent for the data in table 2. Ticino sand was more compressible than the Melbourne sand because of the lower values of relative densities tested. The effect of this difference in compressibility was reflected in the higher value of the normalization factor for the Melbourne sand.

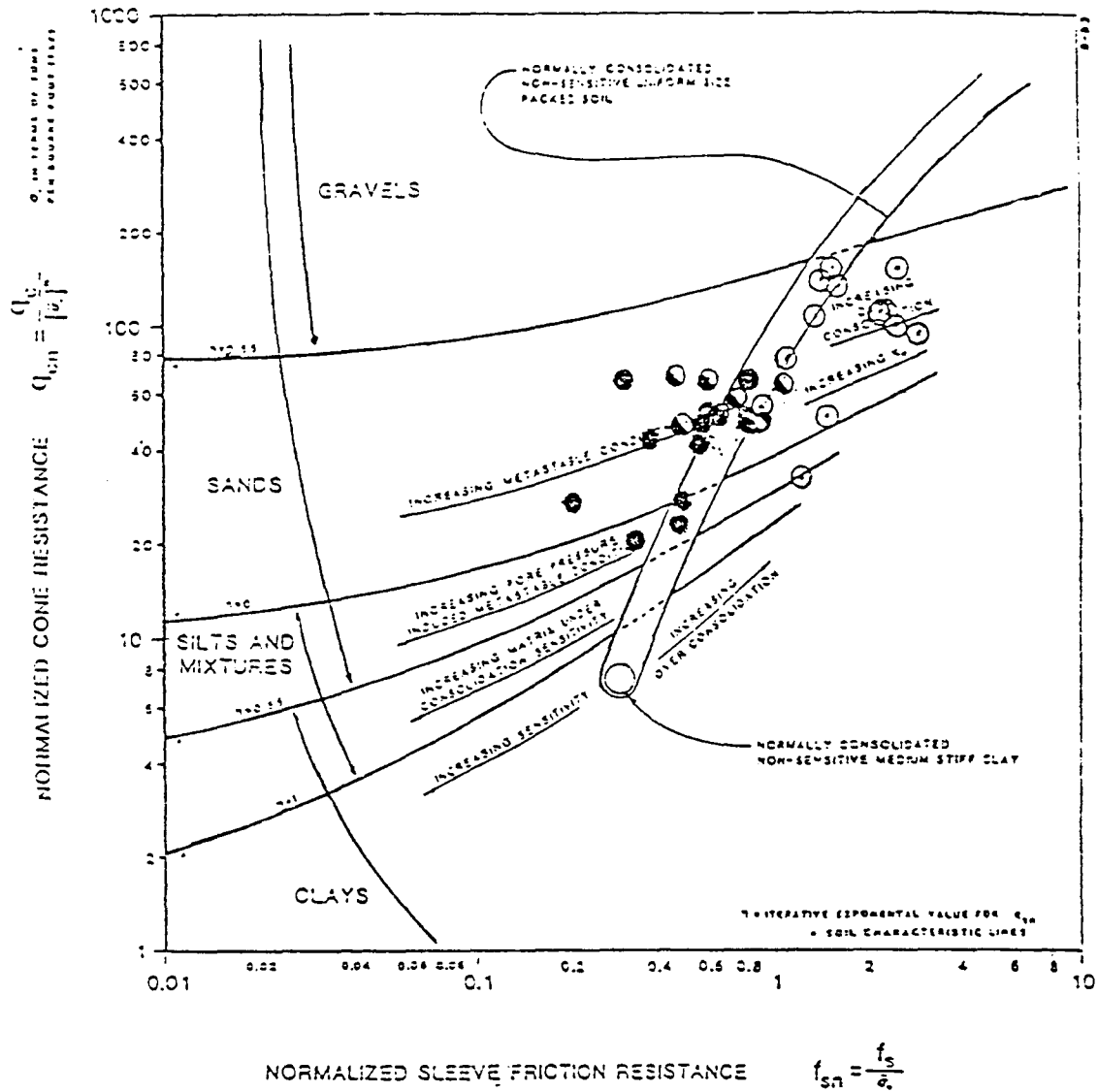
Comparison of Hilton-Mine, Reid Bedford, Ottawa 90, and Edgar 70-140 sands, which have similar ranges of mean grain size and were tested over sim-

ilar ranges of relative density, showed a definite trend of higher values of normalization factor with higher percentages of quartz.

Comparing Hokksund sand having 10 percent mica with Ticino sand having 5 percent mica proved interesting. One would suspect that the Hokksund sand would be more compressible because of its higher mica content. However, figure 29 shows that the effect of mica content on the initial tangent compression modulus is much greater at mica contents ranging from 0 to 5 percent than at those between 5 and 10 percent. The explanation of the higher normalization factor for Hokksund sand is the result of the overriding effects of higher values of relative densities represented in the Hokksund sand test series.

Additional observations of the effect of mineralogy, mean grain size, and angularity may be drawn from the data in tables 2 and 3. However, relative density

# CPT SOIL CHARACTERIZATION CHART



- No liquefaction
  - ◐ Critical FS  $\approx 1.0$
  - Liquefaction
- Liquefaction occurrence from SPT N<sub>160</sub> method

Figure 39. – Summary of normalized tip and sleeve friction CPT data – 1983 U.S.-Japan Joint Study. From [18].

of the sand is by far the most important factor influencing the relationship between compressibility and normalization factor. For soils other than clean sands, permeability must be added to the list of soil parameters influencing the value of the normalization factor. For example, clay soils, which fail in undrained shear during the CPT, are nearly incompressible, and the recommended normalization factor becomes 1.0 [32]. Thus, the normalization factor for a silty sand

would be weighted by density and mean grain-size effects toward a low value of approximately 0.6 and towards a higher value of approximately 0.9 because of its permeability.

Perhaps the most important conclusion of this discussion on the relationship between compressibility and normalization factor is that the measurements obtained from the CPT are a function of both shear

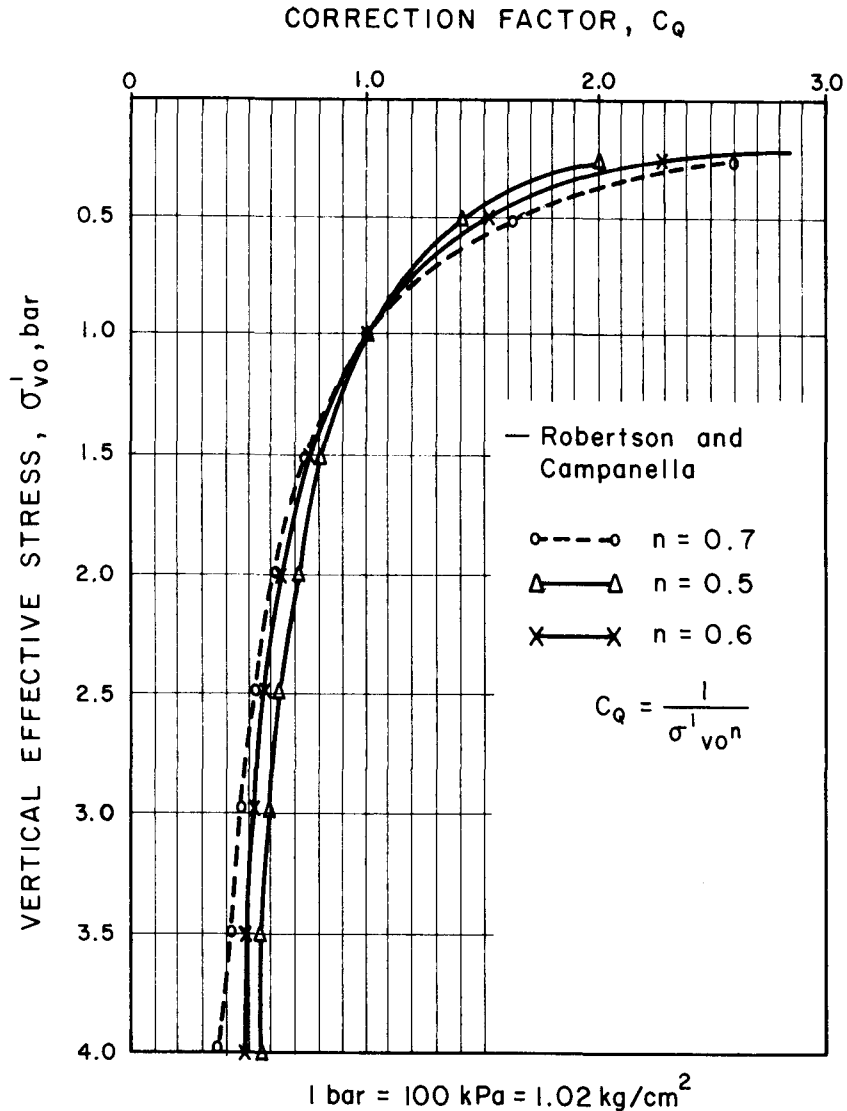


Figure 40. — Relationship between correction factor  $C_Q$  and effective overburden pressure. From [40].

strength and compressibility. To deduce the shear strength or liquefaction susceptibility of a soil, one must estimate the compressibility (i.e., density, permeability, mineralogy, etc.) of the soil and relate this value to the appropriate normalization factor.

#### Analysis of CPT Data to Determine Input Parameters for Use in Liquefaction Analyses

Current emphasis in theoretical liquefaction analysis is on obtaining the steady-state shear strength of a soil (as discussed previously in the subsection entitled "Steady-State Soil Models. . ."). The analysis presumes that the dynamic loading from an earthquake is rapid enough to cause sands to fail in undrained shear while large shear strains develop. As

long as the static shear stresses along a potential failure surface are significantly less than the steady-state shear strength along that surface, the soil will be stable from a flow-deformation theory standpoint.

Within the context of a steady-state analysis, Been et al. [7] proposed to use the cone tip resistance to determine the relationship between the void ratio-static stress state and the steady-state conditions. Realizing that the relationships between relative density and tip resistance was a poor universal indicator of the ambient void ratio of the soil, Been et al. proposed to use the state parameter ( $\psi$ ) developed by Been and Jefferies [6] in place of relative density. The physical meaning of  $\psi$  is illustrated graphically on figure 41, and is defined as:

$$\psi = e_\lambda - e_{ss} \quad (36)$$

Table 2. – Summary of CPT calibration chamber tests. From [22].

Sand type	$D_{50}$ , mm	$\gamma_{max}$ , t/m <sup>3</sup>	$\gamma_{min}$ , t/m <sup>3</sup>	$C_o$	$C_1$	$C_2$	$D_R$ range, %	$R^2$
Edgar 70-140	0.16	1.650	1.311	11.9	3.22	0.685	37 to 70%	0.97
Edgar 30-65	.48	1.750	1.410	11.3	2.39	.824	48 to 99%	.98
Ottawa 90	.21	1.823	1.515	10.5	3.57	.729	20 to 83%	.97
Ottawa 90	.21	1.823	1.515	10.3	3.26	.737	28 to 80%	.97
Reed Bedford	.24	1.748	1.448	12.3	2.79	.788	24 to 81%	.98
Hilton-mine	.20	1.893	1.497	12.1	3.05	.603	30 to 84%	.96
Hilton-mine	.20	1.893	1.497	11.5	2.61	.600	30 to 84%	.97
Ticino	.60	1.700	1.391	13.5	2.84	.584	11 to 95%	.99
Hokksund	.44	1.750	1.414	11.3	3.31	.736	28 to 95%	.99
Melbourne	.32	1.832	1.526	13.6	2.19	.855	52 to 100%	.97

For all considered normalized cone specimens:  $C_o = 11.79$ ;  $C_1 = 2.93$ ;  $C_2 = 0.72$ ;  $R^2 = 0.92$

Table 3. – Properties of sand tested in calibration chamber studies. From [41].

Reference	Sand name	Mineralogy	Shape	Gradation (mm)		Porosity	
				$D_{60}$	$D_{10}$	$n_{max}$	$n_{min}$
Baldi et al. (1981, 1982 [4])	Ticino	Mainly quartz 5%* mica	Subangular to angular	0.65	0.40	0.50	0.41
Villet & Mitchell (1981) [65]	Monterey	Mainly quartz some feldspar	Subrounded to subangular	.40	.25	.45	.36
Schmertmann (1978b) [48]	Ottawa #90	Quartz	Rounded	.24	.13	.44	.33
_____ " _____	Hilton mines	Quartz + mica + feldspar	Angular	.30	.15	.44	.30
Parkin et al (1980)	Hokksund	35% quartz 45% feldspar 10%* mica	Rounded to subangular	.5	.27	.48	.36
Veismanis (1974)	Edgar	Mainly quartz	Subangular	.5	.29	.48	.35
_____ " _____	Ottawa	Quartz	Subangular	.54	.45	.42	.32
Holden (1971)	South Oakleigh	Quartz	Subangular	.19	.12	.47	.35
_____ " _____	_____ " _____	Quartz	Subangular	.37	.17	.43	.29
Chapman & Donald (1981)	Frankston	Mainly quartz	Rounded to subangular	.37	.18	—	—

\* Percent mica by volume

where:

$e_\lambda$  = projected void ratio of a soil at a mean normal stress level of 1 TSF (or 1 MPa), and

$e_{ss}$  = void ratio at which the steady-state line intersects a mean normal stress level of 1 TSF (or 1 MPa).

For the idealized soil model proposed by Robertson [39],  $\psi$  would be represented as shown on figure 42.

The key to this approach is developing independent soil properties as a function of  $\psi$  and the normalized cone resistance ( $q_{c1}$ ) as a function of  $\psi$ . This method requires both extensive laboratory shear testing and large-scale chamber testing of many different sands to develop empirical relationships between  $q_{c1}$  and  $\psi$ . Although the current limited data base for this method is promising (see fig. 43), the method relies

on the concept of steady-state shear strength, which is not yet a universally accepted concept.

### Piezocone as a Possible Indicator of Sand Behavior

Tortensson [58] and Wissa et al. [64] independently developed penetrometers able to measure dynamic pore-water pressures developed during actual penetration. This capability appeared to be a breakthrough in measurement capability that could make the CPT a practical tool for determining soil behavior. It was originally believed that penetrations performed in loose, contractive sands would yield measurements of positive excess pore pressures, whereas penetrations into dense, dilative sands would produce negative excess pore pressures. However, studies performed for the U.S. Army Corps of Engineers [16] and other investigations cast doubt on this hypothesis.

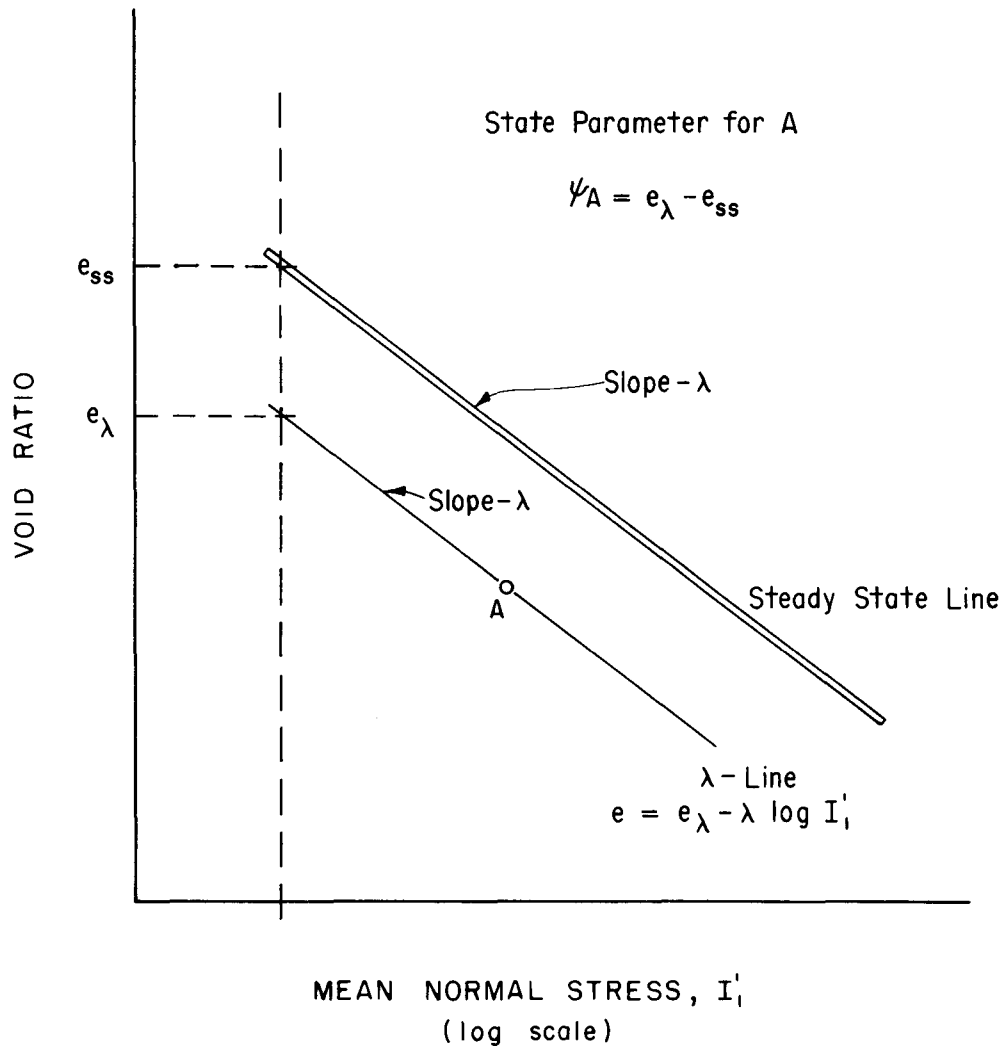


Figure 41. - Definition of state parameter  $\psi$ . From [7].

Three currently used locations of the pore-pressure filter (shown on fig. 44) are (a) on the cone tip, (b) at the middle of the cone, and (c) just behind the cone. Each of these locations has major advantages and disadvantages that have clouded the issue of which location most accurately reflects soil behavior. The tip of the cone is obviously the most forward point of contact between the probe and the soil, but wear on the filter element is extensive in this location. Midway down the cone, the filter element is not subjected to the harsh abrasion of the tip and is still located within the zone of assumed spherical cavity expansion, but (as indicated on fig. 45 [42]), excess pore pressures in this zone always tend to be zero or positive. Pore-pressure measurements just behind the cone tend to be both positive and negative for clays. However, for sands, the disturbance caused by the penetrometer as it expands the soil cavity compacts the sand and results in negative excess pore-pressure measurements behind the cone for

both loose and dense sands. Theoretically, the reason for the negative pore-pressure at this location is the dilation of the sand as the stress state changes from compression on the cone face to shear along the side of the cone. The abrupt change in stress state of a soil element in this vicinity is evident in Allersma's [1] study (fig. 3). Furthermore, from personal experience of pore-pressure measurements made behind the cone, saturation of the filter element is difficult to maintain during penetrations, and dynamic pore-pressure measurements often become unreliable (see figs. 46 and 47).

The excess pore-pressure decay curves shown on figure 47 summarize the various decay patterns observed by this author during field tests with a piezocone penetrometer and filter element located behind the cone. At this writing, no attempt has been made to correlate the observed decay pattern and time scale to soil type, degree of saturation of filter

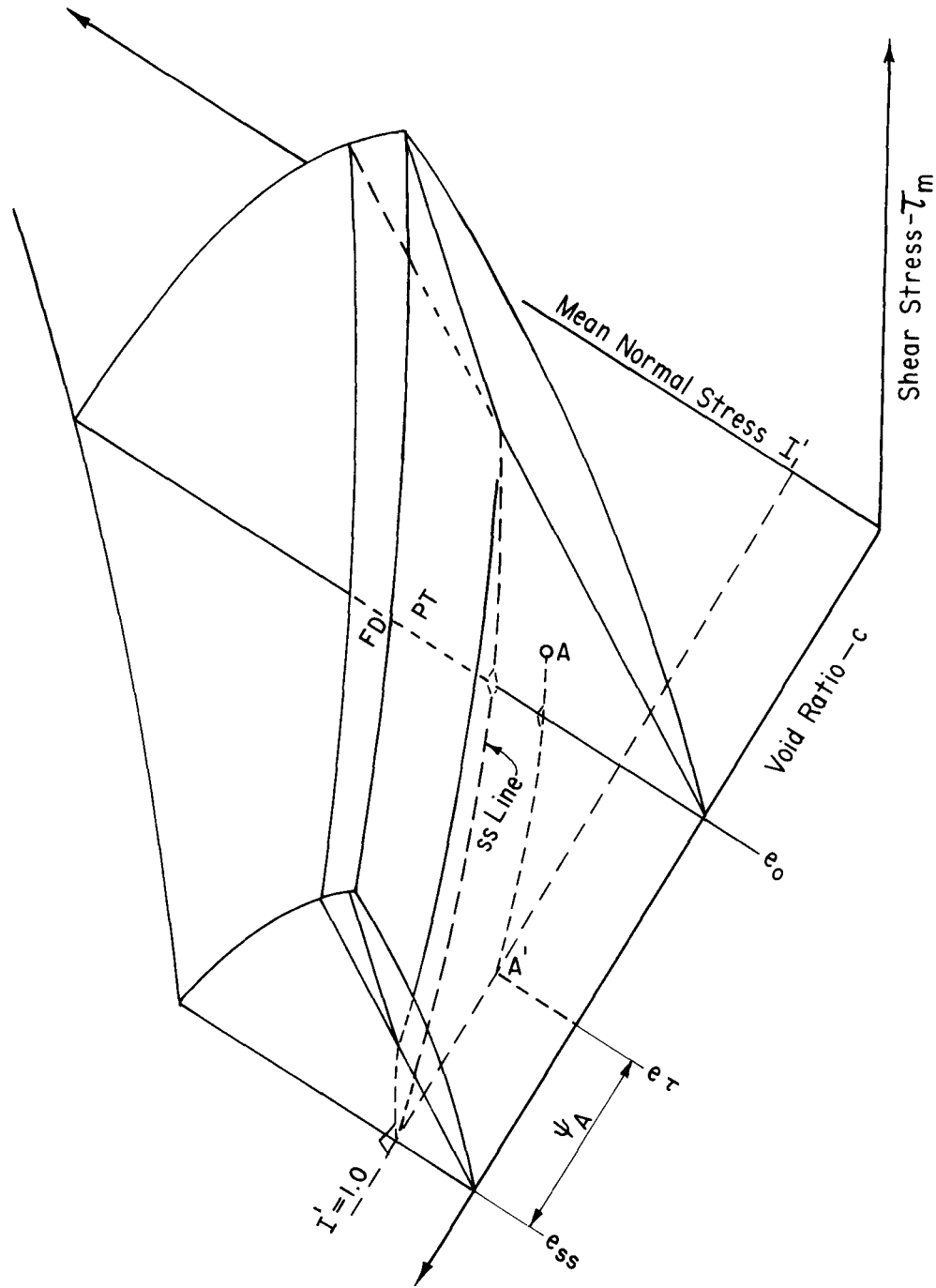


Figure 42. – Definition of state parameter  $\psi$  in idealized soil model proposed by Robertson [39].

element, or stress field and volume change characteristics of the soil surrounding the penetrometer. Difficulty in maintaining saturation of filter elements and lack of knowledge of actual excess pore-pressure development around the penetrometer for granular soils are most likely the causes of many of the contradictory reports on pore-pressure measurements found in the literature.

One successful application of the piezocone penetrometer was reported by Campanella et al. [9]. The piezocone with pore-pressure measurement behind the cone was used to evaluate the effects of dynamic compaction in a sandy and silty deltaic deposit. As shown on figure 48, they were able to detect a change in dynamic pore-pressure measurements before and after treatment of the soil. Although no cor-

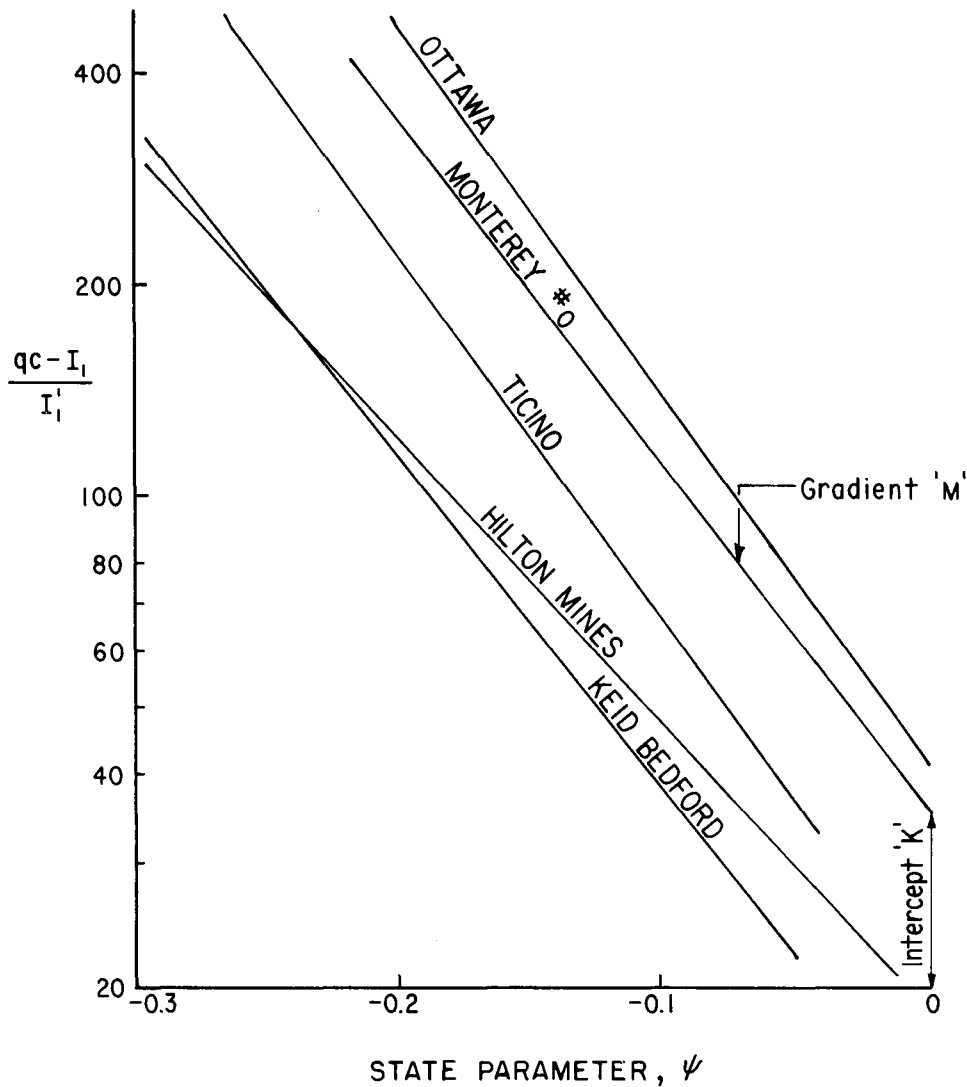


Figure 43. - Summary of normalized cone resistance - state relationships for normally consolidated sands. From [7].

relation of dynamic pore-pressure response to dynamic loading behavior of the soil was attempted in their report, this is the type of evidence that encourages the possible application of the piezocone for evaluating the mechanical properties of silty sands and silts.

#### Use of Relative Density Determinations

One method of liquefaction assessment that has received informal consideration, but little acknowledgment in the literature, is determining the liquefaction susceptibility of a sand as a function of relative density. For this method, the CPT would be used to determine the relative density of the sand.

As discussed previously, this method would require an evaluation of the factors influencing the compress-

ibility of the sand, which are independent of void ratio. The evaluation of those factors would provide the information necessary for the selection of a proper set of relative density versus vertical effective stress curves from the literature. For deposits of sand that are very large and easily accessible for obtaining large sample volumes, a calibration chamber test program could be used to develop the disturbed relative density-CPT relationship for the actual sand in question.

As a preliminary indicator, a procedure of this kind could be used to cover large areas rapidly and to sharply reduce the concern related to unquestionably safe zones of sand and focus attention on questionable zones. This technique may also be conducive to evaluation of soil treatment procedures.

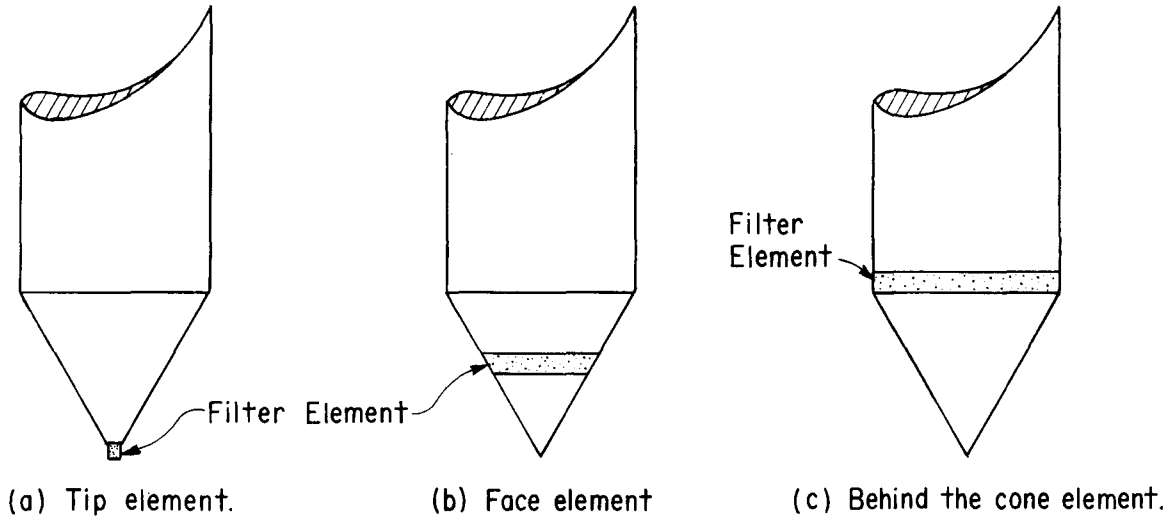


Figure 44. – Location of filter elements for measurement of pore pressure.

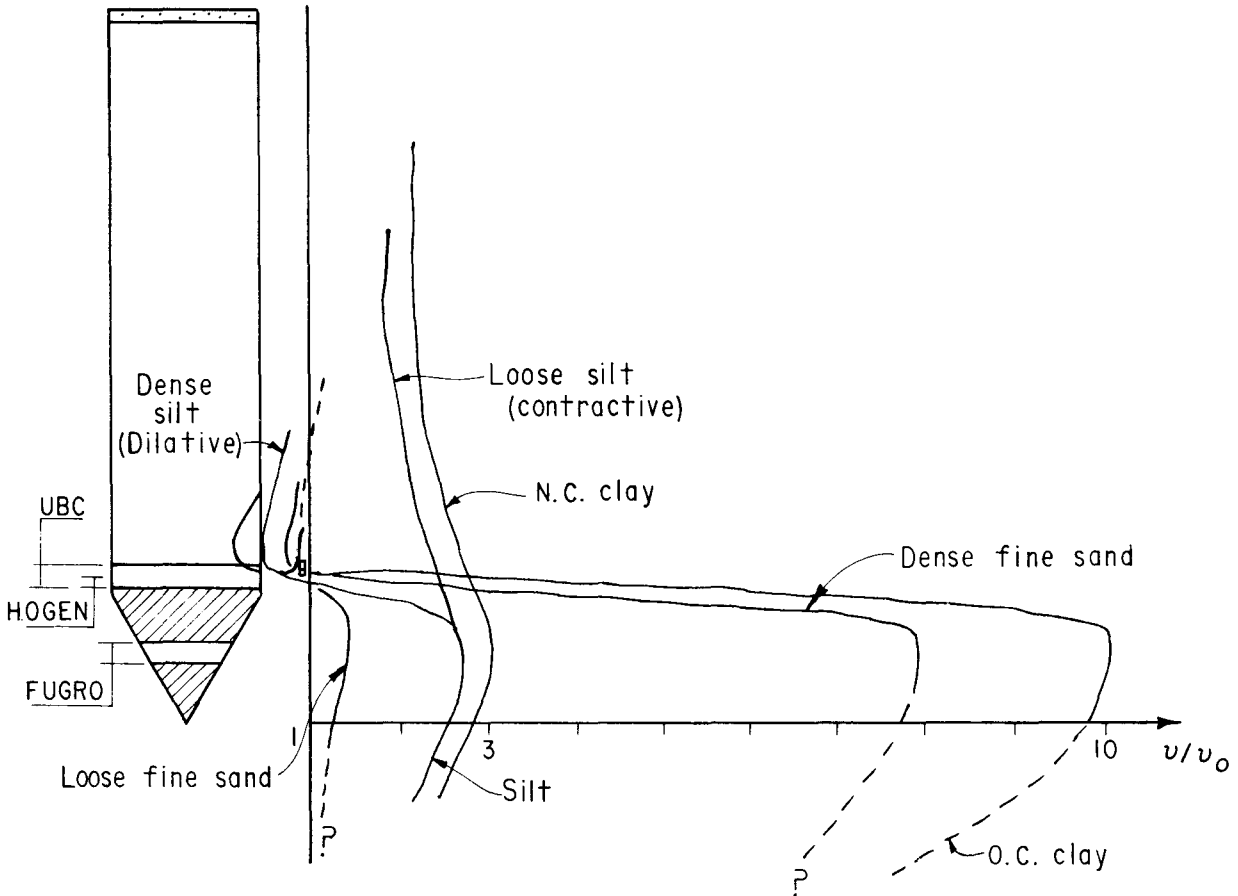


Figure 45. – Conceptual pore pressure distribution in saturated soil during cone penetration. From [42].

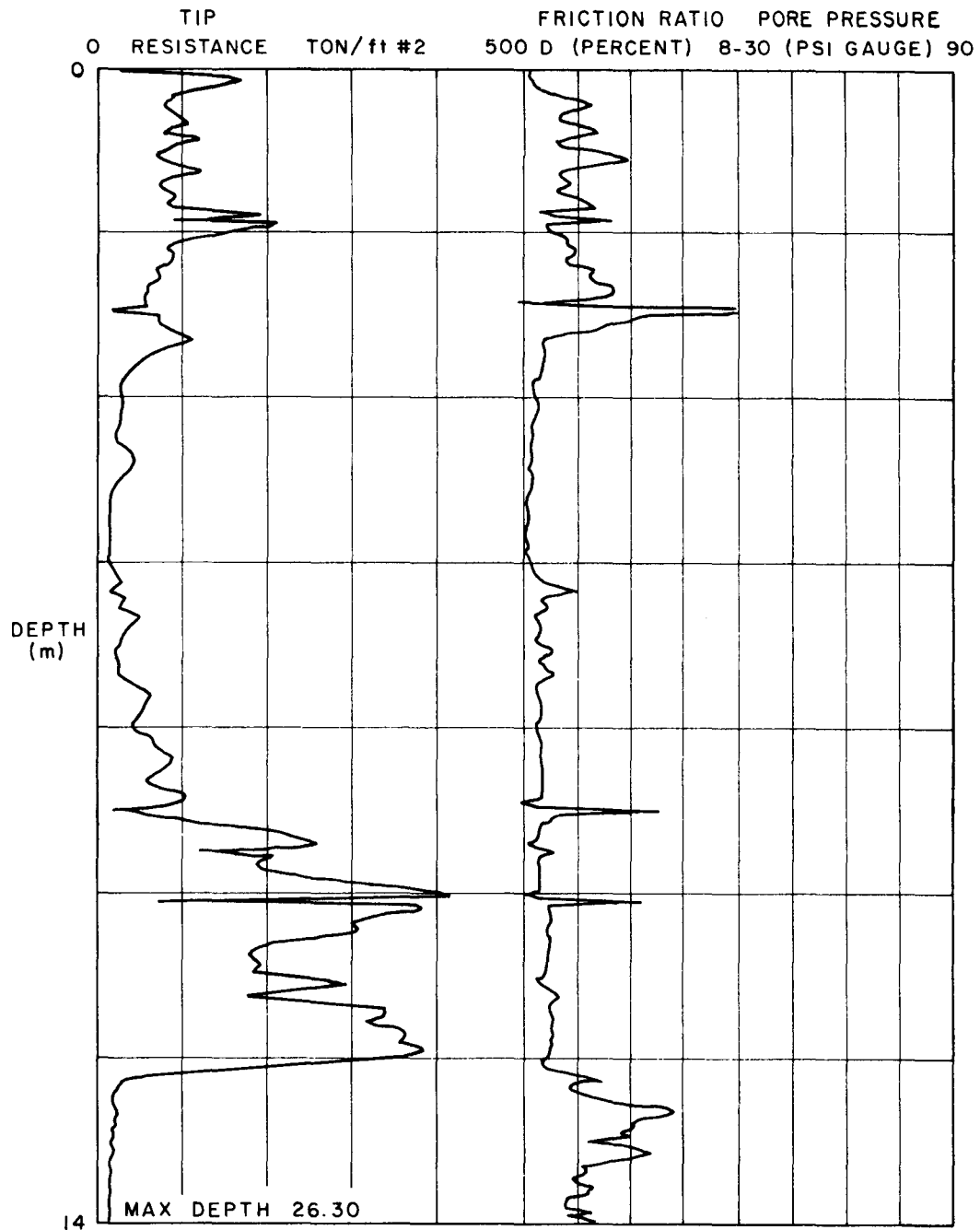


Figure 46. - Piezocone data showing lack of response of pore pressure measurements to changing soil types.

## SUMMARY, CONCLUSIONS, AND RECOMMENDATIONS

### Introduction

This section contains a summary of the report, conclusions on the state of the art related to the use of the CPT to assess liquefaction susceptibility, and proposed recommendations for further research.

### Summary

The section entitled "Soil Behavior Model" discusses the stress and strain fields surrounding the cone penetrometer during steady penetration of a sand deposit, the stress-strain behavior of an element of sand subjected to earthquake loading, and the importance of using a complete soil model to theoret-

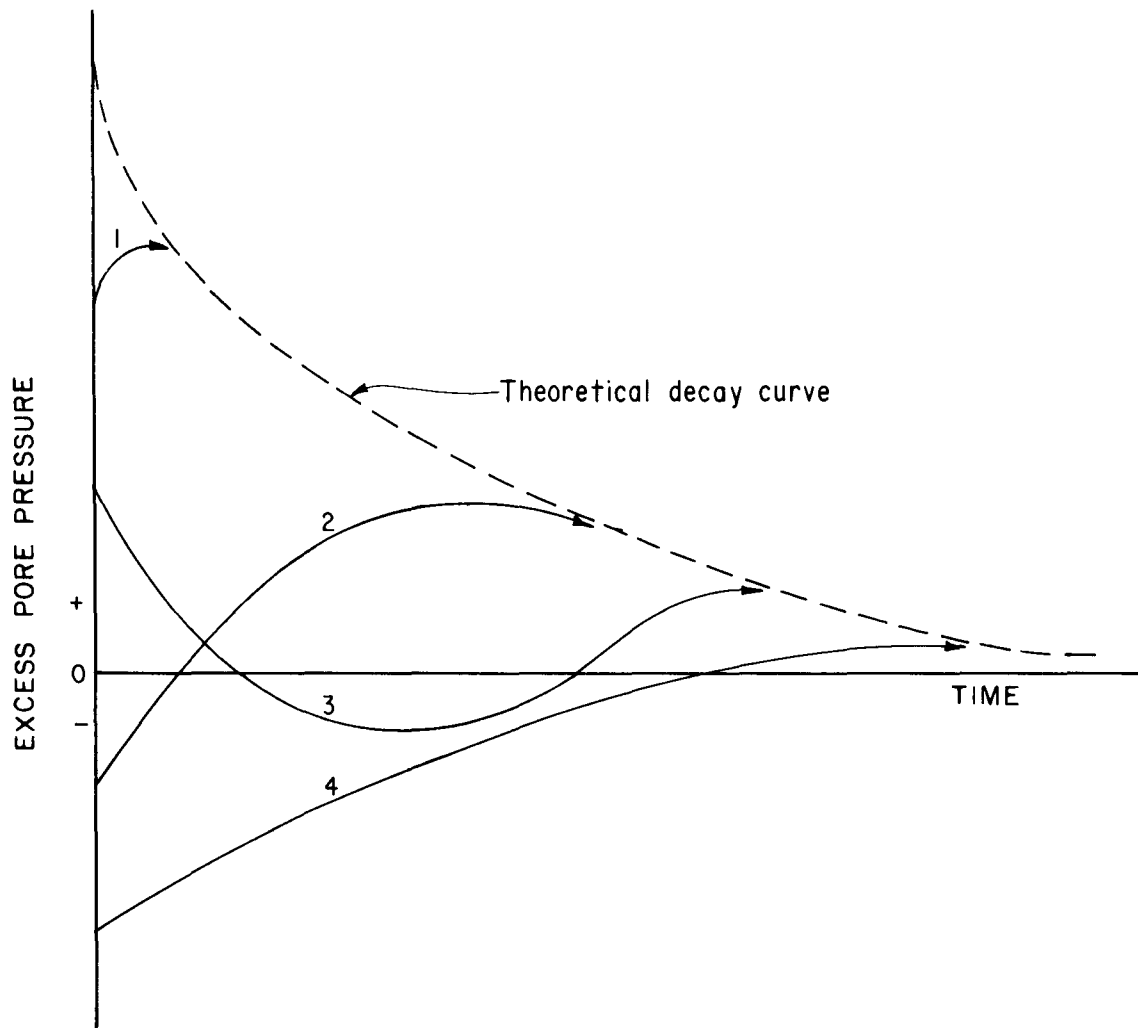
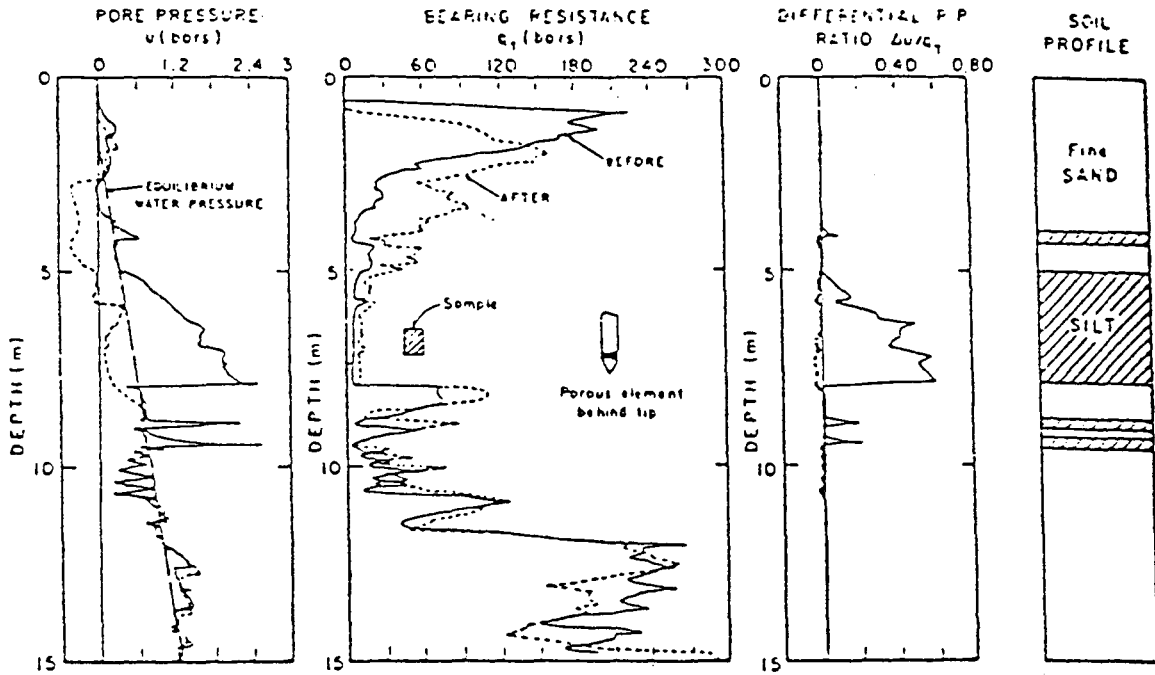


Figure 47. – Conceptual plots of pore-pressure decay patterns measured behind the cone.

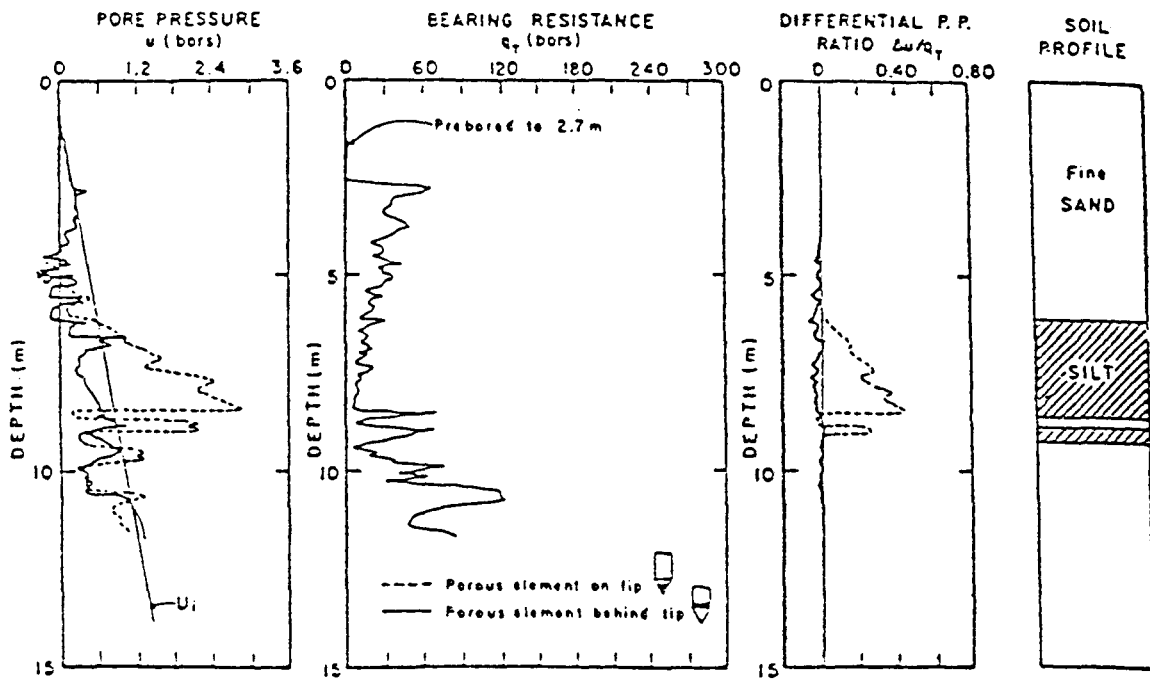
ically link the stress and strain fields induced by the two loading conditions. Theoretical soil modeling of soil behavior during earthquake loading is as little understood as soil behavior during the large strains induced into the soil surrounding the cone penetrometer. Attempts to relate the two behavioral patterns are still highly speculative and premature.

In the section entitled "Cone Penetration Theory," bearing capacity and cavity expansion analyses of CPT results are discussed. Both methods are shown to provide reasonable predictions of the drained shear strength or peak friction angle of a sand as long as the effects related to the compressibility of the sand are recognized when selecting the calculation procedure and variables. For the purpose of liquefaction assessment, it appears that these predictions are currently difficult to use because the relationship of drained shear strength to the liquefaction susceptibility of a sand is currently unclear.

The section entitled "Cone Penetration Practice," discusses the various empirical CPT methods for liquefaction assessment presented in the literature. The proposed methods may be categorized as either (1) CPT-SPT conversion methods, (2) direct interpretation of CPT results to liquefaction susceptibility of a sand methods, or (3) use of CPT data to deduce the void ratio stress state of a sand and relating this deduction to liquefaction assessment of a sand through other laboratory or field experiments. Theoretically, the CPT to SPT conversions are less attractive than the other two procedures; but the CPT-SPT methods offer a means of using the large SPT data base. The methods that attempt to relate the CPT data directly to the liquefaction susceptibility are more theoretically attractive, but the limited data base and lack of knowledge of a complete set of influencing factors for both the CPT data and liquefaction susceptibility of a sand hamper these semi-empirical techniques. Methods of liquefaction assessment that relate CPT data to in situ void ratio



Piezometer cone logging before and after dynamic compaction at New Westminster, B.C. (1 bar = 100 kPa).



After dynamic compaction at sample location: comparison of results for two porous element locations (1 bar = 100 kPa).

Figure 48. – Examples of change in pore-pressure measurements caused by densification of sands and silts. From [9].

and stress condition seem theoretically to be the most attractive. However, they also seem to be the least understood and used because of the lack of understanding of the liquefaction phenomenon itself.

Throughout the discussions in the previous sections, the relationship between shear strength and compressibility of a sand was emphasized. The effects of compressibility and shear strength on the CPT measurements are inseparable. Thus, to deduce one soil parameter or the other from CPT data requires an assumption or knowledge of the other parameter. Associated with the assumptions of strength and compressibility are assumptions of in situ stress condition, drainage condition during penetration, density, cementation, mineralogy, factors related to grain crushing, and others.

### Conclusions

The use of cone penetrometers to assess the liquefaction susceptibility of a sand is currently in its infancy. The largest problems with theoretical evaluation of liquefaction assessment based on the CPT include the lack of a basic understanding of liquefaction, the lack of a closed form solution for interpreting the CPT data, and the limited data base for development of empirical relationships. Problems associated with understanding soil behavior and limited data base may eventually be solved; however, it is doubtful that a closed-form solution will ever be derived for interpreting data obtained by the CPT. The lack of the closed-form solution will require additional assumptions or testing to be performed in conjunction with the CPT for accurate theoretical evaluation of the CPT data. For this reason, the CPT as a liquefaction assessment tool, will most likely remain as an empirical indicator of soil behavior and as an integral part of a larger select group of in situ and laboratory tests designed to complement one another.

### Recommendations

Based on the evidence uncovered in the course of this review, the following recommendations are made:

- (1) A more complete understanding of soil behavior during earthquake loading and large strain shear is necessary for any liquefaction evaluation.
- (2) Continued development of empirical relationships between CPT and observed field behavior of soils is warranted because of lower cost of performing the CPT than the SPT over a large area.
- (3) Continued development of theoretical solutions for the CPT is warranted to develop a more comprehensive understanding of the large-strain

behavior of soils and a complementary set of in situ and laboratory tests for liquefaction assessment.

- (4) Use of the piezocone penetrometers for liquefaction assessment should be pursued for evaluations of silty or clayey sands that may fail in undrained or partially drained shear during the CPT.

## BIBLIOGRAPHY

- [1] Allersma, H. G., "Photoelastic Investigation of the Stress Distribution During Penetration," *Proceedings of the 2d European Symposium on Penetration Testing, ESOPT-II, Amsterdam, 1982.*
- [2] ASTM Designation: D 3441-75T, "Deep Quasi-Static, Cone and Friction Cone Penetration Tests of Soil," 1971.
- [3] Atkinson, J. H., and P. L. Bransby, *The Mechanics of Soils*, McGraw-Hill Company (UK) Limited, England, 1978.
- [4] Baldi, G., R. Bellotti, V. Ghionna, M. Jamiolkowski, and E. Pasqualini, "Design Parameters for Sands from CPT," *Proceedings of the 2d European Symposium on Penetration Testing, ESOPT-II, Amsterdam, 1982.*
- [5] Baligh, M. M., "Cavity Expansion in Sand With Curved Envelopes," *Journal of the Geotechnical Engineers Division, American Society of Civil Engineers*, vol. 102, No. GT 11, pp. 1131-1146. November 1976.
- [6] Been, K., and M. G. Jefferies, "A State Parameter for Sands," *Geotechnique*, vol. 35, 2, pp. 99-112, 1985.
- [7] Been, K., M. Jefferies, J. Crooks, and L. Rothenburg, "The Cone Penetration Test in Sands, Part 2: General Inference of State," Preprint, Submitted for publication in *Geotechnique*, February 1986.
- [8] Buisman, A.S.K., *Grandmechanica*, Waltman, Deft., 1940.
- [9] Campanella, R. G., P. K. Robertson, and Gillespie, "Cone Penetration Testing in Deltaic Soils," *Geotechnique*, vol. 20, pp. 23-35, 1983.
- [10] Casagrande, A., "Liquefaction and Cyclic Deformation of Sands, A Critical Review," *Proceedings of the 5th Pan American Conference, Soil Mechanics and Foundation Engineering*, pp. 80-133, Buenos Aires, 1975.

- [11] Castro, G., "Liquefaction of Sands," Ph.D. Dissertation, Division of Engineering and Applied Physics, Harvard University, 1969.
- [12] Castro, G., "Liquefaction and Cyclic Mobility of Saturated Sands," *Journal of the Geotechnical Engineering Division*, American Society of Civil Engineers, vol. 101, No. GT6, pp. 551-569, June 1975.
- [13] Castro, G., and S. J. Poulos, "Factors Affecting Liquefaction and Cyclic Mobility," *Journal of the Geotechnical Engineering Division*, American Society of Civil Engineers, vol. 106, No. GT6, pp. 501-505, 1977.
- [14] "Cone Penetration Testing and Experience," *Proceedings of a Session Sponsored by the Geotechnical Division*, National Convention, American Society of Civil Engineers, St. Louis, MO, October 1981.
- [15] Cooper, S. S., and A. G. Franklin, "PQS Probe Simultaneous Measurement of Penetration Resistance and Pore Pressure," Final Report GL-82-8, U.S. Army Corps of Engineers, Waterways Experiment Station, Vicksburg, MS, September 1982.
- [16] Douglas, B. J., and R. S. Olsen, "Soil Classification using Electric Cone Penetrometer," Symposium on Cone Penetration Testing and Experience, Geotechnical Engineering Division, ASCE, pp. 209-227, St. Louis, MO, 1981.
- [17] Durgunoglu, H. T., and J. K. Mitchell, "Static Penetration Resistance of Soils: I-Analysis," *Proceedings*, Specialty Conference on In Situ Measurement of Soil Properties, American Society of Civil Engineers, Raleigh, NC, 1975.
- [18] Farrar, J. A., "Study of In Situ Testing for Evaluation of Liquefaction Resistance and Occurrence," Bureau of Reclamation, Special Technical Report, (in draft), 1986.
- [19] Ferritto, J. M., and R. T. Nakamoto, "A Summary of the Prevost Effective Stress Soil Mode," Technical Report R-913, Naval Civil Engineering Laboratory, Port Hueneme, CA, October 1984.
- [20] Harris, W. G., J. C. Parker, and L. W. Zelazny, "Effects of Mica Content on Engineering Properties of Sand," *Journal of Soil Science Society of America*, vol. 48, No. 3, pp. 501-505, 1984.
- [21] "In Situ Measurement of Soil Properties," *Proceedings of the Specialty Conference of Geotechnical Division*, American Society of Civil Engineers, Raleigh, NC, June 1975.
- [22] Jamiolkowski, M., G. Baldi, R. Bellotti, V. Ghionna, and E. Pasqualini, "Penetration Resistance and Liquefaction of Sands," *Proceedings*, 11th International Conference on Soil Mechanics and Foundation Engineering, vol. 4, pp. 1891-1896, 1985.
- [23] Janbu, N., and K. Senneset, "Effective Stress Interpretation of In Situ Static Penetration Tests," *Proceedings of the European Symposium on Penetration Testing*, Stockholm, Sweden, vol. 2.2, pp. 181-193, 1975.
- [24] Levadoux, J. N., and M. M. Baligh, "Pore Pressures During Cone Penetration in Clays," Massachusetts Institute of Technology, Department of Civil Engineering, publication No. R80-15, April 1980.
- [25] *Liquefaction of Soils During Earthquakes*, Report from the Committee on Earthquake Engineering, National Research Council, National Academy Press, Washington, D.C., 1985.
- [26] Lunne, T., and H. P. Christoffersen, "Interpretation of Cone Penetrometer Data for Offshore Sands," Norwegian Geotechnical Institute, Publication No. 156, Oslo, Norway, 1985.
- [27] Lunne, T., T. Eidsmoen, D. Gillespie, and J. D. Howland, "Laboratory and Field Evaluation of Cone Penetrometers," *Use of In Situ Tests in Geotechnical Engineering*, Proceedings of In Situ '86, a Specialty Conference Sponsored by the Geotechnical Division of the American Society of Civil Engineers, Geotechnical special publication No. 6, pp. 714-729. Blacksburg, VA, 1986.
- [28] Matsuoka, H., "Stress-Strain Relationships of Sands Based on the Mobilized Plane," *Soils Foundations*, vol. 14, pp. 47-61, 1974.
- [29] Meyerhof, G. G. "The Ultimate Bearing Capacity of Wedge-Shaped Foundations," *Proceedings of the 5th International Conference of Soil Mechanics and Foundation Engineering*, vol. 2, pp. 105-109, Paris, 1961.
- [30] Mitchell, J. K., and J. M. Keaveny, "Determining Sand Strength by Cone Penetrometer," *Use of In Situ Tests in Geotechnical Engineering*, Proceedings of In Situ '86, a Specialty Conference Sponsored by the Geotechnical Division of the American Society of Civil Engineers, Geotechnical Special Publication No. 6, pp. 823-839, Blacksburg, VA, 1986.
- [31] Nagase, H., "Behavior of Sand in a Multidirectional Irregular Loading," Ph.D. Dissertation, Department of Civil Engineering, University of Tokyo, Japan, 1985.

- [32] Olsen, R. S., "Liquefaction Analysis Using the Cone Penetrometer Test," *Proceedings of the 8th World Conference on Earthquake Engineering*, San Francisco, CA, July 1984.
- [33] Poorooshasb, H. B., I. Holubec, and A. N. Sherbourne, "Yield and Flow of Sand in Triaxial Compression," *Canadian Geotechnical Journal*, Part 1, 3, pp. 179-190, 1966; Parts 2 and 3, 4, pp. 376-397, 1966/67.
- [34] Poorooshasb, H. B., and S. Pietruszczak, "A Generalized Flow Theory for Sand," *Soils and Foundations*, Japanese Society of Soil Mechanics and Foundation Engineering, vol. 26, No. 2, 1986.
- [35] Poulos, S. J., "The Steady-State of Deformation," *Journal of Geotechnical Engineering*, American Society of Civil Engineers, vol. 107, 5, pp. 553-562, pp. 1-15, June 1981.
- [36] *Proceedings of the European Symposium on Penetration Testing*, ESOPT-I, Swedish Geotechnical Society, Stockholm, Sweden, June 1974.
- [37] *Proceedings of the Second European Symposium on Penetration Testing*, ESOPT-II, Amsterdam, Holland, May 1982.
- [38] "Report of the Subcommittee on Standardization of Penetration Testing in Europe", International Society of Soil Mechanics and Foundation Engineering, *Proceedings of the 9th International Conference on Soil Mechanics and Foundation Engineering*, Tokyo, Japan, 1977.
- [39] Robertson, P. K., "In Situ Testing of Soil With Emphasis on Its Application to Liquefaction Assessment," Ph.D. Dissertation, Department of Civil Engineering, University of British Columbia, Vancouver, Canada, 1983.
- [40] Robertson, P. K., and R. G. Campanella, "Interpretation of Cone Penetration Tests – Part I (Sand)," *Canadian Geotechnical Journal*, vol. 20, No. 4, 1983.
- [41] Robertson, P. K., and R. G. Campanella, "Guidelines for Use and Interpretation of the Electronic Cone Penetration Test," Soil Mechanics Series No. 69, Department of Civil Engineering, University of British Columbia, Vancouver, Canada, January 1984.
- [42] Robertson, P. K., R. G. Campanella, D. Gillespie, and J. Greig, "Use of Piezometer Cone Data," *Use of In Situ Tests in Geotechnical Engineering*, a specialty conference sponsored by the technical Division of the American Society of Civil Engineers, Geotechnical special publication No. 6, pp. 1263-1280, Blacksburg, VA, 1986.
- [43] Robertson, P. K., R. G. Campanella, and A. Wightman, "SPT-CPT Correlations," Soil Mechanics Series No. 62, Department of Civil Engineering, University of British Columbia, Vancouver, Canada, October 1982.
- [44] Rowe, P. W., "The Stress-Dilatancy Relation for Static Equilibrium of an Assembly of Particles in Contact," *Proceedings*, Royal Society, vol. 269, series A, pp. 500-527, 1962.
- [45] Sanglerat, G., *The Penetrometer and Soil Exploration*, Elsevier, 1972.
- [46] Schmertmann, J. H., "Predicting the  $Q_c/N$  Ratio," Final Report D-636, Engineering and Industrial Experiment Station, Department of Civil Engineering, University of Florida, Gainesville, FL, 1976.
- [47] Schmertmann, J. H., "Guidelines for Cone Penetration Test, Performance and Design," Federal Highway Administration, Report FHWA-TS-78-209, Washington, D.C., July 1978.
- [48] Scott, R. F., "Plasticity and Constitutive Relations in Soil Mechanics," 19th Terzaghi Lecture, *Journal of Geotechnical Engineering*, American Society of Civil Engineers, vol. 111, No. 5, pp. 559-605, May 1985.
- [49] Seed, H. B., "Some Aspects of Sand Liquefaction Under Cyclic Loading," *Proceedings*, Conference on Behavior of Off-Shore Structures, the Norwegian Institute of Technology, Norway, 1976.
- [50] Seed, H. B., "Soil Liquefaction and Cyclic Mobility Evaluation for Level Ground During Earthquakes," *Journal of the Geotechnical Engineering Division*, American Society of Civil Engineers, vol. 105, No. GT2, pp. 201-255, February 1979.
- [51] Seed, H. B., and I. M. Idriss, "Ground Motions and Soil Liquefaction During Earthquakes," Earthquake Engineering Research Institute, Monograph Series, Berkeley, CA, 1982.
- [52] Seed, H. B., I. M. Idriss, and I. Arango, "Evaluation of Liquefaction Potential Using Field Performance Data," *Journal of Geotechnical Engineering*, American Society of Civil Engineers, vol. 109, No. 3, pp. 458-482, March 1983.

- [53] Seed, H. B., and P. De Alba, "Use of SPT and CPT Tests for Evaluating the Liquefaction Resistance of Sands," *Use of In Situ Tests in Geotechnical Engineering*, a Specialty Conference Sponsored by the Geotechnical Division of the American Society of Civil Engineers, Special Publication No. 6, pp. 281-302, Blacksburg, VA, 1986.
- [54] Shibata, T., H. Yukitomo, M. Miyoshi, "Liquefaction Process of Sand During Cyclic Loading," *Soils and Foundations*, vol. 12, No. 1, pp. 1-16, 1972.
- [55] Tatsuoka, F., "Shear Tests in a Triaxial Apparatus – A Fundamental Study of the Deformation of Sand," Ph.D. Dissertation, Tokyo University, Tokyo, Japan, 1972.
- [56] Tatsuoka, F., and K. Ishihara, "Stress Path and Dilatancy Performance of a Sand," *Proceedings, 8th International Conference on Soil Mechanics and Foundation Engineering*, vol. 1, pp. 419-424, Moscow, 1973.
- [57] Terzaghi, K., *Theoretical Soil Mechanics*, J. Wiley and Sons, New York, NY, 1943.
- [58] Tortensson, B. A., "Pore Pressure Sounding Instrument," Discussion Session I, *Proceedings, American Society of Civil Engineers Special Conference on In Situ Measurement of Soil Properties*, vol. II, pp. 48-54, Raleigh, NC, 1975.
- [59] "Use of In Situ Tests in Geotechnical Engineering," *Proceedings of In Situ '86*, a Specialty Conference Sponsored by the Geotechnical Division of the American Society of Civil Engineers, Geotechnical Special Publication No. 6, Blacksburg, VA, 1986.
- [60] Vesic, A. S., "Expansion of Cavities in Infinite Soil Masses," *Journal of the Soil Mechanics and Foundation Division, American Society of Civil Engineers*, 98, SM3, pp. 265-290, 1972.
- [61] Vesic, A. S., "Principles of Pile Design," Lecture Series on Deep Foundations, Sponsored by the Geotechnical Group, Boston Society of Civil Engineers Section, American Society of Civil Engineers, in Cooperation with Massachusetts Institute of Technology, Cambridge, MA, 1975.
- [62] Vesic, A. S., "Design of Pile Foundations," National Cooperation Highway Research Program, Report No. 42, Transportation Research Board, Washington, D.C., 1977.
- [63] Villet, W. C. B., and J. K. Mitchell (1981), "Cone Resistance, Relative Density, and Friction Angle," Symposium on Cone Penetration Testing and Experience, Geotechnical Engineering Division, American Society of Civil Engineers, St. Louis, MO, October 1981.
- [64] Wissa, A. E. Z., and R. T. Martin, and J. E. Garlanger, "The Piezometer Probe," *Proceedings, American Society of Civil Engineers Specialty Conference in In Situ Measurement of Soil Properties*, vol. I, pp. 536-545, Raleigh, NC, 1975.
- [65] Wroth, C. P., "The Interpretation of In Situ Soil Tests," *Geotechnique*, vol. 34, No. 4, pp. 449-489, 1984.

### **Mission of the Bureau of Reclamation**

*The Bureau of Reclamation of the U.S. Department of the Interior is responsible for the development and conservation of the Nation's water resources in the Western United States.*

*The Bureau's original purpose "to provide for the reclamation of arid and semiarid lands in the West" today covers a wide range of interrelated functions. These include providing municipal and industrial water supplies; hydroelectric power generation; irrigation water for agriculture; water quality improvement; flood control; river navigation; river regulation and control; fish and wildlife enhancement; outdoor recreation; and research on water-related design, construction, materials, atmospheric management, and wind and solar power.*

*Bureau programs most frequently are the result of close cooperation with the U.S. Congress, other Federal agencies, States, local governments, academic institutions, water-user organizations, and other concerned groups.*

A free pamphlet is available from the Bureau entitled "Publications for Sale." It describes some of the technical publications currently available, their cost, and how to order them. The pamphlet can be obtained upon request from the Bureau of Reclamation, Attn D-7923A, P O Box 25007, Denver Federal Center, Denver CO 80225-0007.